LOCALIZATION AND MUTANT ANALYSIS OF THE *ANOPHELES COLUZZII* AMMONIUM TRANSPORTER ACAMT

By

Zi Ye

Dissertation

Submitted to the Faculty of the

Graduate School of Vanderbilt University

in partial fulfillment of the requirements

for the degree of

DOCTOR OF PHILOSOPHY

in

Biological Sciences

May 14, 2021

Nashville, Tennessee

Approved:

Julian F. Hillyer, Ph.D.

Douglas Abbot, Ph.D.

Laurence J. Zwiebel, Ph.D.

Maulik Patel, Ph.D.

Wenbiao Chen, Ph.D.

TABLE OF CONTENTS

LIST OF TABLES

LIST OF FIGURES

LIST OF ABBREVIATIONS

Male accessory gland	MAG
Circumsporozoite protein	CSP
Calcium-dependent protein kinase	CDPK
Plasmodium multidomain scavenger receptor-like protein	PxSR
C-type lectin	CTL
Olfactory sensory neuron	OSN
Tormogen	To
Trichogen	Tr
Thecogen	Th
Odorant receptor	OR
Odorant-binding protein	OBP
Odorant-degrading enzyme	ODE
Odorant receptor-coreceptor	Orco
Ionotropic receptor	IR
Gustatory receptor	GR
Ammonium transporter	Amt
Methylammonium permease	Mep
Rhesus protein	Rh
Anopheles coluzzii ammonium transporter	AcAmt
Drosophila melanogaster ammonium transporter	DmAmt
Aedes aegypti ammonium transporter	AeAmt

Green fluorescence protein	GFP
Discosoma sp. red fluorescence protein	DsRed
AcAmt promoter	AcAmtP
Phosphate-buffered saline with Triton X-100	PBST
Tissue Freezing Medium	TFM
Orco antibody	α-Orco
Horseradish peroxidase antibody	α-HRP
4,6-diamidino-2-phenylindole	DAPI
Digoxigenin	DIG
Saline sodium citrate	SSC
Tris-NaCl-blocking buffer	TNB
Tyramide signal amplification	TSA
Fluorescence in-situ hybridization	FISH
Single sensillum recording	SSR
Grooved peg	GP
Odorant receptor neuron	ORN
Ionotropic receptor neuron	IRN
Gustatory receptor neuron	GRN
Gamma-aminobutyric acid	GABA
Local interneuron	LN
Clustered regularly interspaced short palindromic repeats	CRISPR
CRISPR-associated protein 9	Cas9
RNA interference	RNAi

Electroantennogram	EAG
Electrolabellogram	ELG
single guide RNA	sgRNA
Double-stranded break	DSB
4-(2-hydroxyethyl)-1-piperazineethanesulfonic acid	HEPES
Capillary Feeder	CAFE
α-ketoglutarate	α-KG
Nicotinamide adenine dinucleotide phosphate	NADPH
Glutamate dehydrogenase	GLDH

CHAPTER I

INTRODUCTION: THE MOLECULAR BASIS OF THE AMMONIA SENSING PATHWAY IN THE OLFACTORY SYSTEM OF THE ANOPHELINE MOSQUITO

Anopheles Mosquito Life Cycle

"Mosquito" is the common name for insects in the family Culicidae ("little fly") of Diptera. Mosquitoes have piercing-sucking mouthparts specialized for feeding on liquids, and the majority of mosquito species feed on blood which, in turn, can often lead to pathogen transmission (Mullen and Durden, 2018). Culicidae is divided into two large subfamilies: Anophelinae (represented by the genus *Anopheles*) and Culicinae (represented by the genera *Culex* and *Aedes*) (Reidenbach et al., 2009). Within these groups, notable medically important species include *An. gambiae*, *An. stephensi*, and *An. quadrimaculatus*, which transmit malaria in Africa, India, and North America, respectively; *Cx. pipiens*, which transmits West Nile virus and Saint Louis encephalitis; and *Ae. aegypti* and *Ae. albopictus*, which transmit yellow fever, dengue fever, and Zika virus (Cash-Goldwasser and Barry, 2018; Mullen and Durden, 2018). The malaria mosquito, *An. gambiae*, has undergone a recent speciation event that distinguishes two molecular forms, "M" and "S" (Lehmann and Diabate, 2008). While the S-form retains the species name *An. gambiae*, the M-form has been re-classified as a new species, *An. coluzzii* (Coetzee et al., 2013).

Developmentally, mosquitoes go through a complete metamorphosis over four distinct stages in their life cycles: embryo, larva, pupa, and adult (**Figure 1**). Gravid

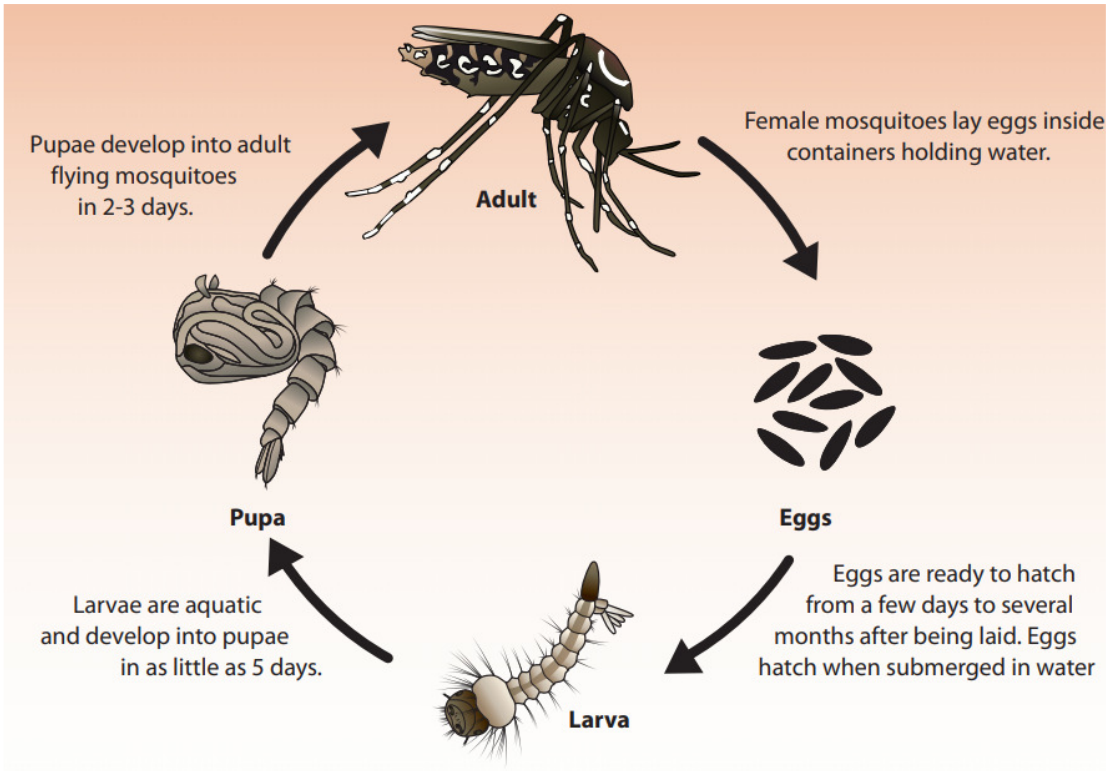

Figure 1. The mosquito life cycle includes 4 stages: egg, larva, pupa, and adult. (Downloaded from Centers for Disease Control and Prevention)

adult female mosquitoes oviposit newly fertilized eggs (embryos) in different largely aquatic habitats, depending on the species. Anopheline mosquitoes oviposit individual embryos and *Culex* mosquitoes deposit groups of embryos held together in “rafts” on the water surface, while *Aedes* often oviposit onto moist soil surfaces that are likely to be subsequently flooded. Embryos are initially pale and then gradually darken as embryogenesis begins. The embryogenesis generally lasts for a few days, and temperature affects the time span of this process. *Anopheles* and *Culex* embryos are oviposited on water and hatch once embryogenesis is complete. In contrast, *Aedes* eggs oviposited on soil surfaces can remain dormant for months and require immersion into water to hatch. Upon hatching from the embryos, mosquito larvae, called “wigglers”, are entirely aquatic and feed primarily on natural algae, which is deficient in protein

(Howland, 1930). Larvae molt three times in total and become pupae. The developmental stage of larvae between each molt is called an “instar”; thus, mosquito larvae go through four instars before becoming pupae. The time required for the larval stage ranges from five to eight days, with temperature, larval density, and food access as the determining factors; additionally, the male larval stage is shorter than that of the female (Barreaux et al., 2018; Lyimo et al., 1992; Marquardt, 2004; Mullen and Durden, 2018). Mosquito pupae, known as “tumblers”, are active during the pupal stage and need to frequently breathe at the surface of the water. When disturbed, they dive deeper into the water using their abdomens. Female pupae are generally larger than males (Marquardt, 2004; Mullen and Durden, 2018).

Mosquito larvae and pupae both need to rest close to the water surface for respiration. Culicine larvae develop a tubular structure called a siphon attached to the 8th abdominal segment. Larvae rest at an angle to the water surface, and the tip of the siphon opens and points at the surface. In contrast, Anopheline larvae lack such a siphon but possess a short spiracle structure on the 8th abdominal segment, by which larvae respire while resting horizontally along the water surface (**Figure 2**; Mullen and Durden, 2018).

Mosquito pupae do not feed and eclose in about two days to become adults in most species (Mullen and Durden, 2018). Adult size and longevity are heavily influenced by larval environment (Barreaux et al., 2018; Lyimo et al., 1992). Males generally emerge earlier than females (Papathanos et al., 2009). In the first few days

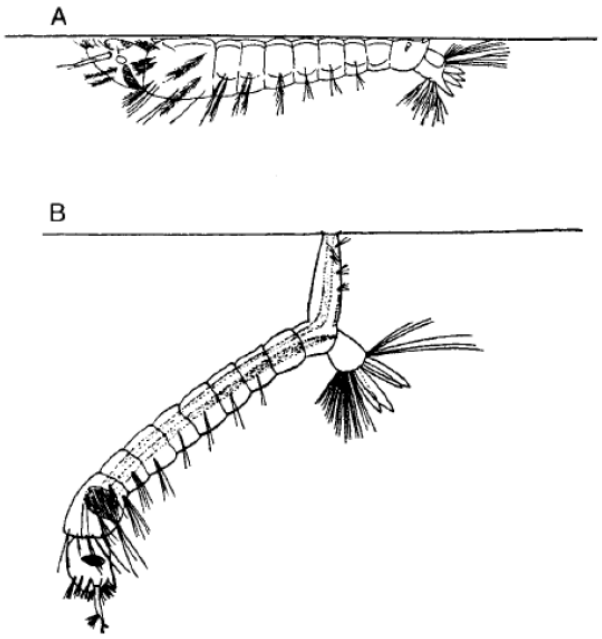

Figure 2. Comparison between **(A)** Anopheline larvae and **(B)** Culicine larvae when resting at the water surface. (Mullen and Durden, 2018)

after emergence, both males and females rely on a range of sensory systems to seek sugar sources (nectar) for survival (Barredo and DeGennaro, 2020). Since protein is limited in the diet during the immature stage and cannot be sufficiently reserved for adults compared to some other insects, females of most mosquito species are obligately haematophagous in that they also must take blood meals from animal hosts in order to acquire sufficient protein stores for egg development, which may be taken after the initial sugar feedings (Klowden, 1995). The majority of mosquito species that require blood meals for reproduction are termed anautogenous, in contrast to a few autogenous species that produce eggs without blood feedings (Tsuji et al., 1990). Although female mosquitoes can substitute sugar with the nutrition in blood for survival,

sufficient access to sugar allows mosquitoes to achieve higher fecundity and fitness (Barredo and DeGennaro, 2020).

Female mosquitoes typically mate once in their lifespan, whereas males can mate multiple times. Males of most species need a few days of sexual maturation to fully development the function of antennal fibrillae, terminalia, and sexual organs; in contrast, females are capable of mating immediately after emergence (Howell and Knols, 2009; Marquardt, 2004; Mullen and Durden, 2018; Oliva et al., 2011; Takken et al., 2006). Copulations of *Anopheles* mosquitoes are generally observed in swarms formed by males that primarily occur in the first hour of the dark phase (Charlwood and Jones, 1979; Howell and Knols, 2009). Males release aggregation pheromones to attract females (Mozūraitis et al., 2020) and erect antennal fibrillae to acoustically locate females by recognizing and matching her wing-beat frequencies (Gibson et al., 2010; Howell and Knols, 2009; Lehmann and Diabate, 2008; Pennetier et al., 2010). The insemination process initiates once a male grasps a female's leg with his tarsal claw on the foreleg and further clamps the female abdomen with his genitalia (Charlwood and Jones, 1979; Howell and Knols, 2009). Males are speculated to detect pheromones on the female cuticle with their gustatory neurons on tarsi in order to assist sexual recognitions prior to inseminations (Diabate and Tripet, 2015). Along with spermatozoa, males ejaculate a mating plug composed of male accessory gland (MAG) substance to block the female spermathecal duct. The MAG substance is suggested to initiate female behavioral changes that prevent remating (Charlwood and Jones, 1979; Howell and Knols, 2009).

Plasmodium Life Cycle

Malaria is a fatal disease, with more than 200 million reported cases and more than 400,000 deaths in 2019. Most of the malaria cases were reported in children in Africa (World Health Organization, 2020). Patients typically show a periodic fever and cold body temperature pattern. Malaria is caused by single-celled eukaryotes in the kingdom protozoa, most of which are free-living and some of which are parasitic (Yaeger, 1996). There are four protozoa species in the genus *Plasmodium* that are responsible for the majority of human malaria cases: *P. falciparum*, *P. vivax*, *P. ovale*, and *P. malariae*. These are vectored to humans and other mammalian blood meal hosts solely by female mosquitoes in the genus *Anopheles*. The malaria pathogen life cycle above can be generalized into several phases: (1) transmission when an infected vector transmits the pathogen to a susceptible host during blood feeding; (2) intrinsic

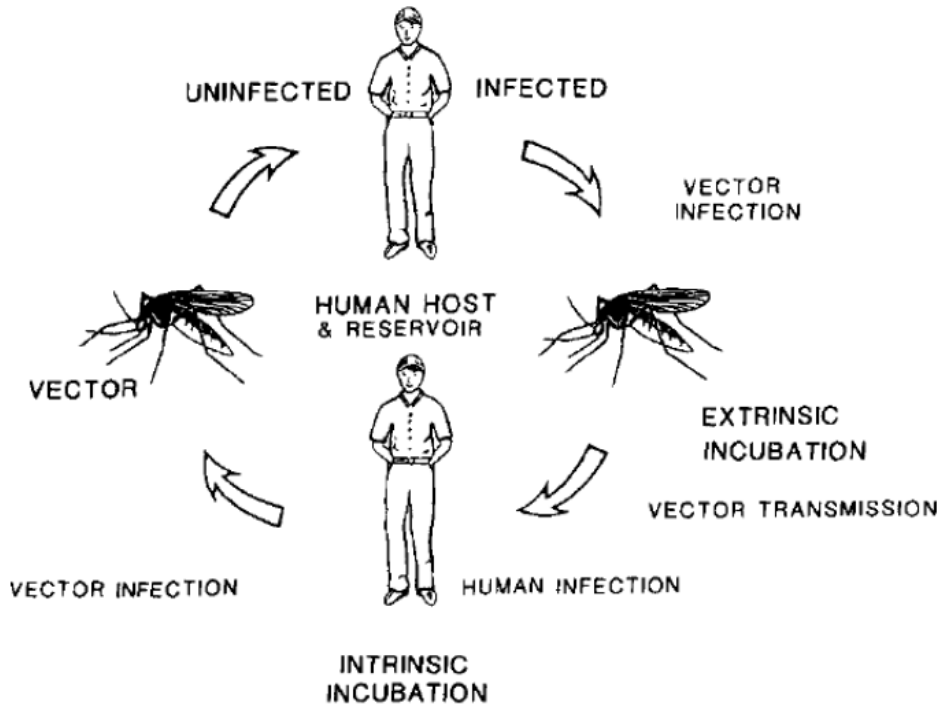

Figure 3. A simplified malaria pathogen transmission cycle. (Mullen and Durden, 2018)

incubation, during which the pathogen develops in the host and becomes infective; (3) extrinsic incubation, during which an uninfected susceptible vector acquires the pathogen from the infected host and the pathogen develops in the vector and becomes infective (**Figure 3**). These interdependent relationships illustrate that diseases such as malaria are closely associated with vectors; as such, vector control has become a crucial approach to reducing vector-borne disease transmission and has shown great success (Mullen and Durden, 2018).

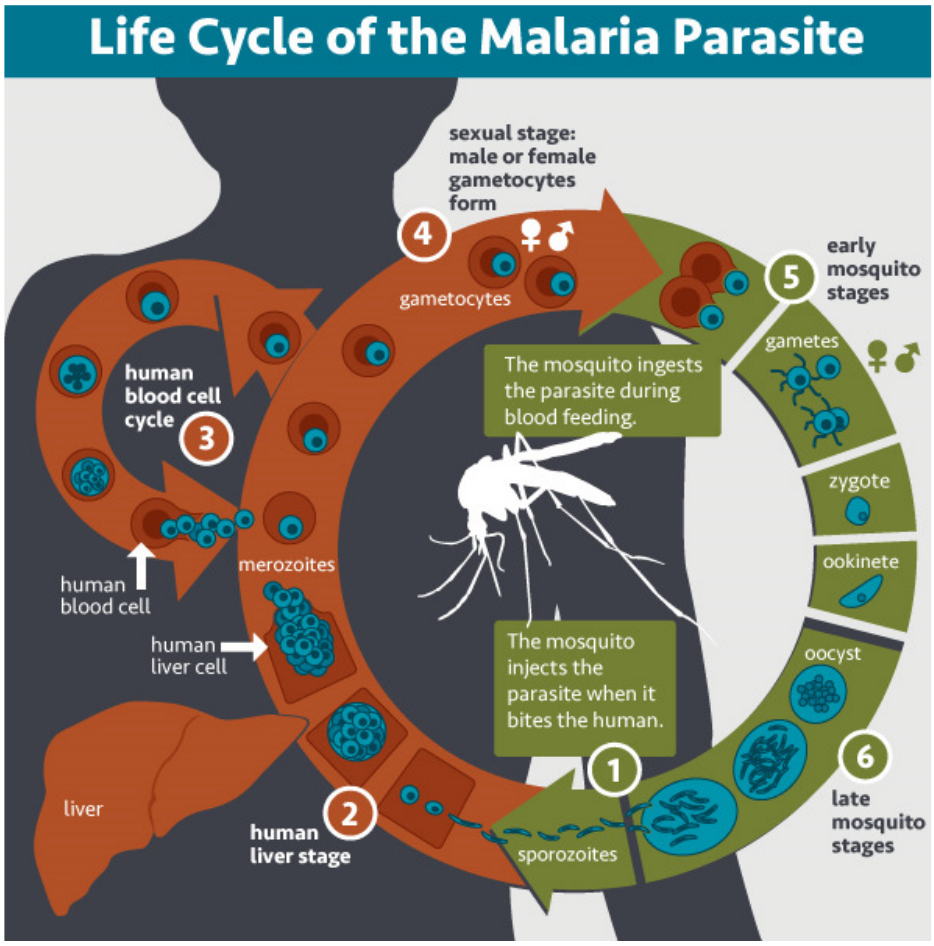

Figure 4. The malaria pathogen life cycle that involves human and mosquito stages. In a human, mosquito transmitted-sporozoites develop into gametocytes that are ingested by mosquitoes through blood meals. (Downloaded from National Institutes of Health)

After transmission to humans through *Anopheles* mosquitoes, *Plasmodium* pathogens usually take up to 30 days to induce symptoms (Ashley et al., 2018; Cash-Goldwasser and Barry, 2018). The malaria pathogen life cycle involves multiple parasitic stages in both humans and mosquitoes (**Figure 4**). Originating from the infected mosquito salivary gland, a small volume of anticoagulant saliva is inoculated by the female mosquito during a blood meal to keep blood flowing, thereby introducing pathogens into the human body. The pathogens infect humans in the form of the sickle-shaped haploid uninucleate sporozoite. It has been suggested that sporozoites are able to independently search for bloodstreams if they are not directly injected into blood vessels by mosquitoes. Sporozoites are then circulated through vessels and invade liver cells, where they develop into multinucleate schizonts. Each liver-stage (exoerythrocytic-stage) schizont comprises a few thousand to 40,000 uninucleate merozoites. The rupture of mature schizonts releases a large amount of merozoites into the bloodstream, where merozoites invade red blood cells (RBCs). Each merozoite can invade one RBC, at which point it develops into either a uninucleate male (microgametocyte) or female (macrogametocyte) gametocyte or a blood-stage (erythrocytic stage) schizont composed of up to 36 merozoites to infect more blood cells. This replication cycle from a merozoite invasion of a blood cell to the bursting of the blood cell that forms more merozoites is called an erythrocytic cycle and causes the symptoms of malaria (Ashley et al., 2018; Barillas-Mury and Kumar, 2005).

At the same time, a small portion of the merozoites differentiate into micro- (male) and macrogametocytes (female) that are not involved in replication in humans but rather are part of the pathogen transmission to mosquitoes (Tuteja, 2007).

Gametocyte formation is determined by numerous factors such as pathogen population and can be influenced by drugs commonly used to treat malaria. Ingested by female mosquitoes during blood meals, gametocytes enter the mosquito midgut lumen. With the changes in temperature and pH and exposure to xanthurenic acid, micro- and macrogametocytes undergo mitosis and produce male (microgamete) and female (macrogamete) haploid gametes, respectively. Male gametes then fertilize female gametes by fusion and form elongated diploid zygotes called ookinetes, in which meiosis occurs to produce sporozoites. Ookinetes are motile and have to invade and penetrate the epithelial cells in order to reach the basal lamina layer and develop into oocysts. After approximately two weeks of development and replication, oocysts rupture and release haploid sporozoites into the hemocoel, where the sporozoites are circulated around the body by hemolymph (Ashley et al., 2018; Josling and Llinás, 2015). The circumsporozoite protein (CSP) that covers the surface of sporozoites plays an essential role in the process by which sporozoites recognize and invade the epithelium cells of the mosquito salivary gland (Barillas-Mury and Kumar, 2005). Sporozoites then penetrate the cells in vacuoles and enter the extracellular secretory cavity, where they further enter the salivary duct in order to be injected along with saliva into new human hosts (Mueller et al., 2010).

The *Plasmodium* life cycle involves complex molecular interactions. As mentioned, CSP has been suggested to have different conformational states to determine the targets (salivary gland or liver) which the sporozoite recognize in different hosts. A member of the calcium-dependent protein kinase (CDPK) family, CDPK4, responds to xanthurenic acid-induced calcium increases in male gametocytes and

regulates the formation of male gametes (Billker et al., 2004). Two ookinete surface proteins, P25 and P28, protect ookinetes from proteases in the midgut and are involved in oocyst formation (Tomas et al., 2001). A *Plasmodium* multidomain scavenger receptor-like protein (PxSR) has been shown to be involved in the production of sporozoites in oocysts (Claudianos et al., 2002). Two C-type lectins (CTLs), CTL4 and CTLMA2, protect ookinetes after the penetration of midgut epithelium cells in the melanization immune response (Barillas-Mury and Kumar, 2005; Osta et al., 2004).

Mosquito Olfactory System

Because malaria pathogens are transmitted to and from blood meal hosts as a direct consequence of mosquito blood feeding that is required for their reproduction, it is essential to understand the fundamental aspects of successful host-seeking preference and recognition (Takken and Knols, 1999; Zwiebel and Takken, 2004). Behaviorally, blood meal host-seeking female mosquitoes are dependent on a large range of host-derived cues, including heat, visual cues, and most importantly, olfactory cues. Together, these allow adult female mosquitoes to track chemical emanations from human and other vertebrate blood meal hosts (Montell and Zwiebel, 2016; Van Breugel et al., 2015). Furthermore, the anthropophilic behavior make *An. gambiae* one of the most efficient vectors for human malaria (Sinka et al., 2010; Takken and Knols, 1999). The mosquito peripheral olfactory system is largely found on a set of bilateral head appendages, including the maxillary palps, labella, and most notably the antennae, which are the principal olfactory appendages in mosquitoes (Lu et al., 2007; Pitts et al., 2004; Qiu et al., 2006; Saveer et al., 2018; Wheelwright et al., 2021; Zwiebel and

Takken, 2004). The surface of the antennae and other olfactory appendages is covered by a large number of diverse sensory hairs known as sensilla, which accommodate several olfactory sensory neurons (OSNs) and auxiliary cells (**Figure 5**) (Kwon et al., 2006; McIver and Siemicki, 1978; McIver, 1982; Pitts and Zwiebel, 2006). Distinct morphological types of antennal sensilla, including trichoid sensilla, coeloconic sensilla, and basiconic sensilla (also known as grooved pegs), are involved in responses to a panel of odorants (**Figure 6**; Pitts and Zwiebel, 2006; Qiu et al., 2006), while only one type of sensilla, known as capitate pegs, was found on the maxillary palps that respond to CO_2 and other odors (Lu et al., 2007). In nature, odorants (acting functionally as agonists for odorant receptors (ORs) and other chemosensory receptors) travel through

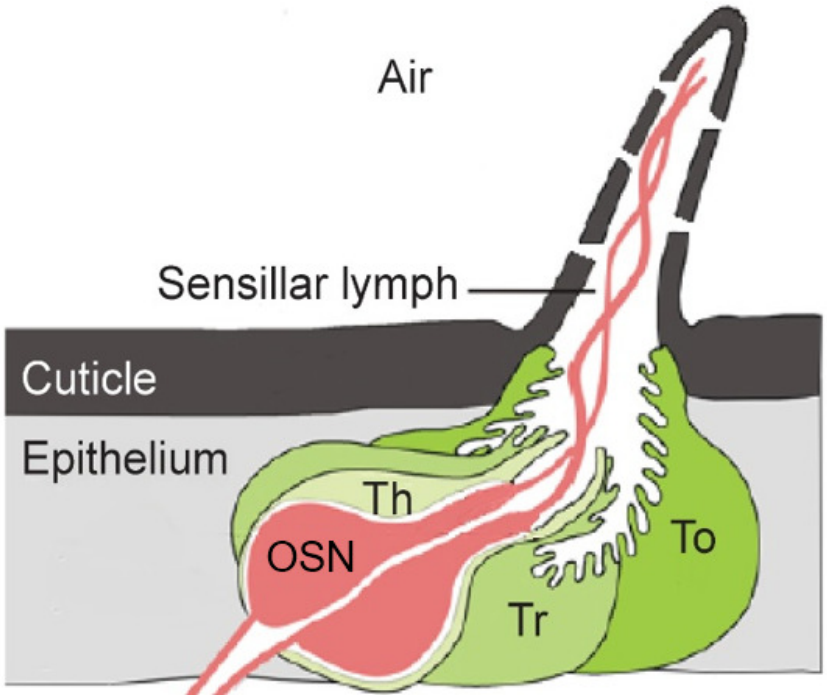

Figure 5. The typical structure of a sensillum. Olfactory sensory neuron (OSN) dendrites are embedded in the sensillum lymph. The cell bodies of OSNs are surrounded by three auxiliary cells: tormogen (To), trichogen (Tr), and thecogen (Th). (Modified from Menuz et al., 2014)

the pores on the surface of the sensillar cuticle where they are transported by odorant-binding proteins (OBPs) or alternatively passively diffuse through the sensillar lymph to activate corresponding OSN dendritic membranes in which signal transduction pathways are centered (Larter et al., 2016; Leal, 2013). Once the signal transduction is complete, the odorants are degraded by odorant-degrading enzymes (ODEs) to rapidly terminate the signaling (Chertemps et al., 2012; Leal, 2013; Younus et al., 2014). The odor-degrading process is particularly important when insects are seeking the odor sources because the interruptions of odor stimulation may suggest they are moving in the wrong direction (Leal, 2013; Maïbèche-Coisne et al., 2004). Both OBPs and ODEs are secreted by the sensillar auxiliary cells surrounding OSNs (**Figure 5**; Laue, 2000; Leal, 2013).

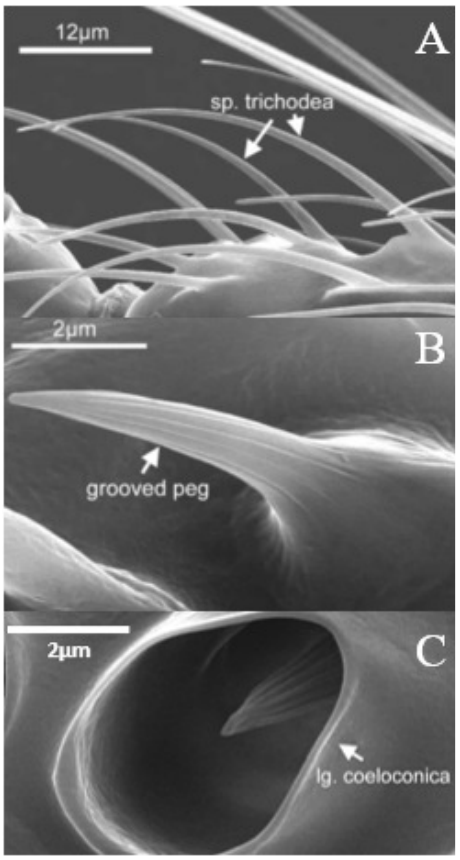

Figure 6. Morphological types of antennal olfactory sensilla on *An. coluzzii*: (A) trichoid sensillum; (B) grooved peg; (C) coeloconic sensillum. (Modified from Pitts and Zwiebel, 2006)

In insects, a large family of highly divergent seven-transmembrane ORs are "tuning ORs", which recognize diverse combinations of chemical stimuli (odorants). Tuning ORs are co-expressed with a highly-conserved OR-coreceptor (Orco) in discrete OSN populations to form a heteromeric ligand-gated cation channel complex that promotes cation flux in response to specific odorant ligands to induce OSN activity (**Figure 7**; Kaupp, 2010; Leal, 2013; Sato et al., 2008; Vosshall and Hansson, 2011). Different OSNs express different OR subunits, while all OSNs express the same Orco subunit. Orco is essential for neuronal functionality as well as OR localization to the dendritic membranes (Degennaro et al., 2013; Larsson et al., 2004; Pitts et al., 2004; Sun et al., 2020). Over the last decade, research has been heavily focused on the functional characterization of canonical ORs and the role they play in mosquito olfactory pathways. A large number of ORs have been functionally characterized as well as implicated in mediating mosquito behaviors (Carey et al., 2010; Hallem et al., 2004; Suh

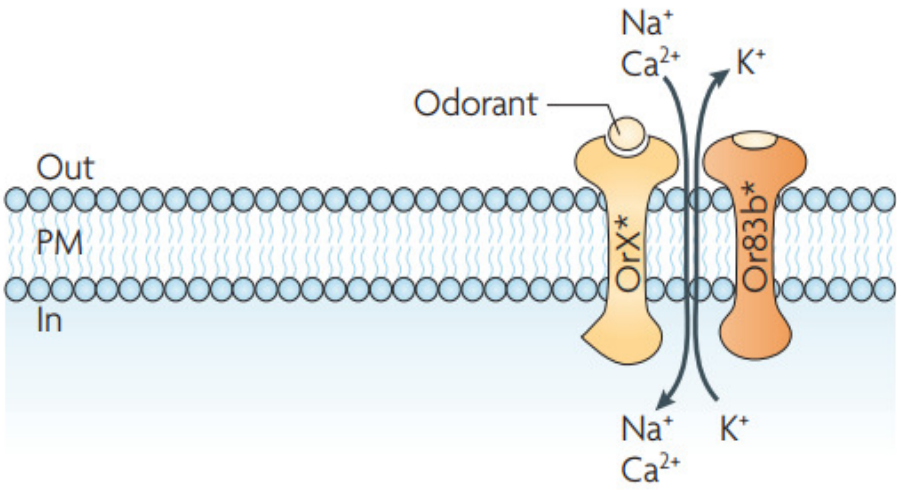

Figure 7. Model of OR/Orco complex where each complex is constructed with a "tuning" OR subunit and an Orco subunit (*OR83b* is the specific gene name for *Orco* in *Drosophila*). (Modified from Kaupp, 2010)

et al., 2014; Wang et al., 2010). However, although Orco is required for the functioning of OR complexes, mutant mosquitoes lacking Orco are still attracted to humans and particularly to a subset of human odors, suggesting the hypothesis that other molecular components are also involved in host-seeking behavior (Degennaro et al., 2013; Potter, 2014). Generally speaking, there has been little attention directed towards other molecular components which must be presumed to act in parallel with ORs to potentially direct the integrative operation of the chemosensory system.

In addition to ORs, a few chemosensory-related membrane protein families have been identified in the last decade, including ionotropic receptors (IRs) as well as gustatory receptors (GRs), although the specific biological function of the majority of these chemosensory receptors in mosquitoes is largely unknown (Benton et al., 2009; Liu et al., 2020; Lu et al., 2007; McMeniman et al., 2014; Pitts et al., 2017; Raji et al., 2019). IRs consist of a family of ionotropic glutamate receptor-related proteins, which was previously suggested to be expressed in a distinct population of neurons aside from OR-expressing neurons that localize in the coeloconic sensilla in *Drosophila* as well as basiconic sensilla (e.g. grooved pegs) in *An. coluzzii*, all of which respond in vivo to acids and amines (Benton et al., 2009; Pitts et al., 2017; Rytz et al., 2013). However, a few recent studies have supported a novel paradigm in which a subset of IRs, ORs, and GRs are co-expressed in the same neurons in antennae and maxillary palps, with different classes of receptors playing complementary roles to ensure neuronal responses to critical semiochemicals (Shankar et al., 2020; Task et al., 2020; Younger et al., 2020). At the molecular level, insect IRs form similar functional complexes to ORs, in which a “tuning” IR is coupled with one or more coreceptors (Ir8a, Ir76b, and

Ir25a) to form a heteromeric ion channel which can be activated by specific agonists and generates action potentials (Benton et al., 2009; Pitts et al., 2017). As their name implies, GRs function as taste receptors that are expressed on insect contact chemosensory appendages, including the maxillary palps, proboscis, and tarsi (Lu et al., 2007; Montell, 2009). In addition, studies have shown that complexes of Gr22/Gr23/Gr24 homologs are co-expressed in mosquito and fly maxillary palps where they act to detect carbon dioxide (CO_2), which is one of the most well-defined human emanations that attracts female mosquitoes (Bowen, 1991; Liu et al., 2020; Lu et al., 2007; McMeniman et al., 2014). Compared to IR and OR signaling complexes, it is unclear whether GRs also act as ion channel complexes with “tuning” and coreceptor subunits (Montell, 2009).

Ammonia Sensing and Ammonium Transporters in Insect Olfactory Systems

It has been demonstrated that human odors are significantly more attractive to female *An. gambiae* than cow odors (Dekker et al., 2009; Pates et al., 2001). While CO_2, a common component of vertebrate breath, generally plays an important role in mosquito host-seeking behaviors (Takken and Knols, 1999), it does not attract *An. gambiae* on its own, which suggests that the anthropophilic character of *An. gambiae* is mediated by other human odors (Takken et al., 1997). Indeed, electrophysiology studies have found human sweat components, including 1-octen-ol, ammonia, L-lactic acid, and some carboxylic acids elicited antennal neuronal activities in *An. gambiae* (Cork and Park, 1996; Meijerink et al., 2001; Qiu et al., 2006). Behavioral assays on these odors revealed that even though the strongest attraction is found in odor blends, ammonia is

the only attractive component when tested alone (Braks et al., 2001; Smallegange et al., 2005). However, ammonia becomes a repellent if the concentration is significantly higher than it is in human sweat (Smallegange et al., 2005), which implies that the mosquito host preference is influenced by the concentration of ammonia (Smallegange et al., 2011). While multiple factors are involved, the ability to identify and locate preferential hosts is mainly determined by the mosquito olfactory system (Takken and Knols, 1999; Zwiebel and Takken, 2004).

In *Drosophila*, Ir92a was found to be extensively co-expressed with the Ir76b, Ir25a, and Ir8a co-receptors and was suggested as the ammonia receptor in the antennal coeloconic sensilla (Benton et al., 2009; Min et al., 2013). Interestingly, the ammonia sensitivity of Ir92a is independent of these co-receptors (Min et al., 2013). In the absence of an obvious Ir92a ortholog, the precise molecular receptor tuned to ammonia has not been identified in mosquitoes. Recently, a novel role of ammonium transporter (Amt) proteins expressed in auxiliary cells was revealed in antennal neuronal responses to ammonia in the fruit fly, *Drosophila melanogaster* (Delventhal et al., 2017; Menuz et al., 2014).

Nitrogen is an essential element required for the survival of living organisms. While nitrogen gas (N_2) makes up about 78% of the atmosphere, its high stability makes it unable to be directly utilized by most organisms. Ammonia (NH_3) is the only nitrogen form that can be incorporated into biological molecules. However, ammonia is toxic when accumulated in cells, which makes it critical for cells to have efficient mechanisms to uptake and transport ammonia (Andrade and Einsle, 2007; Crawford and Forde, 2002). As a hydrophobic gas, ammonia, like O_2 and H_2, is able to passively permeate

cell membranes. However, it is generally accepted that in a typical physiological environment (pH = 7), ammonia is protonated in the form of ammonium cations (NH_4^+), which are membrane-impermeable and require active transportation to travel through the cell membrane. Amt proteins have been identified as facilitating the transportation of ammonium across the cell membrane, including Amts in plants and bacteria, methylammonium permeases (Meps) in yeast, and Rhesus (Rh) proteins in mammals. Although the mechanism of ammonium transportation is debated (Ludewig et al., 2007), Amt is suggested to be a bidirectional transporter involved in the regulation of nitrogen metabolism as a molecular sensor (Andrade and Einsle, 2007; Pitts et al., 2014; Soupene et al., 2002). In *Anopheles* and *Drosophila*, both Amt and Rh proteins have been identified, and in addition to showing expression in the excretory system, Amt transcript is highly abundant in the antenna, one of the primary olfactory appendages (Menuz et al., 2014; Pitts et al., 2014).

Amts are typically four-exon genes encoding proteins with 11 transmembrane helices that were previously thought to serve as a transmembrane channel regulating the transportation of ammonium molecules across the membrane (Andrade and Einsle, 2007; Pitts et al., 2014). Recently, Amt has been shown to be involved in neuronal sensitivity to ammonia in *Drosophila* (Menuz et al., 2014). In the process of having contact with neurons, ammonia must travel through the sensilla lymph, which presumably has a pH of 7 (Böröczky, 2017; Damberger et al., 2013; Leite et al., 2009). Therefore, ammonia molecules are postulated to stimulate OSNs in the form of ammonium cations in the sensillar lymph. In contrast to ORs and other chemosensory receptors expressed in sensory neurons, in the *Drosophila* antennae, *Amt* is expressed

in the auxiliary cells, which are localized around *Ir92a*-expressing neurons where Ir92a transduces signals from ammonia and Amts likely mediate the clearance of excessive ammonium from the extracellular lymph, thereby preventing toxicity and neuronal desensitization by ammonia (Menuz et al., 2014). In *An. coluzzii*, though high levels of *AcAmt* mRNA are detected in the mosquito antenna and its functionality as a transporter has been heterologously validated (Pitts et al., 2014), little information exists as to the mechanistic basis of ammonia detection.

While malaria remains a significant threat to global health, the incremental understanding of essential molecular components in the mosquito olfactory system has shown tremendous potential in decreasing mosquito-human interactions. Among these components, highly conserved molecules, such as Orco and CO_2 receptors, take high priority to be characterized due to their significance in a diverse range of insects (Jones et al., 2011, 2005). As such, the functional investigation of well-conserved AcAmt provides not only the molecular mechanisms of ammonia detection in *An. coluzzii* but also measures the implications of Amt function in other insects of medical and economic importance, such as disease vectors and agricultural pests. Though the exact role that ammonia plays in different insect species is not fully understood, the fact that ammonia elicits neuronal responses in a variety of insects indicates a near universal role of ammonia in insect olfaction-mediated behavior (Haggart and Davis, 1980; Kendra et al., 2005; Yao et al., 2005; Ye et al., 2016).

Along with the well-characterized OR pathway that detects sweat-borne odors such as 1-octen-3-ol (Cork and Park, 1996; Wang et al., 2010) and the GR pathway that detects CO_2 (Liu et al., 2020; Lu et al., 2007), appreciation of the ammonia detection

pathway (most likely IR-dependent) will optimize the disruption of mosquito host-seeking by comprehensively targeting a broad panel of mosquito chemosensory genes. Inasmuch as ammonia represents an essential human cue that plays an important role in host recognition, the characterization of Amt function and localization in *An. coluzzii* contribute to our understanding of mosquito-human interaction, vector control, and global health. Taking advantage of the transgenic and mutagenesis approaches employed here, this study greatly improves insight into mosquito genetic characterization and modification.

References

Andrade, S.L.A., Einsle, O., 2007. The Amt/Mep/Rh family of ammonium transport proteins (Review). Mol. Membr. Biol. 24, 357–365. https://doi.org/10.1080/09687680701388423

Ashley, E.A., Pyae Phyo, A., Woodrow, C.J., 2018. Malaria. Lancet 391, 1608–1621. https://doi.org/10.1016/S0140-6736(18)30324-6

Barillas-Mury, C., Kumar, S., 2005. *Plasmodium*-mosquito interactions: A tale of dangerous liaisons. Cell. Microbiol. https://doi.org/10.1111/j.1462-5822.2005.00615.x

Barreaux, A.M.G., Stone, C.M., Barreaux, P., Koella, J.C., 2018. The relationship between size and longevity of the malaria vector *Anopheles gambiae (s.s.)* depends on the larval environment. Parasites and Vectors 11. https://doi.org/10.1186/s13071-018-3058-3

Barredo, E., DeGennaro, M., 2020. Not just from blood: mosquito nutrient acquisition from nectar sources. Trends Parasitol. https://doi.org/10.1016/j.pt.2020.02.003

Benton, R., Vannice, K.S., Gomez-Diaz, C., Vosshall, L.B., 2009. Variant ionotropic glutamate receptors as chemosensory receptors in *Drosophila*. Cell 136, 149–162. https://doi.org/10.1016/j.cell.2008.12.001

Billker, O., Dechamps, S., Tewari, R., Wenig, G., Franke-Fayard, B., Brinkmann, V., 2004. Calcium and a calcium-dependent protein kinase regulate gamete formation and mosquito transmission in a malaria parasite. Cell. https://doi.org/10.1016/S0092-8674(04)00449-0

Böröczky, K., 2017. Pheromone communication in moths: evolution, behavior, and

application. Am. Entomol. 63, 260–261. https://doi.org/10.1093/ae/tmx069

Bowen, M., 1991. The sensory physiology of host-seeking behavior in mosquitos. Annu. Rev. Entomol. 36, 139–158. https://doi.org/10.1146/annurev.ento.36.1.139

Braks, M.A.H., Meijerink, J., Takken, W., 2001. The response of the malaria mosquito, *Anopheles gambiae*, to two components of human sweat, ammonia and L-lactic acid, in an olfactometer. Physiol. Entomol. 26, 142–148. https://doi.org/10.1046/j.1365-3032.2001.00227.x

Carey, A.F., Wang, G., Su, C.Y., Zwiebel, L.J., Carlson, J.R., 2010. Odorant reception in the malaria mosquito *Anopheles gambiae*. Nature 464, 66–71. https://doi.org/10.1038/nature08834

Cash-Goldwasser, S., Barry, M., 2018. CDC Yellow Book 2018: Health information for international travel. Clin. Infect. Dis. 66, 1157–1158. https://doi.org/10.1093/cid/cix965

Centers for Disease Control and Prevention, 2021. Life cycle of *Aedes aegypti* and *Ae. albopictus* mosquitoes [WWW Document]. URL https://www.cdc.gov/mosquitoes/about/life-cycles/aedes.html

Charlwood, J.D., Jones, M.D.R., 1979. Mating behaviour in the mosquito, *Anopheles gambiae s.l.* I. Close range and contact behaviour. Physiol. Entomol. 4, 111–120. https://doi.org/10.1111/j.1365-3032.1979.tb00185.x

Chertemps, T., François, A., Durand, N., Rosell, G., Dekker, T., Lucas, P., Maïbèche-Coisne, M., 2012. A carboxylesterase, Esterase-6, modulates sensory physiological and behavioral response dynamics to pheromone in *Drosophila*. BMC Biol. 10. https://doi.org/10.1186/1741-7007-10-56

Claudianos, C., Dessens, J.T., Trueman, H.E., Arai, M., Mendoza, J., Butcher, G.A., Crompton, T., Sinden, R.E., 2002. A malaria scavenger receptor-like protein essential for parasite development. Mol. Microbiol. https://doi.org/10.1046/j.1365-2958.2002.03118.x

Coetzee, M., Hunt, R.H., Wilkerson, R., Torre, A. Della, Coulibaly, M.B., Besansky, N.J., 2013. *Anopheles coluzzii* and *Anopheles amharicus*, new members of the *Anopheles gambiae* complex. Zootaxa 3619, 246–274. https://doi.org/10.11646/zootaxa.3619.3.2

Cork, A., Park, K.C., 1996. Identification of electrophysiologically-active compounds for the malaria mosquito, *Anopheles gambiae*, in human sweat extracts. Med. Vet. Entomol. 10, 269–276. https://doi.org/10.1111/j.1365-2915.1996.tb00742.x

Crawford, N.M., Forde, B.G., 2002. Molecular and developmental biology of inorganic nitrogen nutrition. Arab. B. 1, e0011. https://doi.org/10.1199/tab.0011

Damberger, F.F., Michel, E., Ishida, Y., Leal, W.S., Wüthrich, K., 2013. Pheromone discrimination by a pH-tuned polymorphism of the *Bombyx mori* pheromone-binding protein. Proc. Natl. Acad. Sci. U. S. A. 110, 18680–18685. https://doi.org/10.1073/pnas.1317706110

Degennaro, M., McBride, C.S., Seeholzer, L., Nakagawa, T., Dennis, E.J., Goldman, C., Jasinskiene, N., James, A.A., Vosshall, L.B., 2013. Orco mutant mosquitoes lose strong preference for humans and are not repelled by volatile DEET. Nature 498, 487–491. https://doi.org/10.1038/nature12206

Dekker, T., Takken, W., Braks, M.A.H., 2009. Innate preference for host-odor blends modulates degree of anthropophagy of *Anopheles gambiae sensu lato* (Diptera:

Culicidae). J. Med. Entomol. 38, 868–871. https://doi.org/10.1603/0022-2585-38.6.868

Delventhal, R., Menuz, K., Joseph, R., Park, J., Sun, J.S., Carlson, J.R., 2017. The taste response to ammonia in *Drosophila*. Sci. Rep. 7. https://doi.org/10.1038/srep43754

Diabate, A., Tripet, F., 2015. Targeting male mosquito mating behaviour for malaria control. Parasites and Vectors 8. https://doi.org/10.1186/s13071-015-0961-8

Gibson, G., Warren, B., Russell, I.J., 2010. Humming in tune: Sex and species recognition by mosquitoes on the wing. JARO - J. Assoc. Res. Otolaryngol. 11, 527–540. https://doi.org/10.1007/s10162-010-0243-2

Haggart, D.A., Davis, E.E., 1980. Ammonia-sensitive neurones on the first tarsi of the tick, *Rhipicephalus sanguineus*. J. Insect Physiol. 26, 517–523. https://doi.org/10.1016/0022-1910(80)90126-2

Hallem, E.A., Ho, M.G., Carlson, J.R., 2004. The molecular basis of odor coding in the *Drosophila* antenna. Cell 117, 965–979. https://doi.org/10.1016/j.cell.2004.05.012

Howell, P.I., Knols, B.G.J., 2009. Male mating biology. Malar. J. 8. https://doi.org/10.1186/1475-2875-8-S2-S8

Howland, L.J., 1930. The nutrition of mosquito larvae, with special reference to their algal food. Bull. Entomol. Res. 21, 431–439. https://doi.org/10.1017/S0007485300024779

Jones, P.L., Pask, G.M., Rinker, D.C., Zwiebel, L.J., 2011. Functional agonism of insect odorant receptor ion channels. Proc. Natl. Acad. Sci. U. S. A. 108, 8821–8825. https://doi.org/10.1073/pnas.1102425108

Jones, W.D., Nguyen, T.A.T., Kloss, B., Lee, K.J., Vosshall, L.B., 2005. Functional conservation of an insect odorant receptor gene across 250 million years of evolution. Curr. Biol. https://doi.org/10.1016/j.cub.2005.02.007

Josling, G.A., Llinás, M., 2015. Sexual development in *Plasmodium* parasites: Knowing when it's time to commit. Nat. Rev. Microbiol. https://doi.org/10.1038/nrmicro3519

Kaupp, U.B., 2010. Olfactory signalling in vertebrates and insects: Differences and commonalities. Nat. Rev. Neurosci. https://doi.org/10.1038/nrn2789

Kendra, P.E., Montgomery, W.S., Mateo, D.M., Puche, H., Epsky, N.D., Heath, R.R., 2005. Effect of age on EAG response and attraction of female *Anastrepha suspensa* (Diptera: Tephritidae) to ammonia and carbon dioxide. Environ. Entomol. 34, 584–590. https://doi.org/10.1603/0046-225X-34.3.584

Klowden, M.J., 1995. Blood, sex, and the mosquito. Bioscience 45, 326–331. https://doi.org/10.2307/1312493

Kwon, H.W., Lu, T., Rützler, M., Zwiebel, L.J., 2006. Olfactory response in a gustatory organ of the malaria vector mosquito *Anopheles gambiae*. Proc. Natl. Acad. Sci. U. S. A. 103, 13526–13531. https://doi.org/10.1073/pnas.0601107103

Larsson, M.C., Domingos, A.I., Jones, W.D., Chiappe, M.E., Amrein, H., Vosshall, L.B., 2004. Or83b encodes a broadly expressed odorant receptor essential for *Drosophila* olfaction. Neuron 43, 703–714. https://doi.org/10.1016/j.neuron.2004.08.019

Larter, N.K., Sun, J.S., Carlson, J.R., 2016. Organization and function of *Drosophila* odorant binding proteins. Elife 5. https://doi.org/10.7554/eLife.20242

Laue, M., 2000. Immunolocalization of general odorant-binding protein in antennal

sensilla of moth caterpillars. Arthropod Struct. Dev. 29, 57–73. https://doi.org/10.1016/S1467-8039(00)00013-X

Leal, W.S., 2013. Odorant reception in insects: Roles of receptors, binding proteins, and degrading enzymes. Annu. Rev. Entomol. 58, 373–391. https://doi.org/10.1146/annurev-ento-120811-153635

Lehmann, T., Diabate, A., 2008. The molecular forms of *Anopheles gambiae*: A phenotypic perspective. Infect. Genet. Evol. 8, 737–746. https://doi.org/10.1016/j.meegid.2008.06.003

Leite, N.R., Krogh, R., Xu, W., Ishida, Y., Iulek, J., Leal, W.S., Oliva, G., 2009. Structure of an odorant-binding protein from the mosquito *Aedes aegypti* suggests a binding pocket covered by a pH-sensitive “lid.” PLoS One 4. https://doi.org/10.1371/journal.pone.0008006

Liu, F., Ye, Z., Baker, A., Sun, H., Zwiebel, L.J., 2020. Gene editing reveals obligate and modulatory components of the CO_2 receptor complex in the malaria vector mosquito, *Anopheles coluzzii*. Insect Biochem. Mol. Biol. 127. https://doi.org/10.1016/j.ibmb.2020.103470

Lu, T., Qiu, Y.T., Wang, G., Kwon, J.Y., Rutzler, M., Kwon, H.W., Pitts, R.J., van Loon, J.J.A., Takken, W., Carlson, J.R., Zwiebel, L.J., 2007. Odor coding in the maxillary palp of the malaria vector mosquito *Anopheles gambiae*. Curr. Biol. 17, 1533–1544. https://doi.org/10.1016/j.cub.2007.07.062

Ludewig, U., Neuhäuser, B., Dynowski, M., 2007. Molecular mechanisms of ammonium transport and accumulation in plants. FEBS Lett. https://doi.org/10.1016/j.febslet.2007.03.034

Lyimo, E.O., Takken, W., Koella, J.C., 1992. Effect of rearing temperature and larval density on larval survival, age at pupation and adult size of *Anopheles gambiae*. Entomol. Exp. Appl. 63, 265–271. https://doi.org/10.1111/j.1570-7458.1992.tb01583.x

Maïbèche-Coisne, M., Merlin, C., François, M.C., Queguiner, I., Porcheron, P., Jacquin-Joly, E., 2004. Putative odorant-degrading esterase cDNA from the moth *Mamestra brassicae*: Cloning and expression patterns in male and female antennae. Chem. Senses 29, 381–390. https://doi.org/10.1093/chemse/bjh039

Marquardt, W., 2004. Biology of disease vectors. Elsevier.

McIver, S., Siemicki, R., 1978. Fine structure of tarsal sensilla of *Aedes aegypti* (L.) (Diptera: Culicidae). J. Morphol. 155, 137–155. https://doi.org/10.1002/jmor.1051550202

McIver, S.B., 1982. Sensilla of Mosquitoes (Diptera: Culicidae)1, 2. J. Med. Entomol. 19, 489–535. https://doi.org/10.1093/jmedent/19.5.489

McMeniman, C.J., Corfas, R.A., Matthews, B.J., Ritchie, S.A., Vosshall, L.B., 2014. Multimodal integration of carbon dioxide and other sensory cues drives mosquito attraction to humans. Cell 156, 1060–1071. https://doi.org/10.1016/j.cell.2013.12.044

Meijerink, J., Braks, M.A.H., Van Loon, J.J.A., 2001. Olfactory receptors on the antennae of the malaria mosquito *Anopheles gambiae* are sensitive to ammonia and other sweat-borne components. J. Insect Physiol. 47, 455–464. https://doi.org/10.1016/S0022-1910(00)00136-0

Menuz, K., Larter, N.K., Park, J., Carlson, J.R., 2014. An RNA-seq screen of the

Drosophila antenna identifies a transporter necessary for ammonia detection. PLoS Genet. 10. https://doi.org/10.1371/journal.pgen.1004810

Min, S., Ai, M., Shin, S.A., Suh, G.S.B., 2013. Dedicated olfactory neurons mediating attraction behavior to ammonia and amines in *Drosophila*. Proc. Natl. Acad. Sci. U. S. A. 110, 1321–1329. https://doi.org/10.1073/pnas.1215680110

Montell, C., 2009. A taste of the *Drosophila* gustatory receptors. Curr. Opin. Neurobiol. https://doi.org/10.1016/j.conb.2009.07.001

Montell, C., Zwiebel, L.J., 2016. Mosquito sensory systems. Adv. In Insect Phys. 51, 293–328. https://doi.org/10.1016/bs.aiip.2016.04.007

Mozūraitis, R., Hajkazemian, M., Zawada, J.W., Szymczak, J., Pålsson, K., Sekar, V., Biryukova, I., Friedländer, M.R., Koekemoer, L.L., Baird, J.K., Borg-Karlson, A.K., Emami, S.N., 2020. Male swarming aggregation pheromones increase female attraction and mating success among multiple African malaria vector mosquito species. Nat. Ecol. Evol. 4, 1395–1401. https://doi.org/10.1038/s41559-020-1264-9

Mueller, A.K., Kohlhepp, F., Hammerschmidt, C., Michel, K., 2010. Invasion of mosquito salivary glands by malaria parasites: Prerequisites and defense strategies. Int. J. Parasitol. https://doi.org/10.1016/j.ijpara.2010.05.005

Mullen, G.R., Durden, L.A., 2018. Medical and veterinary entomology, Medical and Veterinary Entomology. https://doi.org/10.1016/C2017-0-00210-0

National Institutes of Health, 2021. Malaria parasite, mosquito, and human host [WWW Document]. URL https://www.niaid.nih.gov/diseases-conditions/malaria-parasite

Oliva, C.F., Benedict, M.Q., Lempérière, G., Gilles, J., 2011. Laboratory selection for an accelerated mosquito sexual development rate. Malar. J. 10.

https://doi.org/10.1186/1475-2875-10-135

Osta, M.A., Christophides, G.K., Kafatos, F.C., 2004. Effects of mosquito genes on *Plasmodium* development. Science (80-.). https://doi.org/10.1126/science.1091789

Papathanos, P.A., Bossin, H.C., Benedict, M.Q., Catteruccia, F., Malcolm, C.A., Alphey, L., Crisanti, A., 2009. Sex separation strategies: Past experience and new approaches. Malar. J. https://doi.org/10.1186/1475-2875-8-S2-S5

Pates, H.V., Takken, W., Stuke, K., Curtis, C.F., 2001. Differential behaviour of *Anopheles gambiae sensu stricto* (Diptera: Culicidae) to human and cow odours in the laboratory. Bull. Entomol. Res. 91, 289–296. https://doi.org/10.1079/ber200198

Pennetier, C., Warren, B., Dabiré, K.R., Russell, I.J., Gibson, G., 2010. “Singing on the wing” as a mechanism for species recognition in the malarial mosquito *Anopheles gambiae*. Curr. Biol. 20, 131–136. https://doi.org/10.1016/j.cub.2009.11.040

Pitts, R.J., Derryberry, S.L., Pulous, F.E., Zwiebel, L.J., 2014. Antennal-expressed ammonium transporters in the malaria vector mosquito *Anopheles gambiae*. PLoS One 9. https://doi.org/10.1371/journal.pone.0111858

Pitts, R.J., Derryberry, S.L., Zhang, Z., Zwiebel, L.J., 2017. Variant ionotropic receptors in the malaria vector mosquito *Anopheles gambiae* tuned to amines and carboxylic acids. Sci. Rep. 7. https://doi.org/10.1038/srep40297

Pitts, R.J., Fox, A.N., Zwiebeil, L.J., 2004. A highly conserved candidate chemoreceptor expressed in both olfactory and gustatory tissues in the malaria vector *Anopheles gambiae*. Proc. Natl. Acad. Sci. U. S. A. 101, 5058–5063. https://doi.org/10.1073/pnas.0308146101

Pitts, R.J., Zwiebel, L.J., 2006. Antennal sensilla of two female anopheline sibling

species with differing host ranges. Malar. J. 5. https://doi.org/10.1186/1475-2875-5-26

Potter, C.J., 2014. Stop the biting: Targeting a mosquito's sense of smell. Cell. https://doi.org/10.1016/j.cell.2014.02.003

Qiu, Y.T., van Loon, J.J.A., Takken, W., Meijerink, J., Smid, H.M., 2006. Olfactory coding in antennal neurons of the malaria mosquito, *Anopheles gambiae*. Chem. Senses 31, 845–863. https://doi.org/10.1093/chemse/bjl027

Raji, J.I., Melo, N., Castillo, J.S., Gonzalez, S., Saldana, V., Stensmyr, M.C., DeGennaro, M., 2019. *Aedes aegypti* mosquitoes detect acidic volatiles found in human odor using the Ir8a pathway. Curr. Biol. 29, 1253-1262.e7. https://doi.org/10.1016/j.cub.2019.02.045

Reidenbach, K.R., Cook, S., Bertone, M.A., Harbach, R.E., Wiegmann, B.M., Besansky, N.J., 2009. Phylogenetic analysis and temporal diversification of mosquitoes (Diptera: Culicidae) based on nuclear genes and morphology. BMC Evol. Biol. 9. https://doi.org/10.1186/1471-2148-9-298

Rytz, R., Croset, V., Benton, R., 2013. Ionotropic Receptors (IRs): Chemosensory ionotropic glutamate receptors in *Drosophila* and beyond. Insect Biochem. Mol. Biol. 43, 888–897. https://doi.org/10.1016/j.ibmb.2013.02.007

Sato, K., Pellegrino, M., Nakagawa, Takao, Nakagawa, Tatsuro, Vosshall, L.B., Touhara, K., 2008. Insect olfactory receptors are heteromeric ligand-gated ion channels. Nature 452, 1002–1006. https://doi.org/10.1038/nature06850

Saveer, A.M., Pitts, R.J., Ferguson, S.T., Zwiebel, L.J., 2018. Characterization of chemosensory responses on the labellum of the malaria vector mosquito,

Anopheles coluzzii. Sci. Rep. 8. https://doi.org/10.1038/s41598-018-23987-y

Shankar, S., Tauxe, G.M., Spikol, E.D., Li, M., Akbari, O.S., Giraldo, D., McMeniman, C.J., 2020. Synergistic coding of human odorants in the mosquito brain. bioRxiv. https://doi.org/10.1101/2020.11.02.365916

Sinka, M.E., Bangs, M.J., Manguin, S., Coetzee, M., Mbogo, C.M., Hemingway, J., Patil, A.P., Temperley, W.H., Gething, P.W., Kabaria, C.W., Okara, R.M., Van Boeckel, T., Godfray, H.C.J., Harbach, R.E., Hay, S.I., 2010. The dominant *Anopheles* vectors of human malaria in Africa, Europe and the Middle East: Occurrence data, distribution maps and bionomic précis. Parasites and Vectors 3. https://doi.org/10.1186/1756-3305-3-117

Smallegange, R.C., Qiu, Y.T., van Loon, J.A., Takken, W., 2005. Synergism between ammonia, lactic acid and carboxylic acids as kairomones in the host-seeking behaviour of the malaria mosquito *Anopheles gambiae sensu stricto* (Diptera: Culicidae). Chem. Senses 30, 145–152. https://doi.org/10.1093/chemse/bji010

Smallegange, R.C., Verhulst, N.O., Takken, W., 2011. Sweaty skin: An invitation to bite? Trends Parasitol. https://doi.org/10.1016/j.pt.2010.12.009

Soupene, E., Lee, H., Kustu, S., 2002. Ammonium/methylammonium transport (Amt) proteins facilitate diffusion of NH_3 bidirectionally. Proc. Natl. Acad. Sci. U. S. A. 99, 3926–3931. https://doi.org/10.1073/pnas.062043799

Suh, E., Bohbot, J.D., Zwiebel, L.J., 2014. Peripheral olfactory signaling in insects. Curr. Opin. Insect Sci. 6, 86–92. https://doi.org/10.1016/j.cois.2014.10.006

Sun, H., Liu, F., Ye, Z., Baker, A., Zwiebel, L.J., 2020. Mutagenesis of the orco odorant receptor co-receptor impairs olfactory function in the malaria vector *Anopheles*

coluzzii. Insect Biochem. Mol. Biol. 127. https://doi.org/10.1016/j.ibmb.2020.103497

Takken, W., Costantini, C., Dolo, G., Hassanali, A., Sagnon, N., Osir, E., 2006. Mosquito mating behaviour, in: Bridging Laboratory and Field Research for Genetic Control of Disease Vectors. pp. 183–188. https://doi.org/10.1007/1-4020-3799-6_17

Takken, W., Dekker, T., Wijnholds, Y.G., 1997. Odor-mediated flight behavior of *Anopheles gambiae* giles *sensu stricto* and *An. stephensi* liston in response to CO_2, acetone, and 1-octen-3-ol (Diptera: Culicidae). J. Insect Behav. 10, 395–407. https://doi.org/10.1007/BF02765606

Takken, W., Knols, B.G.J., 1999. Odor-mediated behavior of Afrotropical malaria mosquitoes. Annu. Rev. Entomol. 44, 131–157. https://doi.org/10.1146/annurev.ento.44.1.131

Task, D., Lin, C.C., Afify, A., Li, H., Vulpe, A., Menuz, K., Potter, C.J., 2020. Widespread polymodal chemosensory receptor expression in *Drosophila* olfactory neurons. bioRxiv. https://doi.org/10.1101/2020.11.07.355651

Tomas, A.M., Margos, G., Dimopoulos, G., Van Lin, L.H.M., De Koning-Ward, T.F., Sinha, R., Lupetti, P., Beetsma, A.L., Rodriguez, M.C., Karras, M., Hager, A., Mendoza, J., Butcher, G.A., Kafatos, F., Janse, C.J., Waters, A.P., Sinden, R.E., 2001. P25 and P28 proteins of the malaria ookinete surface have multiple and partially redundant functions. EMBO J. https://doi.org/10.1093/emboj/20.15.3975

Tsuji, N., Okazawa, T., Yamamura, N., 1990. Autogenous and anautogenous mosquitoes: a mathematical analysis of reproductive strategies. J. Med. Entomol. 27, 446–453. https://doi.org/10.1093/jmedent/27.4.446

Tuteja, R., 2007. Malaria - An overview. FEBS J. 274, 4670–4679. https://doi.org/10.1111/j.1742-4658.2007.05997.x

Van Breugel, F., Riffell, J., Fairhall, A., Dickinson, M.H., 2015. Mosquitoes use vision to associate odor plumes with thermal targets. Curr. Biol. 25, 2123–2129. https://doi.org/10.1016/j.cub.2015.06.046

Vosshall, L.B., Hansson, B.S., 2011. A unified nomenclature system for the insect olfactory coreceptor. Chem. Senses. https://doi.org/10.1093/chemse/bjr022

Wang, G., Carey, A.F., Carlson, J.R., Zwiebel, L.J., 2010. Molecular basis of odor coding in the malaria vector mosquito *Anopheles gambiae*. Proc. Natl. Acad. Sci. U. S. A. 107, 4418–4423. https://doi.org/10.1073/pnas.0913392107

Wheelwright, M., Whittle, C.R., Riabinina, O., 2021. Olfactory systems across mosquito species. Cell Tissue Res. 1–16. https://doi.org/10.1007/s00441-020-03407-2

World Health Organization, 2020. World Malaria Report: 20 years of global progress and challenges, World Health Organization.

Yaeger, R.G., 1996. Protozoa: Structure, classification, growth, and development, Medical Microbiology.

Yao, C.A., Ignell, R., Carlson, J.R., 2005. Chemosensory coding by neurons in the coeloconic sensilla of the *Drosophila* antenna. J. Neurosci. 25, 8359–8367. https://doi.org/10.1523/JNEUROSCI.2432-05.2005

Ye, Z., Liu, F., Liu, N., 2016. Olfactory responses of southern house mosquito, *Culex quinquefasciatus*, to human odorants. Chem. Senses 41, 441–447. https://doi.org/10.1093/chemse/bjv089

Younger, M.A., Herre, M., Ehrlich, A.R., Gong, Z., Gilbert, Z.N., Rahiel, S., Matthews,

B.J., Vosshall, L.B., 2020. Non-canonical odor coding ensures unbreakable mosquito attraction to humans. bioRxiv. https://doi.org/10.1101/2020.11.07.368720

Younus, F., Chertemps, T., Pearce, S.L., Pandey, G., Bozzolan, F., Coppin, C.W., Russell, R.J., Maïbèche-Coisne, M., Oakeshott, J.G., 2014. Identification of candidate odorant degrading gene/enzyme systems in the antennal transcriptome of *Drosophila melanogaster*. Insect Biochem. Mol. Biol. 53, 30–43. https://doi.org/10.1016/j.ibmb.2014.07.003

Zwiebel, L.J., Takken, W., 2004. Olfactory regulation of mosquito-host interactions. Insect Biochem. Mol. Biol. 34, 645–652. https://doi.org/10.1016/j.ibmb.2004.03.017

CHAPTER II

HETEROGENEOUS EXPRESSION OF THE AMMONIUM TRANSPORTER *ACAMT* IN CHEMOSENSORY APPENDAGES OF THE MALARIA VECTOR, *ANOPHELES COLUZZII*

Preface

The following chapter was published on *Insect Biochemistry and Molecular Biology* in 2020 (Volume 120, 103360). I was the first author on this paper along with Feng Liu (co-second author), Huahua Sun (co-second author), Mackenzie Barker (fourth author), R. Jason Pitts (fifth author), and Laurence J. Zwiebel (corresponding author). In this study, to employ the binary Q system for *AcAmt* localization, colleagues and I developed a transgenic platform and workflow in the lab to generate an *Anopheles AcAmt promoter-QF* drive line using phiC31 system. The drive line was further crossed to a *QUAS-GFP* effector line to achieve specific *AcAmt* localization in primary chemosensory appendages. Combining immunohistochemistry and fluorescence *in-situ* hybridization, we showed spatial expression pattern of *AcAmt* relative to Orco, Ir76b, and Gr15 in female adults and larvae. I played a leading role in experimental design, data acquisition, data analysis, and manuscript preparation. I want to thank Feng Liu for his electrophysiological supports, Huahua Sun and Mackenzie Barker for their efforts on fluorescence *in-situ* hybridization and immunohistochemistry, R. Jason Pitts and Laurence J. Zwiebel for their mentorship, experimental designs and acquisition of experimental reagents and equipment. The species name in the paper (*Anopheles*

gambiae) was modified to *Anopheles coluzzii* in this chapter to be consistent with the recent nomenclature (Coetzee et al., 2013).

Introduction

Mosquito vectors are responsible for the transmission of a variety of deadly human diseases, including dengue fever, yellow fever, Zika virus, West Nile virus, lymphatic filariasis, and malaria (Van Der Goes Van Naters and Carlson, 2006). In 2016, more than 200 million cases of human malaria occurred worldwide (Alonso and Noor, 2017). The malaria mosquito *Anopheles gambiae* is one of the primary vectors of the most prevalent malaria pathogen *Plasmodium falciparum* (Molina-Cruz et al., 2016; Report, 2007). Female mosquitoes ingest blood meals that are required for egg development and through which pathogens are vectored by *Anopheles* mosquitoes and transmitted between humans (Cox, 2010). Mosquitoes rely on their acute olfactory system to detect volatiles, including CO_2, ammonia, and other specific odors to locate humans and other mammals which represent potential blood meal hosts (Van Der Goes Van Naters and Carlson, 2006; Zwiebel and Takken, 2004).

In mosquitoes, the primary head appendages involved in odorant detection are the antennae, maxillary palps, and the labella of the proboscis. Dispersed along the surface of those appendages are hollow sensory hairs known as sensilla. A large variety of olfactory sensory neurons (OSNs) are housed in the sensilla and respond to distinct spectrums of odorants (Guidobaldi et al., 2014; Montell and Zwiebel, 2016). Based on the morphological features, olfactory sensilla are categorized as trichoid, basiconic (also known as grooved pegs), and coeloconic (Pitts and Zwiebel, 2006).

Although different functional subgroups are present within these classes of sensilla, grooved pegs are generally tuned to acids and amines, trichoid sensilla respond to a broader spectrum of odors (Qiu et al., 2006), while coeloconic sensilla have been associated with both chemo- and thermosensory pathways (McIver, 1973). Within chemosensory sensilla, OSNs are positioned in an aqueous lymph that fills the luminal space and contains odorant binding proteins (OBPs) and odorant-degrading enzymes (ODEs) and other components that are required for odorant recognition and clearage (Leal, 2013). On OSN dendritic membranes, several families of ligand-gated ion channels including odorant receptors (ORs), gustatory receptors (GRs) and ionotropic receptors (IRs), play central roles in olfactory signal transduction as they are activated by specific odorants to generate the action potentials representing peripheral odor coding (Suh et al., 2014).

Ammonia is a volatile component of mammalian sweat and electrophysiological studies have revealed a broad set of neuronal responses to ammonia in antennal trichoid sensilla and grooved pegs (Meijerink et al., 2001; Qiu et al., 2006). As a component of a hyper-effective five-compound mosquito blend, ammonia has been shown to attract female *An. gambiae* (Boverhof et al., 2008; Mukabana et al., 2012; Smallegange et al., 2005, 2002). While studies in *D. melanogaster* have suggested DmIr92a is a functional ammonia receptor, little is known about the molecular and indeed the neuronal receptors responsible for ammonia detection in mosquitoes (Benton et al., 2009; Min et al., 2013), especially as no clear homologs of DmIr92a are encoded in mosquito genomes.

Nitrogen is essential for the survival of mosquitoes and indeed all living organisms and ammonium is the principal ionic target for its fixation and subsequent incorporation into biological molecules. At the same time, ammonia is toxic when it accumulates, which makes it critical for cells to have efficient mechanisms for the uptake and transport of ammonium (Bittsánszky et al., 2015; Crawford and Forde, 2002). Because ammonium is not able to penetrate the cell membrane passively, ammonium transport proteins, including ammonium transporters (Amts), methylammonium/ammonium permeases (Meps), and Rhesus (Rh) proteins, facilitate the cross-membrane transportation of ammonium (Andrade and Einsle, 2007). Recently, several groups have reported the characterization of antennal-expressed Amt proteins in both *Drosophila* and *Anopheles* (Menuz et al., 2014; Pitts et al., 2014a).

In *D. melanogaster, DmAmt* has been shown to be directly involved in ammonia detection as null mutants show significantly reduced olfactory responses to ammonia than the wild type (Menuz et al., 2014). Localization of *DmAmt* in the fruit fly antennae revealed that it is expressed in the auxiliary cells surrounding ammonia sensitive neurons, suggesting that DmAmt is not the receptor/sensor but rather is involved in ammonium clearance from the sensillar lymph (Menuz et al., 2014). This finding suggests that DmAmt's role is to prevent DmIr92a from being prematurely desensitized by the accumulation of environmental (sensory) ammonia or ammonia otherwise produced by cellular metabolism (Menuz et al., 2014; Trussell and Fischbach, 1989). In *Aedes aegypti*, the reduced expression of *AeAmt1* caused accumulation of ammonium in the mosquito larval hemolymph which suggested its role in ammonium excretion (Chasiotis et al., 2016). In *An. coluzzii*, while the functional role of AcAmt in

mediating antennal ammonia sensitivity remains unclear, its transcripts are highly abundant in female antennae and have been functionally shown to modulate ammonium cross-membrane transportation using *Xenopus* heterogeneous expression system (Pitts et al., 2014a). In addition, *Anopheles Amt* was shown to phenotypically rescue the defect of ammonia responses in *DmAmt* mutants (Menuz et al., 2014).
In order to better understand the role of *AcAmt* in ammonia detection in *An. coluzzii*, we now have characterized its tissue and cellular localization utilizing several advanced transgenic tools, including the newly developed “Q system” (Potter et al., 2010). The comprehensive cellular localization of *AcAmt* in the chemosensory system of larval and adult-stage *An. coluzzii* informs our understanding of the role of this transporter in host-seeking and other important behaviors.

Material and Methods

Mosquito Maintenance

An. coluzzii phiC31 docking line E was acquired from The Malaria Research and Reference Reagent Resource Center (Meredith et al., 2011). *An. coluzzii* effector line (*QUAS-mCD8:GFP*) was a generous gift from the lab of Dr. C. Potter at The Johns Hopkins University School of Medicine (Riabinina et al., 2016). All the mosquito lines were reared at 27°C, 75% relative humidity under a 12:12 light-dark cycle and supplied with 10% sugar water in the Vanderbilt University Insectary.

AcAmt promoter-QF2 construct

The 1kb/3kb *AcAmt* upstream sequence was amplified from the wild type *An. coluzzii* genomic DNA using the forward primers (AcAmt_1kb_F: 5'- AAT CCG GAA CAA GCA TCA TCA GAG CGA T -3'; AcAmt_3kb_F: 5'- AAT CCG GAC CCA AGT AAT TAA GTA GTG CT -3') and the reverse primer AcAmt _R (5'- AAG GCG CGC CTG CAG TGC TAA TCA AAC CAA C -3'). The 1kb/3kb *AcAmt promoter* (*AcAmtP*) amplicons were restriction enzyme digested and inserted into the BspEI/AscI restriction site on a pBattB-DsRed construct. Likewise, the *QF2* sequence was sequentially amplified from the pXL-BACII-DsRed-QF2-hsp70 construct (Riabinina et al., 2016) using the primer pair QF2for (5'- AAG GCC GGC CAT GCC ACC CAA GCG CAA AAC-3') and QF2rev (5'- AAG CGA TCG CTC ACT GTT CGT ATG TAT TAA TG- 3') and inserted into the FseI/AsiSi restriction site which is downstream of the *AcAmtP* insertion site.

Mosquito Transgenics

The detailed microinjection protocol was described previously (Pondeville et al., 2014). Briefly, newly laid (approximately 1hr-old) embryos of the phiC31 docking line (Meredith et al., 2011) were immediately collected and aligned on a filter paper moistened with 25mM sodium chloride solution. All the embryos were fixed on a coverslip with double-sided tape and a drop of halocarbon oil 27 was applied to cover the embryos. The coverslip was further fixed on a slide under a Zeiss Axiovert 35 microscope with a 40X objective. The microinjection was performed using Eppendorf FemtoJet 5247 and quartz needles (Sutter Instrument, Novato, CA). The phiC31 integrase was provided by the pENTR R4-vas2-integrase-R3 helper plasmid (a kind gift

from Eric Marois via Addgene plasmid #62299) which was diluted to 200ng/µl in 1x microinjection buffer (5mM KCl, 0.1mM sodium phosphate buffer, pH7.2) before being co-injected with the pBattB-DsRed-AcAmtP-QF2 plasmid at 400ng/µl. The injected embryos were placed into deionized water with artificial sea salt (0.3g/L) and reared in the lab condition.

First generation (G_0) of injected adults were separated based on gender and crossed to 5X phiC31 docking line gender counterparts. Their offspring (F_1) was screened for DsRed-derived red eye fluorescence. Red-eyed F_1 males were individually crossed to 5X docking line females to establish a stable transgenic line. PCR analyses of all individuals were performed (after mating) to validate phiC31 integration using the primer pairs attR_F (5'- TCA AAC TAA GGC GGA GTG G -3') and attR_R (5'- GAT GGG TGA GGT GGA GTA CG -3'); attL_F (5'- GAG GTC GAC GAT GTA GGT CAC -3') and attL_R (5'- ACC TTT TCT CCC TTG CTA CTG AC -3') that covers the junctions between the integrated and endogenous sequences (Meredith et al., 2011). The presence of *1kb/3kb AcAmtP-QF2* sequences was PCR validated using primers 1kb_F (5'- GCC ATC CAA CTC ACC ACA CA -3'), 3kb_F (5'- CGG CAA AAG AAG GGT TTC GG -3'), and QF_R (5'- CAG GGT CGT AGT TGT GGG TC -3').

Whole-mount Appendage Imaging

Because the driver line was not homozygous, all the offspring from the cross between the *AcAmtP-QF2* driver line and the *QUAS-mCD8:GFP* effector line (Riabinina et al., 2016) were collected and screened for the presence of DsRed in the eye. Whole antennae from adult females and larvae were thereafter dissected into 4%

formaldehyde in PBST (0.1% Triton X-100 in PBS) and fixed on ice for 30mins. Samples were washed 3X in PBST for 10mins each and transferred onto slides and mounted in Vectashield fluorescent medium (Vector Laboratories, Burlingame, CA).

Immunocytochemistry

Antibody staining was performed as previously (Pitts et al., 2004) with minor modifications. Antennae, labella, maxillary palps, and tarsi were dissected into 4% formaldehyde in PBST and fixed on ice for 30mins. Samples were wash 3X in PBST for 10mins each and then embedded in TFM Tissue Freezing Medium (General Data Company Inc., Cincinnati, OH). Cryosections were obtained at -20°C with a CM1900 cryostat (Leica Microsystems, Bannockburn, IL). Samples were sectioned at ~10μm and transferred onto Superfrost plus slides (VWR Scientific, Radnor, PA). Slides were air-dried at room temperature (RT) for 30mins and fixed in 4% formaldehyde in PBST for 10mins, followed by 3X rinsing in PBST for 10mins each. Thereafter, 5% normal goat serum (Sigma-Aldrich, St. Louis, MO) in PBST was applied and the slides were blocked in dark at RT for 1hr with HybriWell sealing chambers (Grace Bio-Labs, Bend, OR). Primary antibody (Rabbit α-Orco/Goat α-HRP-Cy3) was diluted 1:500 in 5% normal goat serum in PBST and applied on the slides and incubated overnight at 4°C.
After primary antibody staining, slides were washed 3X in PBST for 10mins each and stained with secondary antibody Goat α-Rabbit-Cy3 (Jackson ImmunoResearch, West Grove, PA) 1:500 in 5% normal goat serum PBST for 2hrs at RT and then rinsed 3X. Nuclei were stained with 300nM DAPI (Invitrogen, Carlsbad, CA) at RT for 10mins. Slides were briefly washed and mounted in Vectashield fluorescent medium (Vector

Laboratories, Burlingame, CA). α-HRP-Cy3 staining was directly visualized without the use of secondary antibody.

The whole-mount larval antennae were dissected into 4% formaldehyde in PBST and fixed on ice for 30mins. Samples were washed 3X in PBST for 10mins each and blocked with 5% normal goat serum (Sigma-Aldrich, St. Louis, MO) in PBST overnight at 4°C. Then 1:500 primary antibody (Rabbit α-Orco/Goat α-HRP-Cy3) was added and the samples were incubated overnight at 4°C. After primary antibody staining, samples were washed 3X in PBST for 10mins each and stained with secondary antibody Goat α-Rabbit-Cy3 (Jackson ImmunoResearch, West Grove, PA) 1:500 in 5% normal goat serum PBST overnight at 4°C and then rinsed 3X. Nuclei were stained with 300nM DAPI (Invitrogen, Carlsbad, CA) at 4°C for 1hr. Samples were transferred onto the slides and mounted in Vectashield fluorescent medium (Vector Laboratories, Burlingame, CA). α-HRP-Cy3 staining was directly visualized without the use of secondary antibody.

Fluorescence In-situ Hybridization (FISH)

The TOPO-TA dual promoter vector (Invitrogen, Carlsbad, CA) was used to subclone full length *AcIr76b* as described in the previous study (Pitts et al., 2017). Similarly, the full length *AcGr15* coding sequence was cloned into the TOPO-TA dual promoter vector and verified by DNA sequence analysis. Antisense/sense probes were thereafter synthesized using SP6/T7 RNA polymerase (NEB, Ipswich, MA) with Digoxigenin (DIG) RNA Labeling Kit (Roche, Switzerland).

Antennal samples were sectioned and fixed as described above. Sequentially, the slides were incubated in acetylation solution (0.1M triethanolamine, 0.65% HCl, 0.375% acetic anhydride) for 10mins at RT. After being washed 3X in PBST, slides were incubated in pre-heated (65°C) hybridization buffer (50% deionized formamide, 5X saline sodium citrate (SSC), 50µg/mL heparin sodium salt, 0.1% tween-20) for 40mins at RT. RNA probes were diluted in the hybridization buffer at 500ng/mL and applied onto the slides which were further incubated with sealing chambers at 65°C for 18hrs. Following the hybridization, slides were washed 3X in 0.2X SSC at 65°C for 20mins each and then placed in TNT buffer (0.1M Tris-HCl, 150mM NaCl, 0.05%Tween-20) at RT for 10mins. TNB buffer (0.1M Tris-HCl, 150mM NaCl, 0.05%Tween-20, 1% blocking reagent from PerkinElmer) was subsequently applied to the slides for blocking for 1hr at RT inside sealed hybridization chambers. Due to the extreme overnight incubation temperature of FISH (65°C) that bleached the fluorescence of GFP, the GFP signal was recovered using GFP antibody (α-GFP) after the FISH experiment. Primary antibodies including 1:200 Chicken α-GFP (Vanderbilt Antibody and Protein Resource) and 1:500 Sheep α-DIG-POD (Roche, Switzerland) in TNB were applied to the slides which were thereafter incubated at 4°C overnight. After washing (3X) in TNT at RT for 5mins each, secondary antibody (1:1000 Donkey α-Chicken-Alexa488; Jackson ImmunoResearch, West Grove, PA) in 5% normal donkey serum TNT was applied to the slides which were incubated for 2hrs at RT. The slides were subsequently washed 3X in TNT at RT for 5mins each. TSA-Cy3 amplification (PerkinElmer, Waltham, MA) was performed according to the manufacturer's instructions at 1:50 in amplification working buffer at

dark, following by 3X washing in TNT for 5mins each and mounting in Vectashield fluorescent medium (Vector Laboratories, Burlingame, CA).

Confocal Microscopy

Confocal microscopy images at 1024*1024 pixel resolution were collected on an Olympus FV-1000 equipped with a 100X oil objective at the Vanderbilt University Cell Imaging Shared Resource Core. Lasers wavelengths of 405nm, 488nm, and 543nm were used to detect DAPI, GFP, and Cy3, respectively.

Electrophysiology

Single sensillum recording (SSR) were carried out as previously described (Liu et al., 2013) with minor modifications. Mated female mosquitoes (4-10 days after eclosion) were mounted on a microscope slide (76 × 26 mm) (Ghaninia et al., 2007). The antennae were fixed using double-sided tape to a cover slip resting on a small bead of dental wax to facilitate manipulation and the cover slip was placed at approximately 30 degrees to the mosquito head. Once mounted, the specimen was placed under an Olympus BX51WI microscope and the antennae viewed at high magnification (1000×). Two tungsten microelectrodes were sharpened in 10% KNO2 at 10 V. The grounded reference electrode was inserted into the compound eye of the mosquito using a WPI micromanipulator and the recording electrode was connected to the preamplifier (10×, Syntech) and inserted into the shaft of the olfactory sensillum to complete the electrical circuit to extracellularly record OSN potentials (Den Otter et al., 1980). Controlled manipulation of the recording electrode was performed using a Burleigh

micromanipulator (Model PCS6000). The preamplifier was connected to an analog to digital signal converter (IDAC-4, Syntech), which in turn was connected to a computer for signal recording and visualization.

Ammonium hydroxide (Sigma-Aldrich, St. Louis, MO) was serially diluted (in water) to 0.01%, 0.05%, 0.1%, 0.5%, 1%, and 5% ammonia solutions. For each concentration, a 10μl aliquot was applied onto a filter paper (3 × 10mm) which was then inserted into a Pasteur pipette to create the stimulus cartridge. A sample containing the solvent (water) alone served as the control. The airflow across the antennae was maintained at a constant 20 ml/s throughout the experiment. Purified and humidified air was delivered to the preparation through a glass tube (10-mm inner diameter) perforated by a small hole 10cm away from the end of the tube into which the tip of the Pasteur pipette could be inserted. The stimulus was delivered to the sensilla by inserting the tip of the stimulus cartridge into this hole and diverting a portion of the air stream (0.5L/min) to flow through the stimulus cartridge for 500ms using a stimulus controller (Syntech). The distance between the end of the glass tube and the antennae was $\leqslant$1cm. Signals were recorded for 10s starting 1 second before stimulation, and the action potentials were counted off-line over a 500ms period before and after stimulation. Spike rates observed during the 500ms stimulation were subtracted from the spontaneous activities observed in the preceding 500ms and counts recorded in units of spikes/s.

Results

Generation of AcAmtP-QF2 Driver Line

Significant efforts to directly localize AcAmt protein or *AcAmt*-derived transcripts proved unsuccessful due to the paucity of specific immunological reagents and riboprobes. To address this deficit, the “Q” binary expression system recently brought to *An. coluzzii* (Riabinina et al., 2016) was utilized to indirectly visualize *AcAmt* expression. Here an *AcAmtP-QF2* driver line was generated and subsequently crossed to a *QUAS-mCD8:GFP* effector line to generate *AcAmtP-QF2*, *QUAS-mCD8:GFP* progeny lines. In this way, *AcAmtP* elements regulate the expression of *QF2* which in turn binds to *QUAS* elements to robustly drive the expression of visible *mCD8:GFP* markers to indirectly reveal the likely sites of *AcAmt* expression. Inasmuch as subsequent studies rely on these indirect binary markers, we acknowledge the inherent caveats of this system in our characterization of *AcAmt* expression.

Injected construct	Injected embryos	Survived adults	Founders
pBattB-DsRed-1kb AcAmtP-QF2	1176	14 males 13 females	≥ 7.4% (2/27)
pBattB-DsRed-3kb AcAmtP-QF2	572	5 females	≥ 20% (1/5)

Table 1. Details of embryo microinjection and the efficiency of phiC31 integration. The survived adults were pooled and crossed to the docking line opposite gender mosquitoes, and therefore the number of founders is the minimum.

To begin with we took advantage of the site-specific integration phiC31 system to generate a driver line by integrating the *AcAmtP-QF2* construct into a pre-defined

genomic site (Meredith et al., 2011). Because of our imprecise understanding of the all the features of the *AcAmtP*, we initially chose to incorporate 1kb and 3kb upstream sequences from the *AcAmt* start codon as potential *AcAmt* regulatory sequences to generate two independent transgenic driver lines (1kb/3kb *AcAmtP-QF2* drivers). Microinjection of preblastoderm embryos was used to deliver the *AcAmtP-QF2* construct containing an *attB* attachment site and a *3xP3-DsRed* marker (pBattB-*DsRed*-1kb/3kb *AcAmtP-QF2*) along with a phiC31 integrase encoding helper plasmid

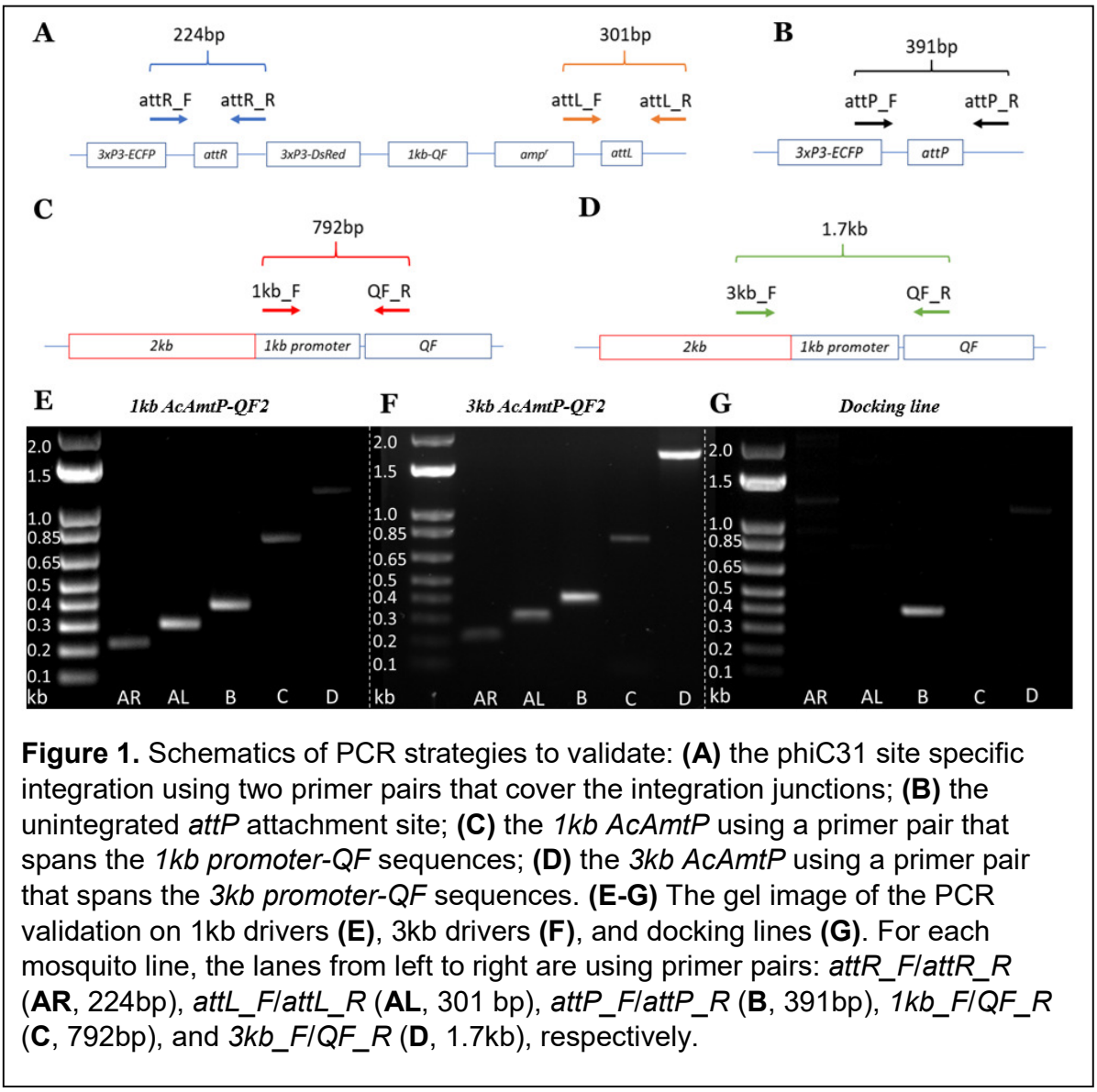

Figure 1. Schematics of PCR strategies to validate: **(A)** the phiC31 site specific integration using two primer pairs that cover the integration junctions; **(B)** the unintegrated *attP* attachment site; **(C)** the *1kb AcAmtP* using a primer pair that spans the *1kb promoter-QF* sequences; **(D)** the *3kb AcAmtP* using a primer pair that spans the *3kb promoter-QF* sequences. **(E-G)** The gel image of the PCR validation on 1kb drivers **(E)**, 3kb drivers **(F)**, and docking lines **(G)**. For each mosquito line, the lanes from left to right are using primer pairs: *attR_F*/*attR_R* (**AR**, 224bp), *attL_F*/*attL_R* (**AL**, 301 bp), *attP_F*/*attP_R* (**B**, 391bp), *1kb_F*/*QF_R* (**C**, 792bp), and *3kb_F*/*QF_R* (**D**, 1.7kb), respectively.

regulated by the vasa2 promoter to induce the integration in germ cells (**Table 1**). Individual males with red fluorescence in the eye and ventral nerve cord fluorescence were crossed to docking line females to establish transgenic lines. The successful integration was confirmed using genomic DNA PCR to show amplicons that cover the junctions between the endogenous and integrated sequences (**Figure 1A-1G**).

Specific AcAmt Localization Driven by the "Q system"

We first examined whole-mount female antennal samples of both the 1kb/3kb *AcAmtP-GFP* progeny where *AcAmtP*-driven expression was specific to the grooved pegs and coeloconic sensilla (1kb *AcAmtP-GFP*: **Figure 2A, 2B;** 3kb *AcAmtP-GFP*: **Figure 2C, 2D**). Importantly, except for the nonspecific expression inherent to the effector line (Riabinina et al., 2016), no *GFP* expression was observed in chemosensory appendages in either parental strain (**Figure S1**).

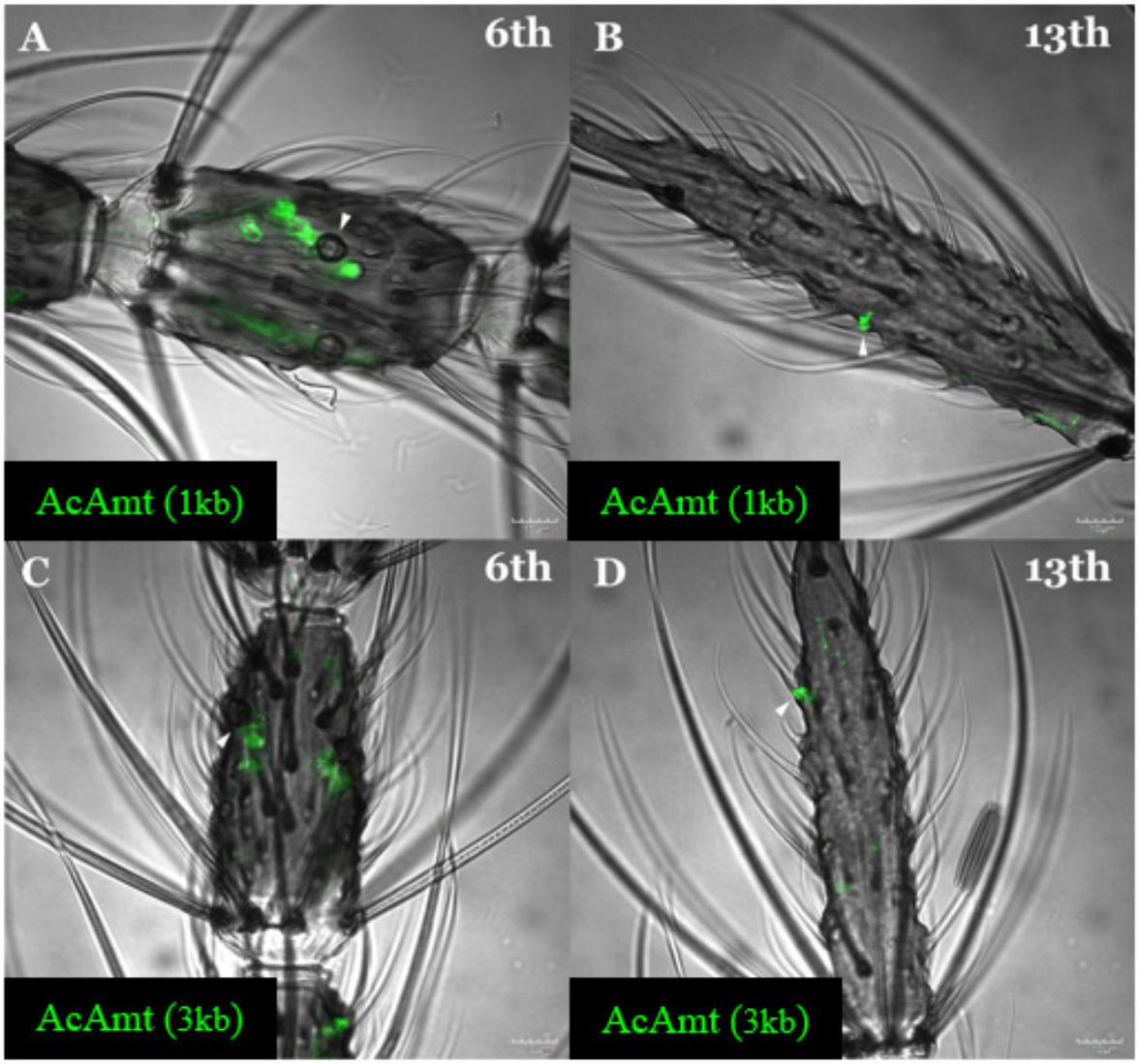

Figure 2. The confocal optical section of the whole-mount female *An. coluzzii* antennae carrying *QUAS-GFP* and either *1kb AcAmtP-QF2* (**A, B**; green) or *3kb AcAmtP-QF2* (**C, D**; green) constructs showing specific expression of *GFP* in coeloconic sensilla on the 6th flagellomere (**A, C**) and grooved pegs on the 13th flagellomere (**B, D**). Sensilla are highlighted with white arrows. Scale bars = 10μm.

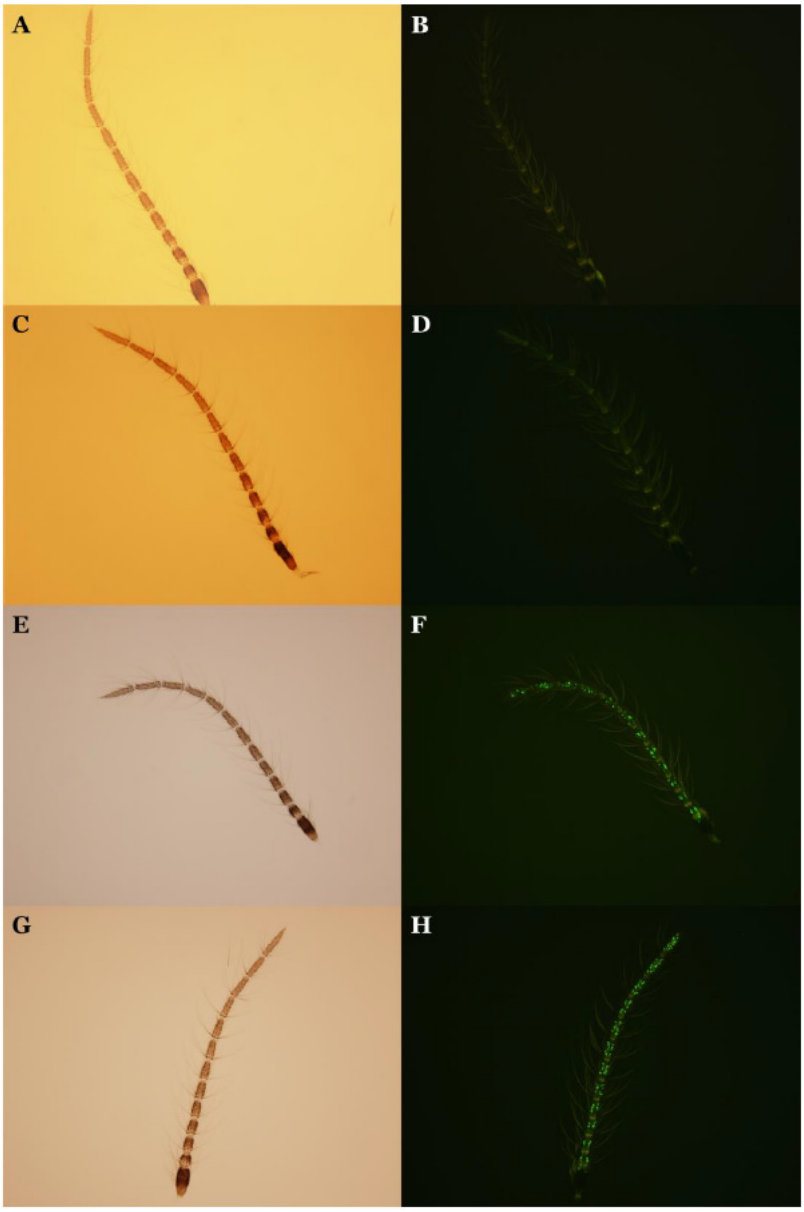

Figure S1. The *An. coluzzii* female antenna from the 1kb driver line under bright field **(A)** and GFP fluorescence filter **(B)**; Effector line female antenna under bright field **(C)** and GFP fluorescence filter **(D)**; 1kb *AcAmt-GFP* progeny antenna under bright field **(E)** and GFP fluorescence filter **(F)**; 3kb *AcAmt-GFP* progeny antenna under bright field **(G)** and GFP fluorescence filter **(H)**.

Flagellomere	1kb Repeat1	1kb Repeat2	1kb Repeat3	3kb Repeat1	3kb Repeat2	3kb Repeat3
2	0	0	0	0	0	0/1
3	1/1	0	0	0	1/1	0
4	1/1	3/3	1/1	3/3	1/1	1/2
5	2/2	3/3	2/2	3/3	3/3	3/3
6	3/3	2/2	2/2	4/5	4/4	5/6
7	5/5	5/5	3/3	5/5	1/1	3/3
8	3/3	6/6	4/4	4/4	4/4	5/5
9	5/5	5/5	6/7	7/7	5/5	5/5
10	4/4	6/6	7/7	7/7	6/6	5/5
11	3/3	6/6	8/8	7/7	9/9	7/7
12	8/8	8/8	10/10	9/9	7/8	9/9
13	4/4	7/7	9/9	10/10	8/8	9/9

Table S1. The comparison table of GFP-labelled female grooved pegs on antennal flagellomere 2nd to 13th between the 1kb and 3kb *AcAmtP-GFP* progeny. Each column presents data from a single antenna sample (n=3). The results are shown as: the number of GFP-labelled sensilla/the number of total sensilla in the view.

Flagellomere	1kb Repeat1	1kb Repeat2	1kb Repeat3	3kb Repeat1	3kb Repeat2	3kb Repeat3
2	3/3	3/3	5/5	1/1	2/2	2/2
3	4/4	4/4	3/3	3/3	3/3	5/5
4	1/1	1/1	4/4	2/2	3/3	4/4
5	3/3	3/3	3/3	2/2	3/3	2/2
6	3/3	3/3	3/3	2/2	2/2	3/3
7	2/2	2/2	2/2	2/2	2/2	2/2
8	1/1	1/1	1/1	0	0	1/1
9	1/1	1/1	0	0	0	1/1

Table S2. The comparison table of GFP-labelled female coeloconic sensilla on antennal flagellomere 2nd to 9th between the 1kb and 3kb *AcAmtP-GFP* progeny. Each column presents data from a single antenna sample (n=3). The results are shown as: the number of GFP-labelled sensilla/the number of total sensilla in the view. All coeloconic sensilla are GFP-labelled in both 1kb and 3kb *AcAmtP-GFP* progeny.

While *AcAmtP*-driven *GFP* is expressed in all coeloconic sensilla, it was only observed in a subset of grooved pegs. In order to assess the relative *GFP* expression patterns of both these lines, the total number of GFP-labelled grooved pegs (**Table S1 & Figure S2A**) and coeloconic sensilla (**Table S2 & Figure S2B**) were counted and compared between the 1kb *AcAmtP-GFP* progeny and the 3kb *AcAmtP-GFP* progeny. These quantitative data suggest there is no significant difference between the percentage of GFP-labelled grooved pegs (**Table S3**; p-value = 0.1061) in the 1kb

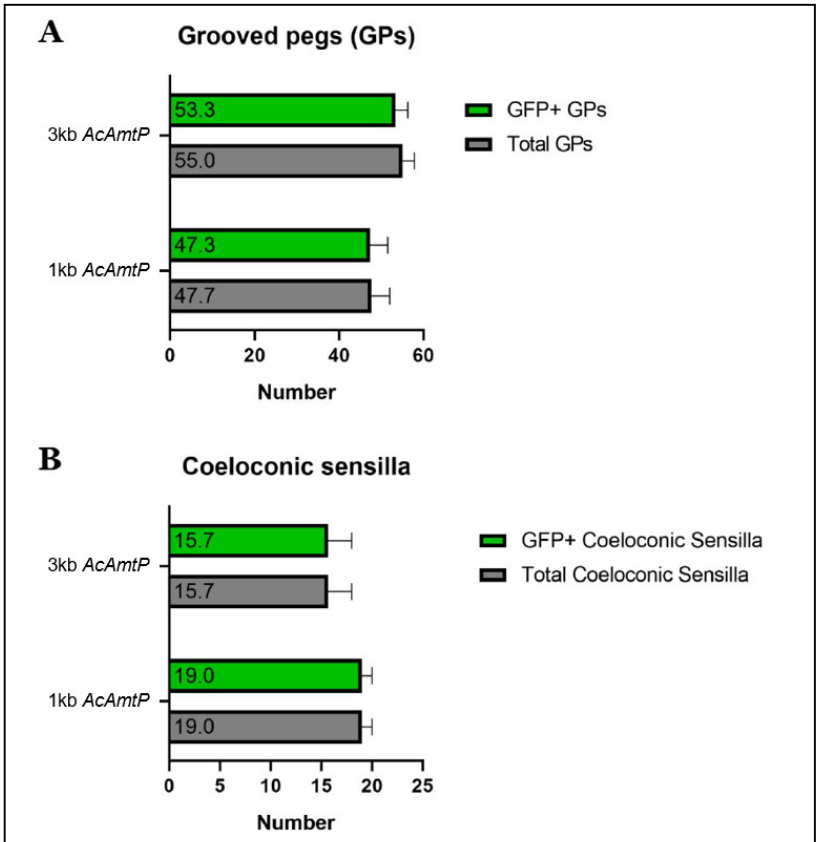

Figure S2. (A) The means of the number of GFP-labelled (GFP+) female grooved pegs (GPs) and the total number of GPs in the view under the regulation of 1kb and 3kb *AcAmtP* (n=3). **(B)** The means of the number of GFP-labelled (GFP+) female coeloconic sensilla and the total number of coeloconic sensilla in the view under the regulation of 1kb and 3kb *AcAmtP* (n=3). Error bars = Standard error of the mean.

(99.30% as the observed percentage in the statistical test) and 3kb (96.97% as the expected percentage in the statistical test) *AcAmtP-GFP* progeny. This suggests that the major regulatory elements that comprise the *AcAmtP* are likely to be contained within the region that is 1kb upstream from the start codon. However, inasmuch as this comparison was not based on cellular expression, we appreciate that there may still be subtle GFP signal expression/intensity differences between the two lines. Nevertheless,

in the absence of significant expression differences, all studies were henceforth carried out using the 1kb *AcAmtP-GFP* progeny.

	1kb	3kb
GFP+ grooved pegs	142	160
GFP- grooved pegs	1	5

Table S3. The contingency table of collective number of GFP-labelled (GFP+) and non-GFP-labelled (GFP-) grooved pegs in 1kb and 3kb *AcAmtP-GFP* progeny (Chi-square goodness of fit test p-value = 0.1061).

Heterogeneous AcAmt Expression in Olfactory Appendages

We first investigated whether *AcAmt* is expressed in non-neuronal auxiliary cells where, as was observed for *DmAmt* (Menuz et al., 2014) it might function in clearing ammonium from the sensillar lymph. Neurons were labelled using a horseradish peroxidase antibody (α-HRP-Cy3), which has been previously used as a general neuronal marker in *Drosophila* and mosquitoes (Jan and Jan, 1982; Loesel et al., 2006; Pitts et al., 2004). An examination of female antennal cryosections revealed that *AcAmtP*-driven *GFP* is expressed in both neuronal and non-neuronal cells across multiple flagellomeres on antennae (**Figure 3A-3D**). Z-axis projections of whole-mount antennal images revealed both coeloconic sensilla and grooved pegs are innervated with likely *AcAmt*-expressing neurons (**Figure 3E-3H**). Here, we observed characteristically distinct cellular morphology between *AcAmtP*-driven GFP labelled neurons and auxiliary cells. While the likely *AcAmt*-expressing neuron cell bodies are typically circular, the shapes of the non-neuronal cells are more irregular, consistent with the expected morphology of thecogen, tormogen, and trichogen sensillar auxiliary cells (McIver, 1982; Shanbhag et al., 2000). In some instances, a partial overlap

between *AcAmt* and α-HRP labelling was observed, which might be due to cell stacking on the z-axis. This also supports a close association between potentially *AcAmt*-expressing auxiliary cells and sensory neurons (**Figure 3I-3L**).

Immunohistochemistry and fluorescence *in-situ* hybridization (FISH) were used to further investigate the relationship between *AcAmt* and discrete sets of chemosensory receptors to discriminate subclasses of chemosensory neurons. In these studies,

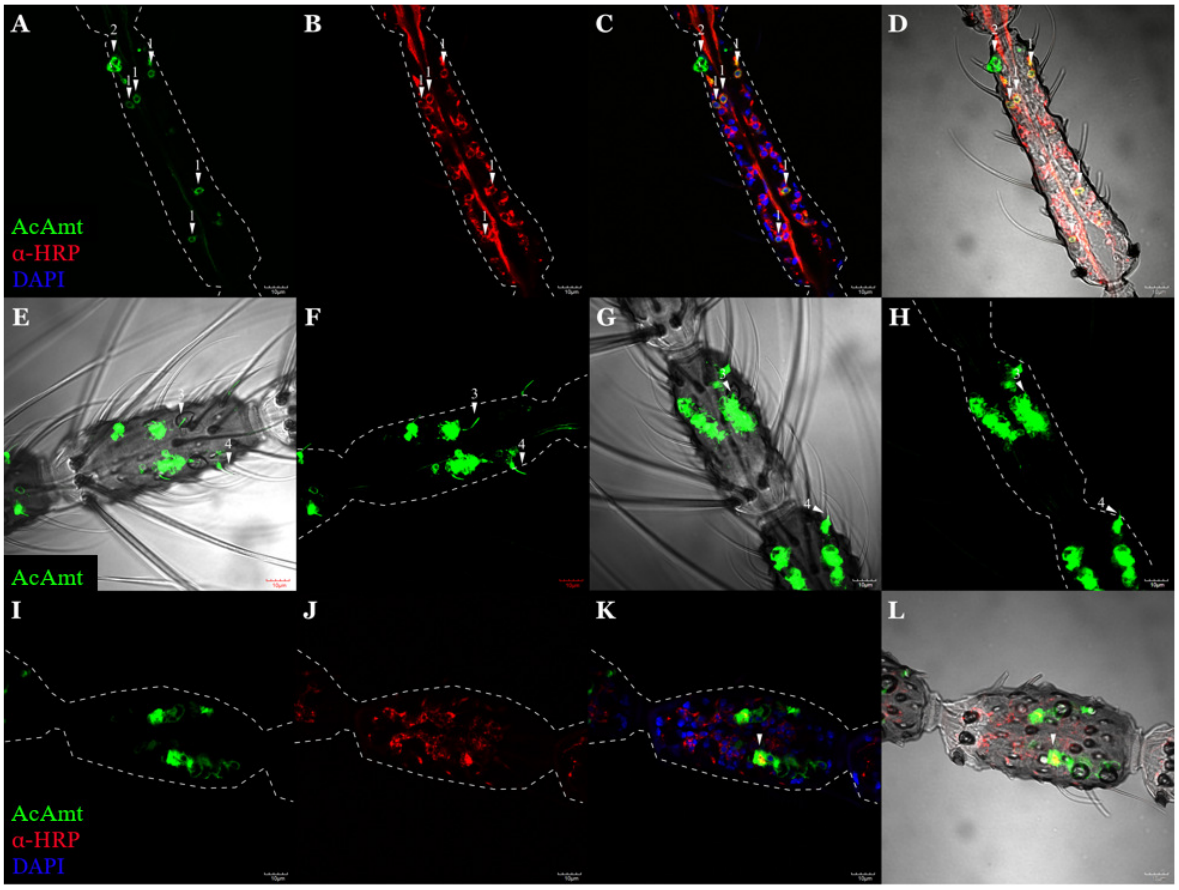

Figure 3. The confocal optical section of immunohistochemistry staining on the female antennae using α-HRP (red) showing *AcAmtP*-driven *GFP* (green) is expressed in both neuronal (arrow 1) and non-neuronal cells (arrow 2) (**A-D**). Z-axis projection of the whole-mount antennal female *An. coluzzii* 6th flagellomere showing *AcAmt* dendritic labelling in coeloconic sensilla (arrow 3) and grooved pegs (arrow 4) of 1kb *AcAmtP-GFP* progeny (**E, F**) and 3kb *AcAmtP-GFP* progeny (**G, H**). The confocal optical section showing a partial overlapping between GFP and α-HRP labeled cells (**I-L**). Scale bars = 10μm.

polyclonal antibodies to the Anopheline orthologs of the OR co-receptor (AcOrco) and riboprobes to the IR co-receptor (AcIr76b) allowed us to label antennal odorant receptor neurons (ORNs) (Pitts et al., 2004) and ionotropic receptor neurons (IRNs) independently (Pitts et al., 2017). We elected to focus on *AcIr76b* as its homolog in *Drosophila* is expressed in the same neurons as the ammonia receptor, *DmIr92a* (Benton et al., 2009). These studies revealed neither co-localization nor a close

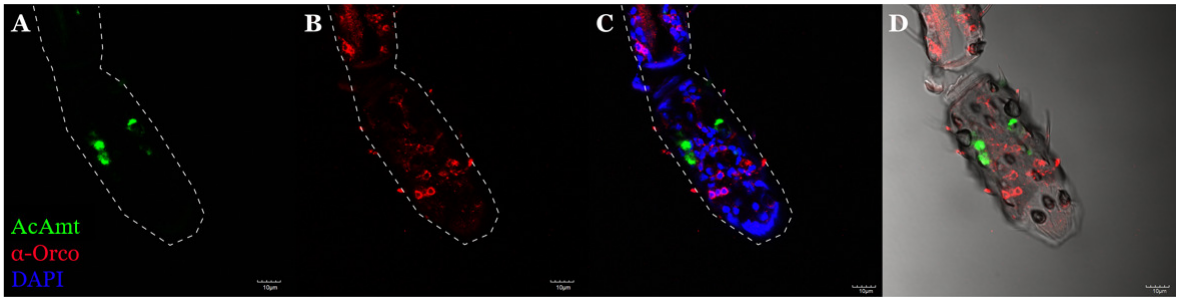

Figure 4. A representative confocal optical section from adult *An. coluzzii* female antennae immunohistochemically stained using α-Orco antibodies (red) showing that *AcAmtP*-driven *GFP* (green) and *Orco* are expressed in distinct cells (**A-D**). Scale bars = 10μm.

association between *AcAmt*- and *Orco*-expressing cells (**Figure 4A-4D**), while *AcIr76b* antisense riboprobes shows a close association between *Ir76b*-expressing IRNs and potentially *AcAmt*-expressing auxiliary cells (**Figure 5A, 5B**). Taken together, these data suggest that *AcAmt* is likely to be expressed in auxiliary cells surrounding *IR*-expressing IRNs. As a negative control, *AcIr76b* sense riboprobes failed to label any cells or structures other than the antennal cuticle (**Figure 5C, 5D**). Surprisingly, in contrast to the labelling studies of the antennae, *AcAmtP*-driven GFP signals were co-localized with a discrete subset of *Orco*-expressing ORNs in the female maxillary palps where only a very small portion of ORNs (approximately less than 5%) were likely to be *AcAmt*-positive (**Figure 6A-6C**).

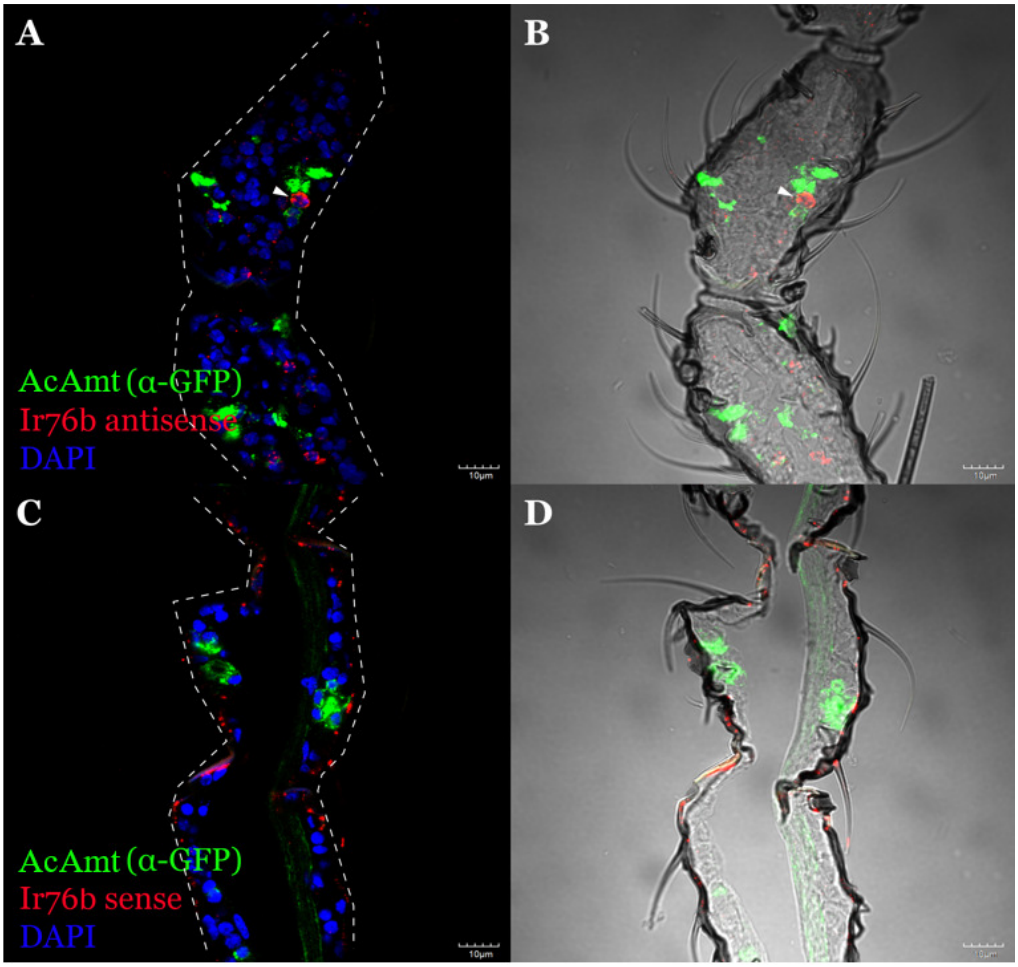

Figure 5. A representative confocal optical section of FISH on the female antennae using *Ir76b* antisense riboprobe (red) and α-GFP showing *AcAmtP*-driven *GFP* (green) is expressed in auxiliary cells closely associated with *Ir76b*-expressing neurons (**A, B**). *Ir76b* sense riboprobe was used as the negative control for riboprobe specificity (**C, D**). An *Ir76b*-expressing cell is highlighted by arrows. Scale bars = 10μm.

Olfactory Responses of Capitate Pegs and Coeloconic Sensilla to Ammonia

The localization of *AcAmtP*-driven GFP in subpopulations of coeloconic sensilla on the antennae and maxillary palp capitate pegs begs the question as to ammonia response profiles of those structures. Single sensillum recordings (SSRs) were carried out to investigate dose-dependent responses of these sensilla to ammonia at 6 different

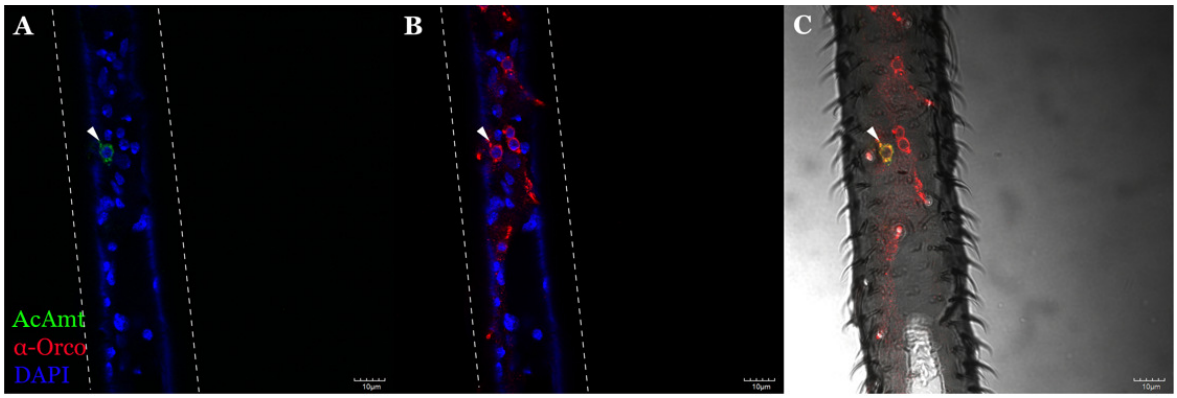

Figure 6. A representative confocal optical section of adult female *An. coluzzii* maxillary palps immunohistochemically stained with α-Orco antibodies (red) showing co-localization of *AcAmtP*-driven GFP (green) and Orco. An *AcAmtP*-derived *GFP* and *Orco* co-expressing cell is highlighted by arrows. Scale bars = 10μm.

concentrations (0.01%-5%), with a specific focus on the 5th-8th antennal flagellomeres where consistent *AcAmtP*-derived GFP expression in coeloconic sensilla was observed. SSR studies identified significant and dose-dependent ammonia responses in all tested antennal coeloconic sensilla (n=14) (**Figure 7A, 7B**). In maxillary palp capitate pegs, the cpB and cpC neurons typically display lower spike amplitudes than cpA neurons (Lu et al., 2007), and were therefore counted together due to the technical difficulty of separation. Dose-dependent excitatory responses to ammonia were identified in only cpB/C neurons; in contrast to either no response or slightly inhibitory responses displayed in cpA neurons (n=6) (Lu et al., 2007) (**Figure 7C, 7D**).

Neuronal AcAmt Expression in Gustatory Appendages

While the labella and tarsi are considered to be the primary gustatory appendages of the mosquito, previous studies have revealed robust olfactory responses in the labial sensilla of *An. coluzzii* (Kwon et al., 2006; Saveer et al., 2018). To investigate the potential role of *AcAmt* in these appendages, cryosections were

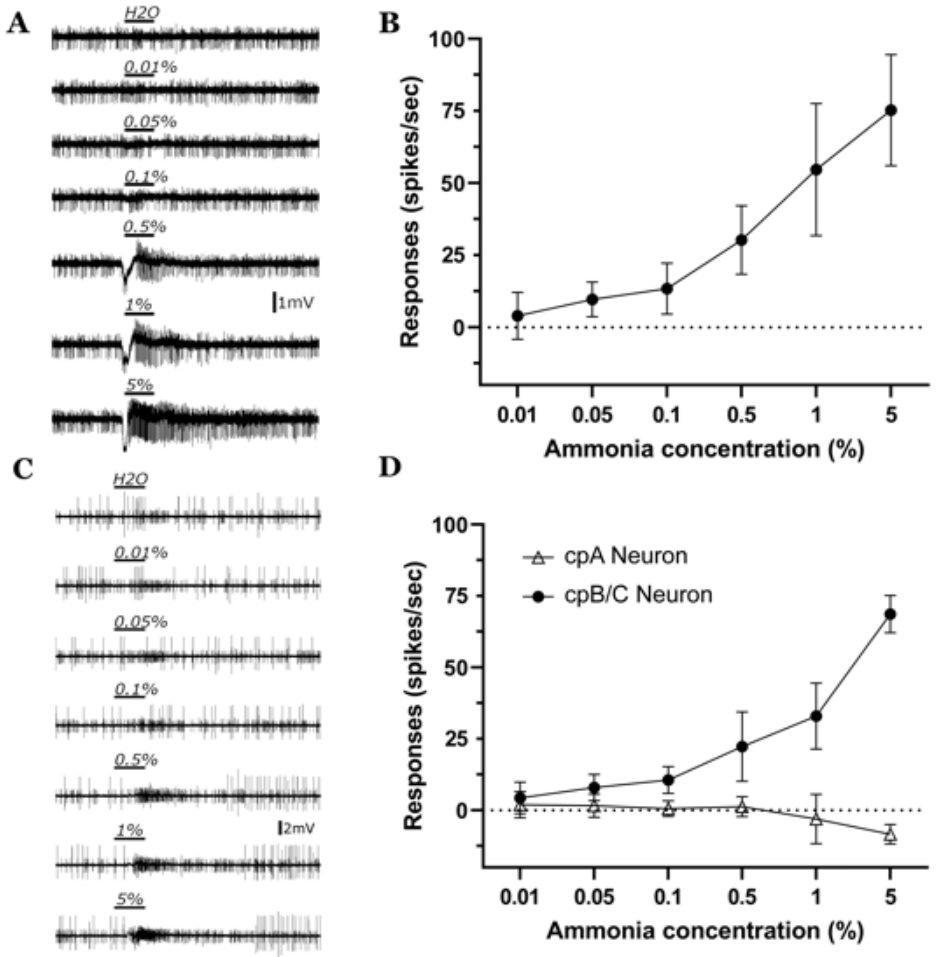

Figure 7. (A) Single sensillum recording signals from a coeloconic sensillum to different concentrations of ammonia and the solvent. The vertical bar denotes the amplitude and the horizontal bar denotes the 0.5s duration of chemical stimulation; **(B)** Mean dose-dependent single sensillum responding patterns of coeloconic sensilla to six concentrations of ammonia; **(C)** Single sensillum recording signals from a capitate peg to different concentrations of ammonia and the solvent. The vertical bar denotes the amplitude and the horizontal bar denotes the 0.5s duration of chemical stimulation; **(D)** Mean dose-dependent single sensillum responding patterns of cpA neurons and cpB/C neurons in capitate pegs to six concentrations of ammonia. Error bars = Standard error of the mean.

examined using immunohistochemistry and FISH. To begin with, GFP-labelled cells were counted and compared in labella between the 1kb *AcAmtP-GFP* and the 3kb

	Repeat1	Repeat2	Repeat3
1kb *AcAmtP-GFP*	53	59	54
3kb *AcAmtP-GFP*	55	57	55

Table S4. The number of GFP-labelled cells in female labella in the 1kb and 3kb *AcAmtP-GFP* progeny. Each column shows data from a labellum sample (n=3).

AcAmtP-GFP lines (**Table S4**). Analysis using unpaired t-tests suggests there is no significant difference in the number of GFP-labelled cells between these lines (**Figure S3;** p-value = 0.874). *Z*-axis projections of labellum whole-mounts showed intensive *AcAmtP*-driven *GFP* expression that was relatively uniform throughout the entire appendage where *AcAmtP*-derived *GFP* expressing neurons were found across the gustatory T1 sensilla (**Figure 8A-8D**) (Saveer et al., 2018), a pattern that is markedly different from the antennae. Furthermore, α-HRP-Cy3 (**Figure 9A-9D**), α-Orco

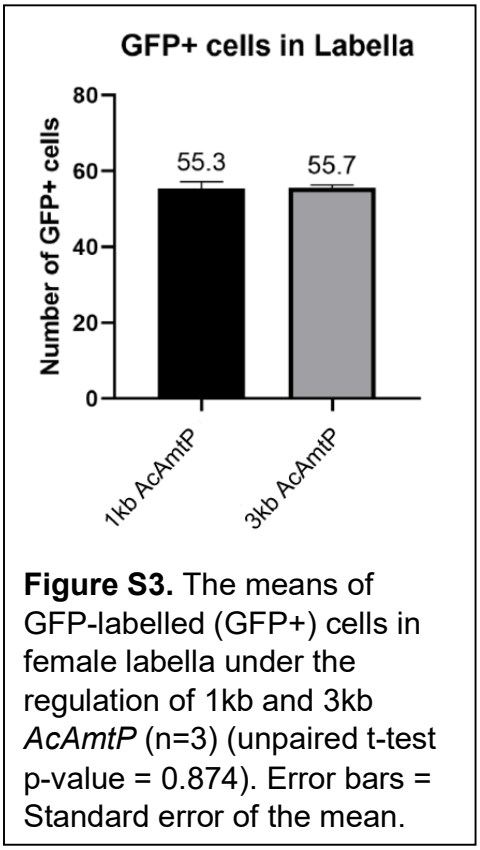

Figure S3. The means of GFP-labelled (GFP+) cells in female labella under the regulation of 1kb and 3kb *AcAmtP* (n=3) (unpaired t-test p-value = 0.874). Error bars = Standard error of the mean.

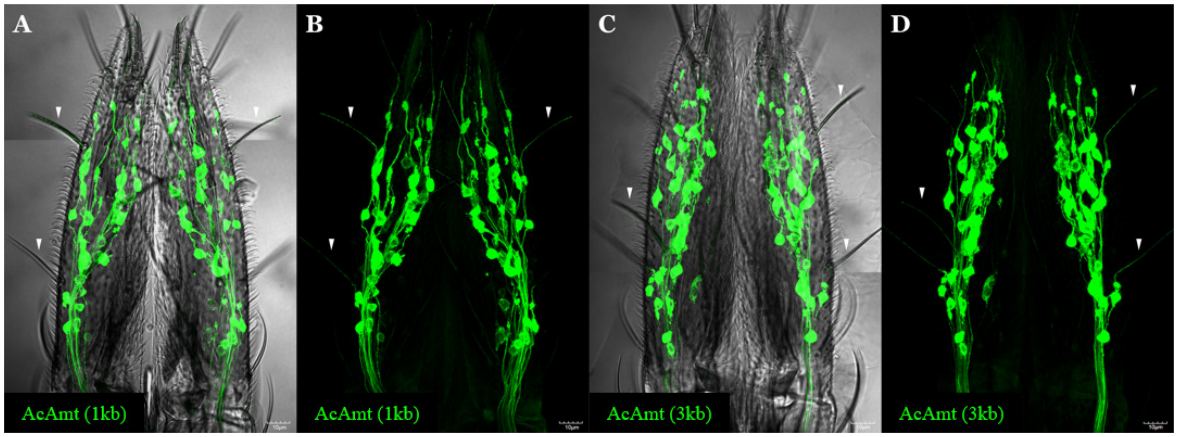

Figure 8. Z-axis projection of whole-mount adult female *An. coluzzii* labellum carrying *QUAS-GFP* and either *1kb AcAmtP-QF2* (**A-B**) or *3kb AcAmtP-QF2* (**C-D**) constructs showing specific expression of *GFP.* Dendritic labelling of *AcAmt* in T1 sensilla is highlighted by arrows. Scale bars = 10μm.

immunostaining (**Figure 9E-9H**) and *AcIr76b* FISH (**Figure 10**), revealed that *AcAmtP*-derived *GFP* expression in the labellum is strictly neuronal, distributed across distinct populations of *AcOrco*-expressing ORNs and *AcIr76b*-expressing IRNs.

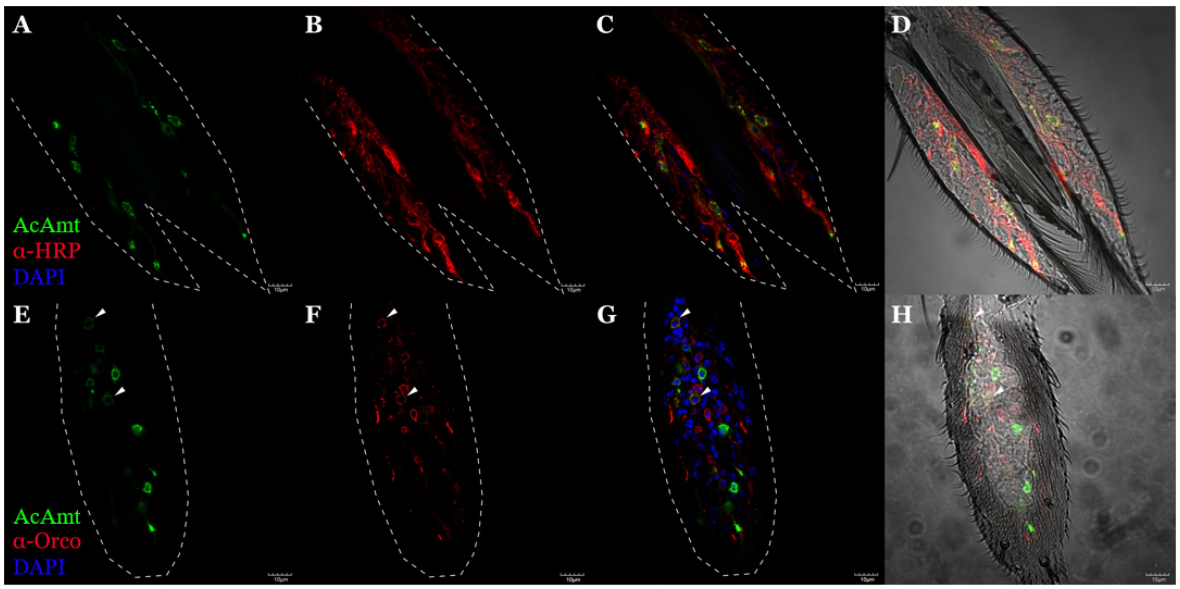

Figure 9. A representative confocal optical section of adult female labellum immunohistochemically stained with α-HRP **(A-D**; red**)** and α-Orco **(E-H**; red**)** showing *AcAmtP*-driven *GFP* (green) is expressed in neurons and partially in ORNs. *AcAmtP*-derived *GFP* and *Orco* co-expressing cells are highlighted by arrows. Scale bars = 10μm.

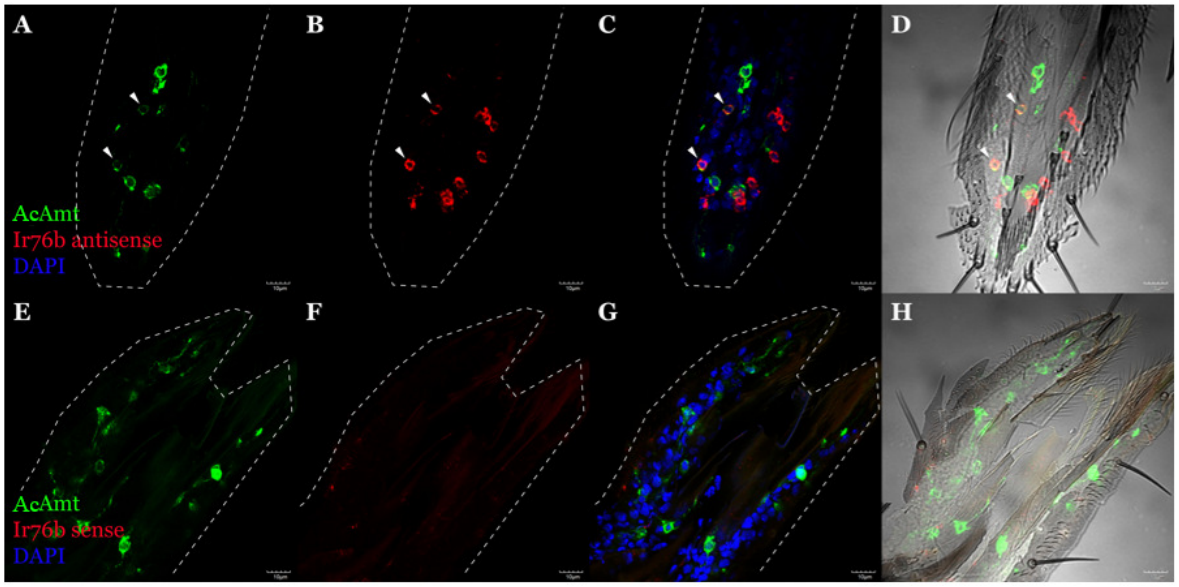

Figure 10. A representative confocal optical section of the adult female labellum stained for FISH using *Ir76b* antisense riboprobes (red) and α-GFP showing partial *AcAmtP*-derived *GFP* (green) expression in *Ir76b*-expressing neurons **(A-D).** *Ir76b* sense riboprobes were used as the negative control for riboprobe specificity **(E-H).** *AcAmtP*-derived *GFP* and *Ir76b* co-expressing cells are highlighted by arrows. Scale bars = 10μm.

In the *D. melanogaster* labellum, *DmAmt* is not involved in volatile or contact-based ammonia sensing but instead is expressed in sugar sensing *Gr5a* neurons (Delventhal et al., 2017). To investigate whether *AcAmt* has a similar expression pattern, we used FISH to localize *AcGr15* which is the homolog to *DmGr5a*. In these studies, we found extensive co-localization between *AcAmtP*-driven GFP and *AcGr15* (**Figure 11A-11D**; negative control with *AcGr15* sense riboprobe: **Figure 11E-11H**). In the *An. coluzzii* tarsi, *AcAmtP*-derived *GFP* expression was uniformly observed across all 5 tarsal segments of prothoracic, mesothoracic, and metathoracic tarsi where it co-localizes with α-HRP-Cy3, indicating once more that *AcAmtP*-derived *GFP* is expressed in neurons (**Figure 12A-12C**). These likely *AcAmt*-expressing cells are localized to the distal half of each tarsal segment in close proximity to the joints between segments where a cluster of neurons are localized.

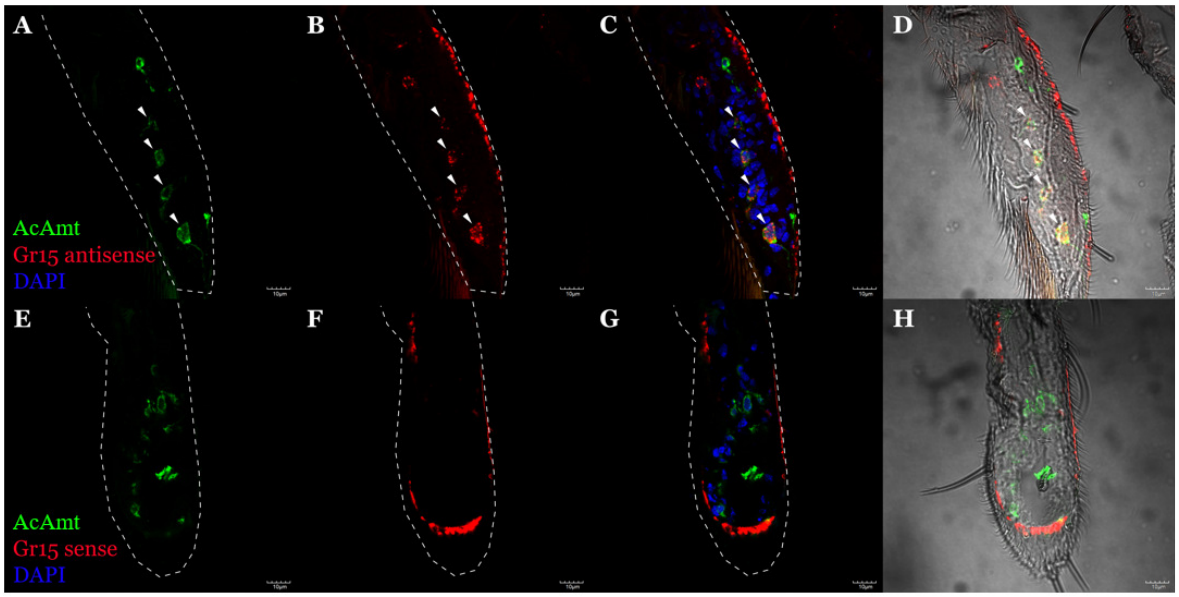

Figure 11. A representative confocal optical section of the adult female labellum stained for FISH using *Gr15* antisense riboprobes (red) and α-GFP (green) showing partial *AcAmtP*-derived *GFP* expression in the *Gr15*-expressing neurons **(A-D).** *Gr15* sense riboprobes were used as the negative control for riboprobe specificity **(E-H).** *AcAmtP*-driven *GFP* and *Gr15* co-expressing cells are highlighted by arrows. Scale bars = 10μm.

Larval AcAmt Expression

Larval progeny from both the 1kb and 3kb *AcAmtP-QF2* driver lines house a cluster of GFP+ potentially *AcAmt*-expressing cells proximal to the sensory cone **(Figure 13)**, which is the major olfactory structure on the multi-articulated larval antennae (Xia et al., 2008). Interestingly, significantly fewer cells were labelled in the 1kb *AcAmtP-GFP* progeny (**Figure 13A**) as compared to the 3kb progeny (**Figure 13B**), suggesting the presence of larval specific transcriptional control elements between 1kb and 3kb upstream of the *AcAmt* translational start site. As such, sequential experiments were conducted using the 3kb *AcAmtP-GFP* progeny. Consistent with the adult female antennae, whole-mount immunostaining with α-HRP-Cy3 revealed that *AcAmtP*-driven

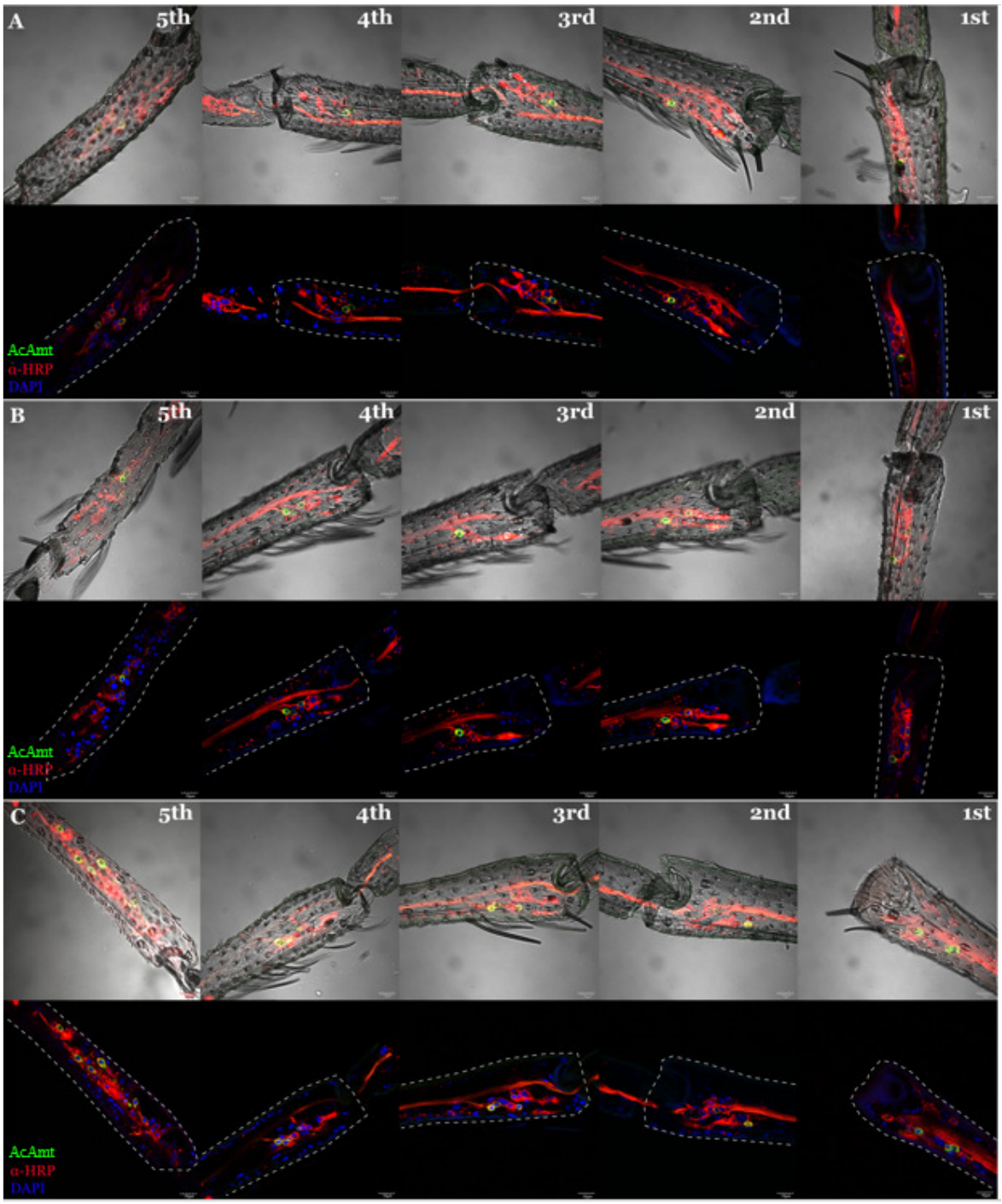

Figure 12. A representative confocal optical section of adult female tarsi immunohistochemically stained with α-HRP (red) showing *AcAmtP-GFP* (green) is expressed in neurons in all five segments (1st-5th labelled on images) of protarsi **(A)**, mesotarsi **(B)**, and metatarsi **(C)**. Scale bars = 10μm.

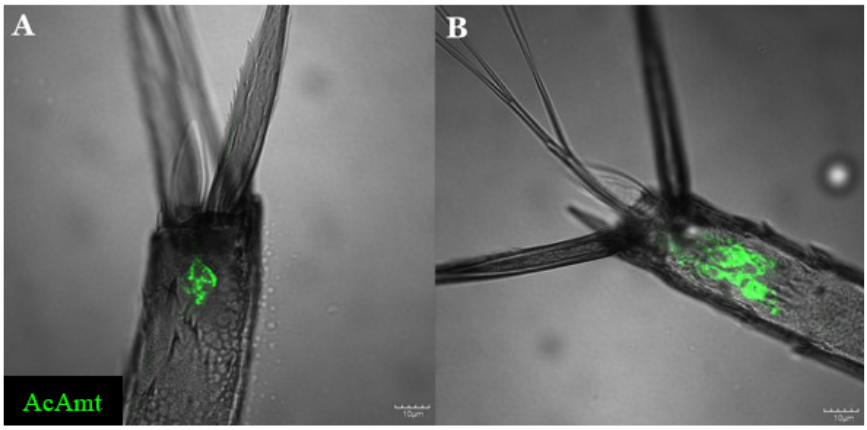

Figure 13. A representative confocal optical section of whole-mount *An. coluzzii* larval antennae carrying either *1kb* **(A)** or *3kb* **(B)** *AcAmtP-QF2* and *QUAS-GFP* showing *AcAmtP-GFP* (green) expression closely associated with the antennal sensory cone. Scale bars = 10μm.

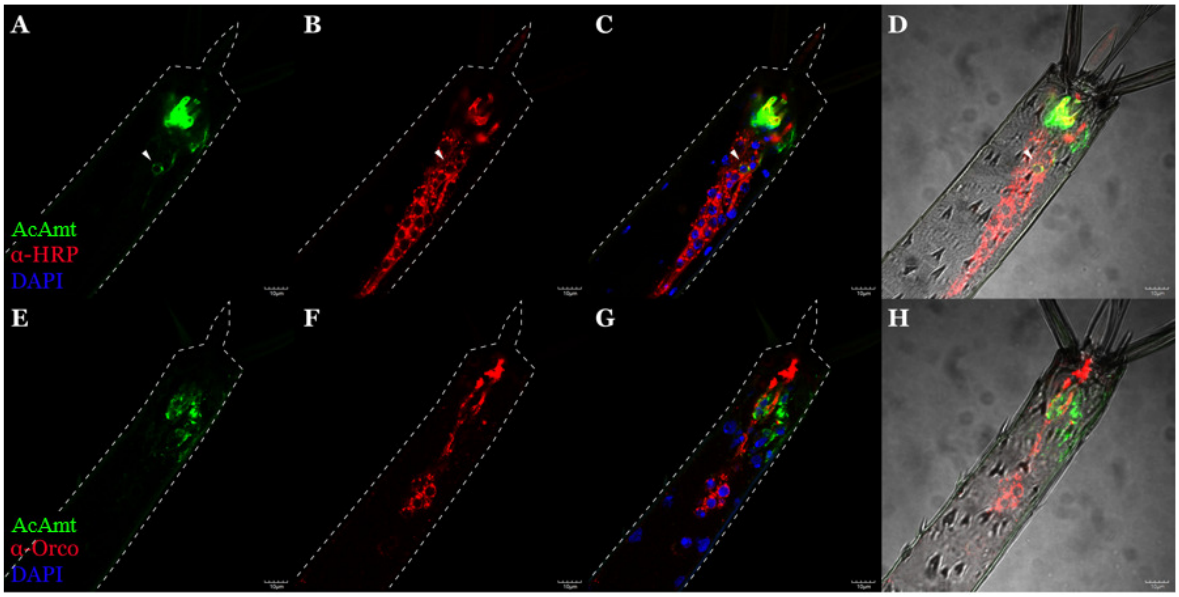

Figure 14. A representative confocal optical section of whole-mount *An. coluzzii* larval antennae from 3kb *AcAmtP-GFP* (green) progeny immunohistochemically stained with α-HRP **(A-D**; red**)** and α-Orco **(E-H**; red**)** showing *AcAmtP*-driven *GFP* expression in both neuronal cells and auxiliary cells which envelope the neurons. An *AcAmtP-GFP*-expressing neuron is highlighted by arrows. Scale bars = 10μm.

GFP is expressed in both neuronal and auxiliary cells in the larval antennae (**Figure 14A-14D**). The *AcAmtP*-driven *GFP* expressing auxiliary cells surround, or are

proximate to, most if not all of the α-HRP labelled neurons, which is consistent with a previous description of larval auxiliary cells (**Figure 14A-14D**) (Zacharuk et al., 1971). As expected, α-Orco polyclonal antibodies marked ORNs comprise a subset of these larval neurons (**Figure 14B, 14F**) and a close association between ORNs and what are likely to be *AcAmt*-expressing larval auxiliary cells was observed (**Figure 14E-14H**).

Discussion

Heterogeneous Localization of AcAmt in Olfactory and Gustatory Appendages

From a technical perspective, the generation of a set of *AcAmtP-QF2* driver lines involved the development of a high-efficiency adaptation that brings together the phiC31 integration (Meredith et al., 2011) and Q system (Riabinina et al., 2016) in the malaria vector *An. gambiae* which until recently has been largely refractory to such genetic manipulations. We have utilized the phiC31 site-specific integration system to generate a Q system driver line thereby avoiding positional effects and potential fitness costs introduced by random-insertion transposon systems (Labbé et al., 2010). Additionally, the large integration capacity of the phiC31 system ensures the practicability of generating driver lines with larger transcriptional regulatory elements (Nimmo et al., 2006). Indeed, the relatively high integration efficiency of driver constructs we observed in *An. coluzzii* is likely due to the use of the phiC31 helper plasmid as the source of integrase, as the plasmid is likely to be more stable and therefore better able to express integrase activity than co-injected mRNA (Gratz et al., 2014; Kistler et al., 2015). In this manner, we have developed a technical workflow where the driver line, and potentially,

a modified effector line can be rapidly generated in *An. coluzzii*. These substantial improvements in utility result in a highly efficient Q system that represents a powerful tool for the genetic characterization and manipulation of *An. coluzzii* target genes in future studies.

In order to further characterize the role of *AcAmt* insofar as ammonia sensitivity and metabolic processes that are salient for host-seeking and other mosquito behaviors, we examined the spatial localization in the chemosensory appendages of the adult and larval peripheral nervous system of *An. coluzzii*. Previous studies examining the localization of *DmAmt*, the *Amt* homolog in the chemosensory appendages of *D. melanogaster*, revealed an unexpected heterogeneity in which *DmAmt* is found in non-neuronal antennal auxiliary cells whereas in the labella and tarsi, *DmAmt* is neuronal (Delventhal et al., 2017; Menuz et al., 2014). Importantly, these *Drosophila* studies also revealed *DmAmt*'s functional heterogeneity; in which antennal expression is required for olfactory responses to ammonia, while null mutants which showed no labellum-expression also displayed wild-type gustatory responses to ammonium solutions (Delventhal et al., 2017; Menuz et al., 2014).

While acknowledging the reliance on *AcAmtP*-driven GFP signals, our localization studies in female *An. coluzzii* antennae build upon the theme of heterogeneity by demonstrating that *AcAmtP*-derived *GFP* is widely expressed in both neuronal and non-neuronal cells (**Figures 2-5**). More specifically, and in contrast to *DmAmt* which is expressed only in a narrow subtype of antennal coeloconic sensilla (ac1) (Menuz et al., 2014), *AcAmtP*-driven *GFP* is expressed in the auxiliary cells in all coeloconic sensilla as well as what appears to be the majority of grooved pegs. Even

more complexity is evident as neuronal *AcAmtP*-derived *GFP* expression seems to be localized to non-OSNs as these cells are not labelled by either α-Orco antibodies or *Ir76b* riboprobes. As is the case in *Drosophila* antennae (Menuz et al., 2014), we did not observe *AcAmtP*-derived *GFP* expression in any trichoid sensilla despite studies demonstrating ammonia sensitivity across these sensilla (Qiu et al., 2006). Therefore the significant diversity we observed in *AcAmtP*-driven *GFP* expression presumably correlates with heterogenous function along the antennae of *An. coluzzii*.

The chemosensory ultrastructure of the *An. coluzzii* maxillary palps has long been thought to contain a single, homogeneous class of olfactory sensilla, the capitate pegs, in which 3 distinct neurons are present: two ORNs and one CO_2 sensing gustatory receptor neuron (GRN) (Lu et al., 2007). However, our expression data challenges this model as in contrast to the antennae, where *AcAmt* appears to be expressed in auxiliary cells and non-ORN neurons, *AcAmt*-driven *GFP* is expressed only in a subset of the maxillary palp ORNs. This suggests there is a previously undescribed heterogeneity among the maxillary palp capitate peg ORNs of *An. coluzzii* that may impact functionality and sensitivity to ammonia and perhaps other stimuli on this important chemosensory appendage.

In the proboscis and tarsi that encompass the adult gustatory appendages, the complete spectrum of labial chemosensory neurons (ORNs, IRNs, and GRNs) appear to express *AcAmt*. Moreover, all segments in the tarsi display *AcAmtP*-driven *GFP* expression compared to only up to 4 *DmAmt*$^{+}$ segments in *Drosophila* (Delventhal et al., 2017). Consistent with studies showing that *DmAmt* is expressed in the sugar sensing *DmGr5a* neurons instead of the ammonium sensing *DmGr66a* neurons (Delventhal et

al., 2017), *AcAmtP*-driven *GFP* is expressed in the putative mosquito sugar sensing *AcGr15* neurons in the labellum. Inasmuch as mosquito tarsi have not been shown to display ammonia sensitivity, these data raise the possibility that the function of neuronal AcAmt is fundamentally different from the auxiliary cell AcAmt and indeed may not be directly involved in environmental ammonium sensing.

The *Anopheles* larval antennae is a single tubular appendage in which the primary olfactory structure, the sensory cone, is located at the distal tip and is innervated by a group of subtended chemosensory neurons that are enveloped by auxiliary cells (Xia et al., 2008; Zacharuk et al., 1971). Although studies have revealed the potential olfactory function of the sensory cone (Xia et al., 2008), no electrophysiological studies have thus far been conducted to characterize the chemosensory responses of neurons in the larval antennae (Liu et al., 2010; Xia et al., 2008). Given that *AcAmtP*-driven GFP is localized in auxiliary cells surrounding a group of α-HRP labelled neurons among which ORNs only compose a subset, our data suggests that in larvae, AcAmt functionality is associated with other chemosensory neurons besides ORNs. Therefore, given the strong correlation between *Ag/DmAmt* expression and ammonia sensitivity that we and others have demonstrated (Delventhal et al., 2017; Menuz et al., 2014), it is reasonable to speculate that other structures/chemosensory neurons on the larval antennae, along with the ORN-innervated sensory cone (Xia et al., 2008), are involved in chemosensory processing of ammonia-based stimuli (Zacharuk and Blue, 1971).

In addition to the expression of *AcOrco* and *AcOR*s that define ORNs, *AcIR* expression has been reported in larval IRNs and shown to mediate larvae behaviors

(Liu et al., 2010). In light of previous studies in the larval antennae where ORNs seem to be exclusively present in the sensory cone (Xia et al., 2008) and in the adult chemosensory system that suggest IRNs and ORNs are distinct cell populations (Pitts et al., 2017) it is reasonable to speculate that larval *AcIRs* are expressed in chemosensory appendages other than the ORN-rich sensory cone that may correlate to larval ammonia sensitivity.

A Model for Neuronal Amt Function

While it has been suggested that *DmAmt* expression in *Drosophila* antennal auxiliary cells is involved in ammonium clearance from the sensillar lymph to ameliorate receptor desensitization (Menuz et al., 2014), the function of neuronal *DmAmt* on the labellum remains cryptic (Delventhal et al., 2017). In contrast, apart from our observation of non-neuronal *AcAmtP*-driven *GFP* expression in antennal coeloconic and basiconic auxillary cells, *AcAmt* is largely neuronal across all the chemosensory appendages of *An. coluzzii*. This begs the general question as to the function of neuronal ammonium transporters in the malaria mosquito.

It is reasonable to suggest that insect chemosensory neurons must transport ammonium for a variety of metabolic and/or neurobiological purposes that could be addressed by bidirectional *Amt* transporters (Durant and Donini, 2018; Soupene et al., 2002). Indeed, in honeybees it has been observed that ammonium is produced in the conversion of glutamine to glutamate in glutamatergic neurons and is released from photoreceptor neurons and transported to glial cells (Marcaggi and Coles, 2001; Tsacopoulos et al., 1997), where neuronal expressing *Amt* may be involved. While the

ammonium excretion from neurons remains largely uncharacterized, it was suggested that the Na^+-K^+-$2Cl^-$ co-transporter plays a role in transporting ammonia into the honeybee glial cells by substituting the K^+ with ammonium (Bak et al., 2006; Marcaggi and Coles, 2001). However, this co-transporter has a moderate affinity for ammonium and is therefore less efficient in its transport (Bakouh et al., 2006). It is therefore possible that Amt is acting as a potential supporting element in this process. While glutamatergic interneurons have been characterized in the antennal lobes of *Drosophila*, no glutamatergic OSNs have been described in other insects. In addition to glutamate, gamma-aminobutyric acid (GABA) has also been shown to serve as an inhibitory neurotransmitter in insects (Wilson and Laurent, 2005). The GABAergic neurons requires a similar ammonia clearance system as the glutamatergic neurons where Amt can also be functional (Bak et al., 2006). While many studies suggest a large portion of glutamatergic/GABAergic cells act as local interneurons (LNs) concentrated in the insect antennal lobes, antennal GABAergic neurons have also been identified in the sphinx moth (Hoskins et al., 1986). Additionally, it is possible that neuronal Amt plays a role in the metabolism of biogenic amines which modulate neuronal activity (Zhukovskaya and Polyanovsky, 2017). Moreover, serotoninergic neurons were found in olfactory and gustatory appendages in mosquitoes (Siju et al., 2008; Zhukovskaya and Polyanovsky, 2017), where the uptake/excretion of ammonia could be essential for the regulation of serotonin synthesis (Coleman and Neckameyer, 2005; Grippon et al., 1986). While the function of DmAmt in gustatory appendages remains unknown, the high labial expression level of *Amt* in *Drosophila*, *Anopheles*, and *Aedes* suggests that a significant role of ammonium transporters in gustation or in labial-based olfaction that

has been shown to occur in *An. coluzzii* (Kwon et al., 2006; Matthews et al., 2016; Menuz et al., 2014; Pitts et al., 2014a; Saveer et al., 2018).

IRs are Implicated in Ammonia Detection

While Anopheline *OR*s are widely expressed on antennae and have been shown to recognize diverse combinations of chemical stimuli, they are not expressed in the ammonia-sensitive grooved pegs (Carey et al., 2010; Pitts et al., 2004; Wang et al., 2010). The characterization of *Drosophila IRs* as amine and acid receptors revealed *DmIr92a* is co-expressed with *DmIr76b* and *DmIr25a* co-receptors that together are responsible for olfactory responses to ammonia in ac1 coeloconic sensilla (Ai et al., 2010; Benton et al., 2009; Min et al., 2013). Recently, several similar amine and acid-sensitive *An. coluzzii IR*s have been characterized (Pitts et al., 2017) although in the absence of a clear *DmIr92*a homolog, the Anopheline ammonia receptor has not yet been identified.

We have found a strong association between *AcAmt* and ammonia sensing neurons. In addition to the grooved pegs as previously demonstrated (Qiu et al., 2006), all of the putative *AcAmt*-expressing sensilla on the antennae and maxillary palps showed neuronal responses to ammonia. Moreover, the localization of antennal *AcAmtP*-driven GFP is highly correlated with *AcIr76b*, which suggests that, in keeping with the data from *Drosophila* (Menuz et al., 2014), mosquito ammonia receptors are likely to be *IR*s. In light of the high correlation between the response spectrum of *DmIRs* and *AcIRs* and the odor response profiles of *Anopheles* grooved pegs (Benton et al., 2009; Pitts et al., 2017; Qiu et al., 2006), which are orthologous to *Drosophila*

coeloconic sensilla (Ray, 2015), it is reasonable to suggest these sensilla are innervated by IRNs instead of ORNs, and that *AcIRs* are ammonia sensing receptors in Anopheline grooved pegs.

It is noteworthy that we did not observe *AcAmtP*-driven *GFP* expression in the trichoid sensilla, a subpopulation of which has been shown to house ammonia sensitive neurons (Qiu et al., 2006). This suggests there are *AcAmt*-independent ammonia sensing pathways in *An. coluzzii*. Furthermore, inasmuch as *An. coluzzii* trichoid sensilla express *Orco* and presumably a range of tuning *OR*s, it is likely this alternative pathway is *OR*-mediated and perhaps involves the antennal-expressed *Rh50* transporter (Pitts et al., 2014a).

Acknowledgements

We thank Zhen Li for mosquito rearing, Dr. Ahmed Saveer (North Carolina State University) and Dr. Zhiwei Zhang (Shanxi Agricultural University) for technical training, and all members of the Zwiebel lab for valuable advice and comments throughout the course of this work. We also thank Dr. Julian Hillyer, Dr. Maulik Patel, Dr. Wenbiao Chen, and Dr. Patrick Abbot (Vanderbilt University) for critical suggestions. We are especially grateful for the generous gift of expertise and Q system mosquito lines from Dr. Christopher Potter (the Johns Hopkins University School of Medicine). Lastly, we acknowledge The Vanderbilt University Cell Imaging Shared Resource Core for training and use of the Olympus FV-1000 confocal microscope and Dr. James Patton (Vanderbilt University) for cryostat access. This work was conducted with the support of

Vanderbilt University and funded by the National Institutes of Health (NIAID, R21-113960) to LJZ.

Author Contributions

Conceived experiments: ZY, FL, HHS, MB, RJP and LJZ; Performed research: ZY, FL, HHS, and MB; Analyzed data: ZY, FL, HHS, and MB; Wrote the paper: ZY, FL, HHS, MB, RJP and LJZ. Approved the final manuscript: ZY, FL, HHS, MB, RJP and LJZ.

References

Ai, M., Min, S., Grosjean, Y., Leblanc, C., Bell, R., Benton, R., Suh, G.S.B., 2010. Acid sensing by the *Drosophila* olfactory system. Nature 468, 691–695. https://doi.org/10.1038/nature09537

Alonso, P., Noor, A.M., 2017. The global fight against malaria is at crossroads. Lancet 390, 2532–2534. https://doi.org/10.1016/S0140-6736(17)33080-5

Andrade, S.L.A., Einsle, O., 2007. The Amt/Mep/Rh family of ammonium transport proteins (Review). Mol. Membr. Biol. 24, 357–365. https://doi.org/10.1080/09687680701388423

Bak, L.K., Schousboe, A., Waagepetersen, H.S., 2006. The glutamate/GABA-glutamine cycle: Aspects of transport, neurotransmitter homeostasis and ammonia transfer. J. Neurochem. 98, 641–653. https://doi.org/10.1111/j.1471-4159.2006.03913.x

Bakouh, N., Benjelloun, F., Cherif-Zahar, B., Planelles, G., 2006. The challenge of understanding ammonium homeostasis and the role of the Rh glycoproteins. Transfus. Clin. Biol. 13, 139–146. https://doi.org/10.1016/j.tracli.2006.02.008

Benton, R., Vannice, K.S., Gomez-Diaz, C., Vosshall, L.B., 2009. Variant Ionotropic Glutamate Receptors as Chemosensory Receptors in *Drosophila*. Cell 136, 149–162. https://doi.org/10.1016/j.cell.2008.12.001

Bittsánszky, A., Pilinszky, K., Gyulai, G., Komives, T., 2015. Overcoming ammonium toxicity. Plant Sci. 231, 184–190. https://doi.org/10.1016/j.plantsci.2014.12.005

Boverhof, D.R., Wiescinski, C.M., Botham, P., Lees, D., Debruyne, E., Repetto-Larsay, M., Ladics, G., Hoban, D., Gamer, A., Remmele, M., Wang-Fan, W., Ullmann, L.G., Mehta, J., Billington, R., Woolhiser, M.R., 2008. Interlaboratory validation of 1%

pluronic L92 surfactant as a suitable, aqueous vehicle for testing pesticide formulations using the murine local lymph node assay. Toxicol. Sci. 105, 79–85. https://doi.org/10.1093/toxsci/kfn117

Carey, A.F., Wang, G., Su, C.Y., Zwiebel, L.J., Carlson, J.R., 2010. Odorant reception in the malaria mosquito *Anopheles gambiae*. Nature 464, 66–71. https://doi.org/10.1038/nature08834

Chasiotis, H., Ionescu, A., Misyura, L., Bui, P., Fazio, K., Wang, J., Patrick, M., Weihrauch, D., Donini, A., 2016. An animal homolog of plant Mep/Amt transporters promotes ammonia excretion by the anal papillae of the disease vector mosquito *Aedes aegypti*. J. Exp. Biol. 219, 1346–1355. https://doi.org/10.1242/jeb.134494

Coleman, C.M., Neckameyer, W.S., 2005. Serotonin synthesis by two distinct enzymes in *Drosophila melanogaster*. Arch. Insect Biochem. Physiol. 59, 12–31. https://doi.org/10.1002/arch.20050

Cox, F.E., 2010. History of the discovery of the malaria parasites and their vectors. Parasites and Vectors 3. https://doi.org/10.1186/1756-3305-3-5

Crawford, N.M., Forde, B.G., 2002. Molecular and developmental biology of inorganic nitrogen nutrition. Arab. B. 1, e0011. https://doi.org/10.1199/tab.0011

Delventhal, R., Menuz, K., Joseph, R., Park, J., Sun, J.S., Carlson, J.R., 2017. The taste response to ammonia in *Drosophila*. Sci. Rep. 7. https://doi.org/10.1038/srep43754

Den Otter, C.J., Behan, M., Maes, F.W., 1980. Single cell responses in female *Pieris brassicae* (Lepidoptera: Pieridae) to plant volatiles and conspecific egg odours. J. Insect Physiol. 26, 465–472. https://doi.org/10.1016/0022-1910(80)90117-1

Durant, A.C., Donini, A., 2018. Ammonia excretion in an osmoregulatory syncytium is facilitated by AeAmt2, a novel ammonia transporter in *Aedes aegypti* larvae. Front. Physiol. 9. https://doi.org/10.3389/fphys.2018.00339

Ghaninia, M., Ignell, R., Hansson, B.S., 2007. Functional classification and central nervous projections of olfactory receptor neurons housed in antennal trichoid sensilla of female yellow fever mosquitoes, *Aedes aegypti*. Eur. J. Neurosci. 26, 1611–1623. https://doi.org/10.1111/j.1460-9568.2007.05786.x

Gratz, S.J., Ukken, F.P., Rubinstein, C.D., Thiede, G., Donohue, L.K., Cummings, A.M., Oconnor-Giles, K.M., 2014. Highly specific and efficient CRISPR/Cas9-catalyzed homology-directed repair in *Drosophila*. Genetics 196, 961–971. https://doi.org/10.1534/genetics.113.160713

Grippon, P., le Poncin Lafitte, M., Boschat, M., Wang, S., Faure, G., Dutertre, D., Opolon, P., 1986. Evidence for the role of ammonia in the intracerebral transfer and metabolism of tryptophan. Hepatology 6, 682–686. https://doi.org/10.1002/hep.1840060424

Guidobaldi, F., May-Concha, I.J., Guerenstein, P.G., 2014. Morphology and physiology of the olfactory system of blood-feeding insects. J. Physiol. Paris 108, 96–111. https://doi.org/10.1016/j.jphysparis.2014.04.006

Hoskins, S.G., Homberg, U., Kingan, T.G., Christensen, T.A., Hildebrand, J.G., 1986. Immunocytochemistry of GABA in the antennal lobes of the sphinx moth *Manduca sexta*. Cell Tissue Res. 244, 243–252. https://doi.org/10.1007/BF00219199

Jan, L.Y., Jan, Y.N., 1982. Antibodies to horseradish peroxidase as specific neuronal markers in *Drosophila* and in grasshopper embryos. Proc. Natl. Acad. Sci. U. S. A.

79, 2700–2704. https://doi.org/10.1073/pnas.79.8.2700

Kistler, K.E., Vosshall, L.B., Matthews, B.J., 2015. Genome engineering with CRISPR-Cas9 in the mosquito *Aedes aegypti*. Cell Rep. 11, 51–60. https://doi.org/10.1016/j.celrep.2015.03.009

Kwon, H.W., Lu, T., Rützler, M., Zwiebel, L.J., 2006. Olfactory response in a gustatory organ of the malaria vector mosquito *Anopheles gambiae*. Proc. Natl. Acad. Sci. U. S. A. 103, 13526–13531. https://doi.org/10.1073/pnas.0601107103

Labbé, G.M.C., Nimmo, D.D., Alphey, L., 2010. Piggybac- and PhiC31-mediated genetic transformation of the Asian tiger mosquito, *Aedes albopictus* (Skuse). PLoS Negl. Trop. Dis. 4. https://doi.org/10.1371/journal.pntd.0000788

Leal, W.S., 2013. Odorant Reception in Insects: Roles of Receptors, Binding Proteins, and Degrading Enzymes. Annu. Rev. Entomol. 58, 373–391. https://doi.org/10.1146/annurev-ento-120811-153635

Liu, C., Pitts, R.J., Bohbot, J.D., Jones, P.L., Wang, G., Zwiebel, L.J., 2010. Distinct olfactory signaling mechanisms in the malaria vector mosquito *Anopheles gambiae*. PLoS Biol. 8, 27–28. https://doi.org/10.1371/journal.pbio.1000467

Liu, F., Chen, L., Appel, A.G., Liu, N., 2013. Olfactory responses of the antennal trichoid sensilla to chemical repellents in the mosquito, *Culex quinquefasciatus*. J. Insect Physiol. 59, 1169–1177. https://doi.org/10.1016/j.jinsphys.2013.08.016

Loesel, R., Weigel, S., Bräunig, P., 2006. A simple fluorescent double staining method for distinguishing neuronal from non-neuronal cells in the insect central nervous system. J. Neurosci. Methods 155, 202–206. https://doi.org/10.1016/j.jneumeth.2006.01.006

Lu, T., Qiu, Y.T., Wang, G., Kwon, J.Y., Rutzler, M., Kwon, H.W., Pitts, R.J., van Loon, J.J.A., Takken, W., Carlson, J.R., Zwiebel, L.J., 2007. Odor coding in the maxillary palp of the malaria vector mosquito *Anopheles gambiae*. Curr. Biol. 17, 1533–1544. https://doi.org/10.1016/j.cub.2007.07.062

Marcaggi, P., Coles, J.A., 2001. Ammonium in nervous tissue: Transport across cell membranes, fluxes from neurons to glial cells, and role in signalling. Prog. Neurobiol. 64, 157–183. https://doi.org/10.1016/S0301-0082(00)00043-5

Matthews, B.J., McBride, C.S., DeGennaro, M., Despo, O., Vosshall, L.B., 2016. The neurotranscriptome of the *Aedes aegypti* mosquito. BMC Genomics 17. https://doi.org/10.1186/s12864-015-2239-0

McIver, S.B., 1973. Fine structure of antennal sensilla coeloconica of culicine mosquitoes. Tissue Cell 5, 105–112. https://doi.org/10.1016/S0040-8166(73)80009-6

McIver, S.B., 1982. Sensilla of mosquitoes (Diptera: Culicidae)1, 2. J. Med. Entomol. 19, 489–535. https://doi.org/10.1093/jmedent/19.5.489

Meijerink, J., Braks, M.A.H., Van Loon, J.J.A., 2001. Olfactory receptors on the antennae of the malaria mosquito *Anopheles gambiae* are sensitive to ammonia and other sweat-borne components. J. Insect Physiol. 47, 455–464. https://doi.org/10.1016/S0022-1910(00)00136-0

Menuz, K., Larter, N.K., Park, J., Carlson, J.R., 2014. An RNA-Seq screen of the *Drosophila* antenna identifies a transporter necessary for ammonia detection. PLoS Genet. 10. https://doi.org/10.1371/journal.pgen.1004810

Meredith, J.M., Basu, S., Nimmo, D.D., Larget-Thiery, I., Warr, E.L., Underhill, A.,

McArthur, C.C., Carter, V., Hurd, H., Bourgouin, C., Eggleston, P., 2011. Site-specific integration and expression of an anti-malarial gene in transgenic *Anopheles gambiae* significantly reduces *Plasmodium* infections. PLoS One 6. https://doi.org/10.1371/journal.pone.0014587

Min, S., Ai, M., Shin, S.A., Suh, G.S.B., 2013. Dedicated olfactory neurons mediating attraction behavior to ammonia and amines in *Drosophila*. Proc. Natl. Acad. Sci. U. S. A. 110, 1321–1329. https://doi.org/10.1073/pnas.1215680110

Molina-Cruz, A., Zilversmit, M.M., Neafsey, D.E., Hartl, D.L., Barillas-Mury, C., 2016. Mosquito vectors and the globalization of *Plasmodium falciparum* malaria . Annu. Rev. Genet. 50, 447–465. https://doi.org/10.1146/annurev-genet-120215-035211

Montell, C., Zwiebel, L.J., 2016. Mosquito sensory systems. Adv. In Insect Phys. 51, 293–328. https://doi.org/10.1016/bs.aiip.2016.04.007

Mukabana, W.R., Mweresa, C.K., Otieno, B., Omusula, P., Smallegange, R.C., van Loon, J.J.A., Takken, W., 2012. A novel synthetic odorant blend for trapping of malaria and other African mosquito species. J. Chem. Ecol. 38, 235–244. https://doi.org/10.1007/s10886-012-0088-8

Nimmo, D.D., Alphey, L., Meredith, J.M., Eggleston, P., 2006. High efficiency site-specific genetic engineering of the mosquito genome. Insect Mol. Biol. 15, 129–136. https://doi.org/10.1111/j.1365-2583.2006.00615.x

Pitts, R.J., Derryberry, S.L., Pulous, F.E., Zwiebel, L.J., 2014. Antennal-expressed ammonium transporters in the malaria vector mosquito *Anopheles gambiae*. PLoS One 9. https://doi.org/10.1371/journal.pone.0111858

Pitts, R.J., Derryberry, S.L., Zhang, Z., Zwiebel, L.J., 2017. Variant ionotropic receptors

in the malaria vector mosquito *Anopheles gambiae* tuned to amines and carboxylic acids. Sci. Rep. 7. https://doi.org/10.1038/srep40297

Pitts, R.J., Fox, A.N., Zwiebeil, L.J., 2004. A highly conserved candidate chemoreceptor expressed in both olfactory and gustatory tissues in the malaria vector *Anopheles gambiae*. Proc. Natl. Acad. Sci. U. S. A. 101, 5058–5063. https://doi.org/10.1073/pnas.0308146101

Pitts, R.J., Zwiebel, L.J., 2006. Antennal sensilla of two female anopheline sibling species with differing host ranges. Malar. J. 5. https://doi.org/10.1186/1475-2875-5-26

Pondeville, E., Puchot, N., Meredith, J.M., Lynd, A., Vernick, K.D., Lycett, G.J., Eggleston, P., Bourgouin, C., 2014. Efficient φc31 integrase-mediated site-specific germline transformation of *Anopheles gambiae*. Nat. Protoc. 9, 1698–1712. https://doi.org/10.1038/nprot.2014.117

Potter, C.J., Tasic, B., Russler, E. V., Liang, L., Luo, L., 2010. The Q system: A repressible binary system for transgene expression, lineage tracing, and mosaic analysis. Cell 141, 536–548. https://doi.org/10.1016/j.cell.2010.02.025

Qiu, Y.T., van Loon, J.J.A., Takken, W., Meijerink, J., Smid, H.M., 2006. Olfactory coding in antennal neurons of the malaria mosquito, *Anopheles gambiae*. Chem. Senses 31, 845–863. https://doi.org/10.1093/chemse/bjl027

Ray, A., 2015. Reception of odors and repellents in mosquitoes. Curr. Opin. Neurobiol. 34, 158–164. https://doi.org/10.1016/j.conb.2015.06.014

Report, W.M., 1980. World. Chem. Eng. News 58, 28. https://doi.org/10.1016/S0264-410X(07)01183-8

Riabinina, O., Task, D., Marr, E., Lin, C.C., Alford, R., O'Brochta, D.A., Potter, C.J., 2016. Organization of olfactory centres in the malaria mosquito *Anopheles gambiae*. Nat. Commun. 7. https://doi.org/10.1038/ncomms13010

Saveer, A.M., Pitts, R.J., Ferguson, S.T., Zwiebel, L.J., 2018. Characterization of chemosensory responses on the labellum of the malaria vector mosquito, *Anopheles coluzzii*. Sci. Rep. 8. https://doi.org/10.1038/s41598-018-23987-y

Shanbhag, S.R., Müller, B., Steinbrecht, R.A., 2000. Atlas of olfactory organs of *Drosophila melanogaster* 2. Internal organization and cellular architecture of olfactory sensilla. Arthropod Struct. Dev. 29, 211–229. https://doi.org/10.1016/S1467-8039(00)00028-1

Siju, K.P., Hansson, B.S., Ignell, R., 2008. Immunocytochemical localization of serotonin in the central and peripheral chemosensory system of mosquitoes. Arthropod Struct. Dev. 37, 248–259. https://doi.org/10.1016/j.asd.2007.12.001

Smallegange, R.C., Geier, M., Takken, W., 2002. Behavioural responses of *Anopheles gambiae* to ammonia, lactic acid and a fatty acid in a y-tube olfactometer. Proc. Exp. Appl. Entomol. 13, 147–152.

Smallegange, R.C., Qiu, Y.T., van Loon, J.A., Takken, W., 2005. Synergism between ammonia, lactic acid and carboxylic acids as kairomones in the host-seeking behaviour of the malaria mosquito *Anopheles gambiae* sensu stricto (Diptera: Culicidae). Chem. Senses 30, 145–152. https://doi.org/10.1093/chemse/bji010

Soupene, E., Lee, H., Kustu, S., 2002. Ammonium/methylammonium transport (Amt) proteins facilitate diffusion of NH_3 bidirectionally. Proc. Natl. Acad. Sci. U. S. A. 99, 3926–3931. https://doi.org/10.1073/pnas.062043799

Suh, E., Bohbot, J.D., Zwiebel, L.J., 2014. Peripheral olfactory signaling in insects. Curr. Opin. Insect Sci. 6, 86–92. https://doi.org/10.1016/j.cois.2014.10.006

Trussell, L.O., Fischbach, G.D., 1989. Glutamate receptor desensitization and its role in synaptic transmission. Neuron 3, 209–218. https://doi.org/10.1016/0896-6273(89)90034-2

Tsacopoulos, M., Poitry-Yamate, C.L., Poitry, S., 1997. Ammonium and glutamate released by neurons are signals regulating the nutritive function of a glial cell. J. Neurosci. 17, 2383–2390. https://doi.org/10.1523/jneurosci.17-07-02383.1997

Van Der Goes Van Naters, W., Carlson, J.R., 2006. Insects as chemosensors of humans and crops. Nature 444, 302–307. https://doi.org/10.1038/nature05403

Wang, G., Carey, A.F., Carlson, J.R., Zwiebel, L.J., 2010. Molecular basis of odor coding in the malaria vector mosquito *Anopheles gambiae*. Proc. Natl. Acad. Sci. U. S. A. 107, 4418–4423. https://doi.org/10.1073/pnas.0913392107

Wilson, R.I., Laurent, G., 2005. Role of GABAergic inhibition in shaping odor-evoked spatiotemporal patterns in the *Drosophila* antennal lobe. J. Neurosci. 25, 9069–9079. https://doi.org/10.1523/JNEUROSCI.2070-05.2005

Xia, Y., Wang, G., Buscariollo, D., Pitts, R.J., Wenger, H., Zwiebel, L.J., 2008. The molecular and cellular basis of olfactory-driven behavior in *Anopheles gambiae* larvae. Proc. Natl. Acad. Sci. U. S. A. 105, 6433–6438. https://doi.org/10.1073/pnas.0801007105

Zacharuk, R.Y., Blue, S.G., 1971. Ultrastructure of a chordotonal and a sinusoidal peg organ in the antenna of larval *Aedes aegypti* (L.). Can. J. Zool. 49, 1223–1230. https://doi.org/10.1139/z71-185

Zacharuk, R.Y., Yin, L.R., Blue, S.G., 1971. Fine structure of the antenna and its sensory cone in larvae of *Aedes aegypti* (L.). J. Morphol. 135, 273–297. https://doi.org/10.1002/jmor.1051350303

Zhukovskaya, M.I., Polyanovsky, A.D., 2017. Biogenic amines in insect antennae. Front. Syst. Neurosci. 11. https://doi.org/10.3389/fnsys.2017.00045

Zwiebel, L.J., Takken, W., 2004. Olfactory regulation of mosquito-host interactions. Insect Biochem. Mol. Biol. 34, 645–652. https://doi.org/10.1016/j.ibmb.2004.03.017

CHAPTER III

MUTAGENESIS OF THE AMMONIUM TRANSPORTER *ACAMT* REVEALS A REPRODUCTIVE ROLE AND A NOVEL AMMONIA-SENSING MECHANISM IN THE MALARIA VECTOR MOSQUITO *ANOPHELES COLUZZII*

Preface

The following chapter was published on bioRxiv in 2021 and under the review of *Insect Biochemistry and Molecular Biology*. I was the co-first author on this paper along with Feng Liu (co-first author), Stephen T. Ferguson (third author), Adam Baker (fourth author), R. Jason Pitts (fifth author), and Laurence J. Zwiebel (corresponding author). In this study, to characterize the function of AcAmt through mutagenesis, I employed CRISPR/Cas9 system to induce a deletion of majority of *AcAmt* and a fluorescence marker knock-in at the target site. The mutants were phenotypically assessed using a range of electrophysiological, behavioral, and biochemical measurements. I played a leading role in experimental design, data acquisition, data analysis, and manuscript preparation. I want to thank Feng Liu for his electrophysiological supports, Stephen T. Ferguson for his contributions to mosquito locomotor bioassay and analysis, Adam Baker for his electrophysiological data analysis and mutation confirmation, R. Jason Pitts and Laurence J. Zwiebel for their mentorship, experimental designs and acquisition of experimental reagents and equipment.

Introduction

Several species of Anopheline mosquitoes make up the primary vectors of *Plasmodium* pathogens that are the causative agents for human malaria resulting in hundreds of thousands of deaths worldwide every year (World Health Organization, 2019). Pathogen transmission occurs exclusively as a consequence of the blood meals that female mosquitoes require in order to complete their reproductive cycles. The mosquito's olfactory system provides the ability to sense and discriminate a broad spectrum of semiochemical cues that drive host preference and seeking behaviors that ultimately lead to blood feeding (Carey and Carlson, 2011; Montell and Zwiebel, 2016; Zwiebel and Takken, 2004). In that process, ammonia along with several carboxylic acids derived from human sweat act as attractants that promote mosquito-human interactions (Smallegange et al., 2011). Anopheline females are attracted to ammonia without the presence of other sweat-derived cues (Braks et al., 2001).

A complex array of molecular components, which most notably include two classes of chemosensory receptors, odorant receptors (ORs) and ionotropic receptors (IRs), are highly expressed on the antennae and other olfactory appendages of Anopheline females where they have been implicated in the neuronal sensitivity to a range of odorant stimuli (Pitts et al. 2004; Pitts et al. 2017; Sun et al. 2020). While *Ir92a* has been characterized in *Drosophila* as an ammonia receptor expressed in antennal neurons, the molecular pathway of ammonia detection in mosquitoes has remained cryptic due to the lack of a direct homolog to *Drosophila Ir92a* (Benton et al., 2009; Min et al., 2013).

The transportation of ammonium in bacteria, insects, and other animals occurs through the aptly named ammonium transporter (Amt) (Andrade and Einsle, 2007; Pitts et al., 2014a; Tremblay and Hallenbeck, 2009). While bacteria rely on Amt for both ammonium uptake and diffusion (Soupene et al., 2002; Thomas et al., 2000), in *Aedes aegypti*, *AeAmt1* expressed in the anal papillae is involved in ammonium excretion and *AeAmt1* RNAi treated larvae display significantly higher concentrations of ammonium ions in the hemolymph than wild-type mosquitoes (Chasiotis et al., 2016; Durant and Donini, 2018).

More recently, several studies focused on Amt revealed a novel function in mediating ammonia sensitivity in insect chemosensory systems (Delventhal et al., 2017; Menuz et al., 2014; Pitts et al., 2014a). In *Drosophila melanogaster*, the ammonium transporter (*DmAmt*) is expressed in the auxiliary cells of coeloconic ac1 sensilla, in which null mutations result in a loss of antennal sensitivity to ammonia (Menuz et al., 2014). Furthermore, the expression of *DmAmt* in auxiliary cells, as opposed to the olfactory sensory neurons (OSNs), suggested it may not be a molecular sensor of ammonia but rather could be involved in ammonium clearance which prevents neuron desensitization. Studies in *Anopheles coluzzii* (formerly *An. gambiae*; Coetzee et al. 2013) suggested that AcAmt facilitates cross-membrane transport of ammonium ions in a heterogeneous expression system (Pitts et al., 2014a), and, importantly, *AcAmt* is localized in the antennal auxiliary cells of basiconic (grooved pegs) and coeloconic sensilla (Ye et al., 2020). These data suggest there may be conserved functionality between *Drosophila* and mosquitoes, in the latter case where ammonia sensing pathways plays a substantial role in host seeking (Ye et al., 2020). Thus far, technical

difficulties in gene editing in *Anopheles* mosquitoes has precluded elucidation of the olfactory function of AcAmt *in vivo*.

Here we used CRISPR/Cas9 to generate an *AcAmt* null mutant line to examine the hypothesis that *AcAmt* is essential for ammonia responses in *Anopheles* mosquitoes. Surprisingly, *AcAmt* mutants failed to display a significant difference in ammonia peripheral responses in antennal single sensillum recordings (SSRs) as well as in electroantennogram (EAG) and electrolabellogram (ELG) assays compared with wild-type *An. coluzzii*. These results suggest a divergence of ammonia-sensing pathways between *Drosophila* and mosquitoes. Furthermore, we observed *AcAmt* null mutants to be dramatically less efficient in mating and pupal eclosion. A series of behavioral and biochemical assessments were undertaken to investigate the potential mechanisms underlying these behavioral defects.

Material and Methods

Mosquito Rearing

An. coluzzii (SUA 2La/2La), previously known as *Anopheles gambiae sensu stricto* “M-form”(Coetzee et al., 2013), originated from Suakoko, Liberia, were reared using previously described protocols (Fox et al., 2001; Qiu et al., 2004). Briefly, all mosquito lines were reared at 27°C, 75% relative humidity under a 12:12 light:dark cycle (11 h ~250 lux full light, 11 h darkness, with 1 h dawn/dusk gradient transitions in between) and supplied with 10% sugar water in the Vanderbilt University Insectary (Fox

et al., 2001; Suh et al., 2016). Mosquito larvae were reared in 500mL distilled water with 100 larvae per rearing pan. Larval food was prepared by dissolving 0.12g/mL Kaytee Koi's Choice premium fish food (Chilton, WI, US) and 0.06g/mL yeast in distilled water and incubating at 4°C overnight for fermentation. For 0- to 4-day-old larvae, 0.12mL of larval food solution was added daily into each rearing pan; for larvae ≥5 days old, 0.16mL was added.

Mosquito Mutagenesis

CRISPR/Cas9 gene editing in *An. coluzzii* was carried out as previously described (Liu et al., 2020), with minor modifications. The CRISPR gene-targeting vector was a kind gift from Dr. Andrea Crisanti of Imperial College London, UK (Hammond et al., 2016). The single guide RNA (sgRNA) sequences for *AcAmt* gene *Exon 1* and *Exon 4* were designed by CHOPCHOP (http://chopchop.cbu.uib.no/) with high efficiency (**Table 1**) and were synthesized (Integrated DNA Technologies, Coralville, IA) and subcloned into the CRISPR vector by Golden Gate cloning (New England Biolabs, Ipswich, MA). The homologous templates were constructed based on a pHD-DsRed vector (a gift from Kate O'Connor-Giles; Addgene plasmid #51434; http://n2t.net/addgene:51434; RRID:Addgene 51434), in which the 2-kb homologous arms extending either direction from the double-stranded break (DSB) sites were PCR amplified (**Table 1**) and sequentially inserted into the *AarI* and *SapI* restriction sites on the vector, respectively.

The microinjection protocol was carried out as described (Pondeville et al., 2014; Ye et al., 2020). Briefly, newly laid (approximately 1-h old) embryos of the wild-type *An. coluzzii* were immediately collected and aligned on a filter paper moistened with 25mM

Primer	Sequence	Label
forward sgRNA oligo EXON1	5'-TGCTGTGGCCAACGGCACAACGATG-3'	A
reverse sgRNA oligo EXON1	5'-AAACCATCGTTGTGCCGTTGGCCAC-3'	A
forward sgRNA oligo EXON4	5'-TGCTGCTACGCATGGATACGACGAG-3'	B
reverse sgRNA oligo EXON4	5'-AAACCTCGTCGTATCCATGCGTAGC-3'	B
AarI_EXON1_F	5'-GGTACACCTGCGCAGTCGCGTCCAACAAGGGTGCTATAG-3'	C
AarI_EXON1_R	5'-GGACCACCTGCCCTCTTATCGTTGTGCCGTTGGCCATTG-3'	C
SapI_EXON4_F	5'-GAGTGCTCTTCTTATGAGCGGACGATCGGGACTCT-3'	D
SapI_EXON4_R	5'-GGCTGCTCTTCGGACCGATTCGATCACAACATTCAC-3'	D
AcAmt_F	5'-GCGTTTGTGATGCAATAGAACAG-3'	E
AcAmt_R	5'-TTAATCAATCCACGCAAAGTTGCG-3'	E

Table 1. The oligonucleotide primers used in this study. (**A**) sgRNA oligos targeting *Exon 1* of *AcAmt*; (**B**) sgRNA oligos targeting *Exon 4* of *AcAmt*; (**C**) Primers amplifying the homologous arm extending from the DSB site in *Exon 1* which was inserted into the *AarI* site of the homologous template; (**D**) Primers amplifying the homologous arm extending from the DSB site in *Exon 4* which was inserted into the *SapI* site of the homologous template; (**E**) Primers used in the PCR confirmation of *AcAmt* mutagenesis.

sodium chloride solution. All the embryos were fixed on a coverslip with double-sided tape, and a drop of halocarbon oil 27 (Sigma-Aldrich, St. Louis, MO) was applied to cover the embryos. The coverslip was further fixed on a slide under a Zeiss Axiovert 35 microscope with a 40X objective (Zeiss, Oberkochen, Germany). The microinjection was performed using Eppendorf FemtoJet 5247 and quartz needles (Sutter Instrument, Novato, CA). The gene targeting vectors at 300ng/μL were co-injected with the homologous template at 300ng/μL. The injected embryos were placed into deionized water with artificial sea salt (0.3g/L) and reared under lab conditions.

First-generation (G0) injected adults were separated based on sex and crossed with 5X wild-type sex counterparts. Their offspring (F1) were screened for DsRed-derived red eye fluorescence. Red-eyed F1 males were individually crossed with 5X

wild-type females to establish a stable mutant line. PCR analyses of all individuals were performed (after mating) to validate the fluorescence marker insertion using primers that cover the DSB site (**Table 1**). The PCR products were further sequenced to confirm the accurate insertion. The heterozygous mutant lines were back-crossed with the wild-type partners for at least eight generations before putative homozygous individuals were manually screened for DsRed-derived red-eye fluorescence intensity. Putative homozygous mutant individuals were mated to each other before being sacrificed for genomic DNA extraction and PCR analyses (as above) to confirm their genotypes.

Single Sensillum Recording (SSR)

SSR was carried out as previously described (Liu et al., 2013) with minor modifications. Non-blood-fed female mosquitoes (4-10 days post-eclosion) were mounted on a microscope slide (76 x 26 mm) (Ghaninia et al., 2007). The antennae were fixed using double-sided tape to a cover slip resting on a small bead of dental wax to facilitate manipulation, and the cover slip was placed at approximately 30 degrees to the mosquito head. Once mounted, the specimen was placed under an Olympus BX51WI microscope and the antennae viewed at high magnification (1000X). Two tungsten microelectrodes were sharpened in 10% KNO_2 at 10 V. The grounded reference electrode was inserted into the compound eye of the mosquito using a WPI micromanipulator, and the recording electrode was connected to the preamplifier (10X, Syntech) and inserted into the shaft of the olfactory sensillum to complete the electrical circuit to extracellularly record OSN potentials (Den Otter et al., 1980). Controlled manipulation of the recording electrode was performed using a Burleigh

micromanipulator (Model PCS6000). The preamplifier was connected to an analog-to-digital signal converter (IDAC-4, Syntech), which in turn was connected to a computer for signal recording and visualization.

Stock odorants of highest available purity were diluted in paraffin oil to make 10^{-2} (v/v) working solutions. Ammonium hydroxide (Sigma-Aldrich, St. Louis, MO) was serially diluted in water to 0.01, 0.05, 0.1, 0.5, 1, and 5% ammonia solutions. For each odorant, a 10-µL aliquot was applied onto a filter paper (3 x 50mm), which was then inserted into a Pasteur pipette to create the stimulus cartridge. A sample containing the solvent (water/paraffin oil) alone served as the control. The airflow across the antennae was maintained at a constant 20 mL/s throughout the experiment. Purified and humidified air was delivered to the preparation through a glass tube (10-mm inner diameter) perforated by a small hole 10cm away from the end of the tube into which the tip of the Pasteur pipette could be inserted. The stimulus was delivered to the sensilla by inserting the tip of the stimulus cartridge into this hole and diverting a portion of the air stream (0.5L/min) to flow through the stimulus cartridge for 500ms using a stimulus controller (Syntech). The distance between the end of the glass tube and the antennae was ≤ 1cm. Signals were recorded for 10s starting 1s before stimulation, and the action potentials were counted off-line over a 500-ms period before and after stimulation. Spike rates observed during the 500-ms stimulation were subtracted from the spontaneous activities observed in the preceding 500ms and counts recorded in units of spikes/sec.

Electroantennogram (EAG) and Electrolabellogram (ELG)

The EAG and ELG protocols were derived from previous studies (Kwon et al., 2006; Suh et al., 2016; Sun et al., 2020). Briefly, a non-blood-fed, 5- to 10-day-old female mosquito was decapitated with forceps. Two sharp borosilicate glass (1B100F-3; World Precision Instruments, Sarasota, FL) electrodes were prepared using an electrode puller (P-2000; Sutter Instruments, Novato, CA) and filled with Ringer solution (96mM NaCl, 2mM KCl, 1mM $MgCl_2$, 1mM $CaCl_2$, 5mM HEPES, pH = 7.5), in which a AgCl-coated sliver wire was placed in contact to complete a circuit with a reference electrode inserted into the back of the head. Antennal/labellar preparations were continuously exposed to a humidified air flow (1.84L/min) transferred through a borosilicate glass tube (inner diameter = 0.8cm) that was exposed to the preparation at a distance of 10mm. Stimulus cartridges were prepared by transferring 10µl of test or control stimuli solutions to filter paper (3 x 50mm), which was then placed inside a 6-inch Pasteur pipette. Odorant stimuli were delivered to antennal preparations for 500ms through a hole placed on the side of the glass tube located 10cm from the open end of the delivery tube (1.08L/min), where it was mixed with the continuous air flow using a dedicated stimulus controller (Syntech, Hilversum, The Netherlands). An air flow (0.76L/min) was simultaneously delivered from another valve through a blank pipette into the glass tube at the same distance from the preparation in order to minimize changes in flow rate during odor stimulation. The resulting signals were amplified 10x and imported into a PC via an intelligent data acquisition controller (IDAC-232; Syntech, Hilversum, The Netherlands) interface box, and the recordings were analyzed offline using EAG software (EAG Version 2.7, Syntech, Hilversum, The Netherlands). Maximal

response amplitudes of each test stimuli were normalized after dividing by the control (solvent alone) responses.

Pupation and Eclosion Rate Quantification

Each replicate consisted of 80-100 newly hatched 1st instar larvae reared under the same conditions with a density of 10 larvae/50μL dH_2O. Pupae from each replicate were then collected into a mosquito bucket and allowed to eclose. Total pupae were counted and divided by the initial 1st instar larval counts to calculate the pupation rate. The successfully eclosed adults were counted and divided by the pupal counts to measure the eclosion success rate.

Mating Bioassay

Newly emerged wild-type females and males were separated for 1 day. 15 females and 10 males were then placed in a rearing bucket and allowed to freely mate for 5 days. All surviving females were then collected and their spermathecae were dissected under a compound microscope. The spermathecae were then placed in the buffer (145mM NaCl, 4mM KCl, 1mM $MgCl_2$, 1.3mM $CaCl_2$, 5mM D-glucose, 10mM HEPES) (Pitts et al., 2014b) with 300nM DAPI and a cover slip was used to gently press and break the spermathecae to release the sperm. The spermathecae were examined to assess the insemination status under a 1000X compound microscope (BX60; Olympus, Tokyo, Japan). The insemination rate was calculated by dividing the number of inseminated females by the total number of females in each bucket.

Mosquito Locomotor Activity Bioassay

Individual adult mosquitoes (3- to 9-days old) were first anesthetized on ice, then placed in wells of a six-well CytoOne tissue-culture plate (CC7672-7506; USA Scientific, Ocala, FL), and thereafter allowed to recover for at least 30 min prior to trial start. The wells were supplied with a cotton ball soaked in 0.5mL of 10% sugar water. Activity was digitally recorded and analyzed starting at ZT12 (the onset of the dark cycle) and continued through to ZT17. Activity recordings were collected with VideoVelocity software (v3.7.2090, Vancouver, Canada) at one image per second using a USB camera (Spinel, Newport Beach, CA) with built-in 850nm IR light placed ~20cm above the six-well plate.

Digital recordings were analyzed *post hoc* using EthoVision software (v8.5, Noldus, Wageningen, NL) to generate the following activity/mobility parameters: (1) distance travelled, defined as movement of the center-point of the animal (cm); (2) time spent moving relative to time spent not moving using the following parameters defined according to the software: averaging interval, 1 sample; start velocity, 1.00cm/s; stop velocity, 0.90cm/s; (3) clockwise and counterclockwise turns, defined as a cumulative turn angle of 180° with a minimum distance travelled by the animal of at least 0.5cm, with turns in the opposite direction of less than 45.00° ignored; and (4) time the mosquito spent in the half of the well containing the sugar water.

Capillary Feeder (CAFE) Bioassay

The CAFE bioassay was conducted following a previous study with minor modifications (Dennis et al., 2019). Each trial started at ZT12 and ended at ZT18 for 6h. Four 4- to 8-day-old mosquitoes were provided with water but otherwise fasted for 22h before being anesthetized on ice briefly and placed into a *Drosophila* vial (24.5mm x 95mm; Fisher Scientific, Waltham, MA). A borosilicate glass capillary (1B100F-3; World Precision Instruments, Sarasota, FL) was filled with 10% sucrose water and embedded into a cotton plug. The vial opening was then blocked with the cotton plug and the capillary was placed slightly protruding from the plug into the vial for mosquitoes to feed on. The sugar level in the capillary was compared before and after each trial to generate the initial sugar consumption value. At least four control vials with no mosquitoes inside were used to assess the evaporation at the same time. The final sugar consumption was calculated by subtracting the evaporation from the initial sugar consumption value.

Mass Measurements

Individual 3- to 6-day-old mosquitoes were briefly anesthetized on ice and weighed using a XSR Analytical Balance (Mettler Toledo, Columbus, OH).

Ammonia Quantifications

The total ammonia context of adult and pupal stage *An. coluzzii* was assessed according to (Scaraffia et al., 2005) with minor modifications. Here, two 3- to 5-day-old adults or a single ≥1-day-old pupa were homogenized in 150μL distilled water and centrifuged at max speed in a table centrifuge for 2min at 4°C. 100μL supernatant was

used for ammonia level measurement following the manufacturer's instructions of the Ammonia Reagent Set (Pointe Scientific, Canton, MI) (Scaraffia et al., 2005).The absorbance was read at 340nm wavelength using a SmartSpec 3000 spectrophotometer (Bio-Rad, Hercules, CA) and compared with an ammonia standard curve prepared with ammonium chloride to calculate the ammonia concentration.

Carbohydrate Quantification

The total carbohydrate content of adult and pupal stage *An. coluzzii* was assessed according to (Ahmed, 2013; Ellison et al., 2015) with minor modifications. Here, four 3- to 6-day-old mosquitoes or ≥1-day-old pupae were collected between ZT11 and ZT12 and homogenized in 200µL ddH_2O; the homogenate was centrifuged at maximum speed for 1min at 4°C. 10µL of the supernatant was collected from the homogenate and added to a phenol solution of 195µL ddH_2O and 5µL 100% phenol. 500µL sulfuric acid was subsequently added to the solution and briefly vortexed. The colorimetric reaction stood at room temperature for 10min and then the absorbance was read at 490nm wavelength using a SmartSpec 3000 spectrophotometer (Bio-Rad, Hercules, CA). The absorbance was compared with a standard curve prepared with glucose to calculate the carbohydrate content.

Results

Generation of the AcAmt Null Mutant

A complete *AcAmt* null mutant strain was generated using CRISPR/Cas9 gene editing via embryonic microinjection of two targeting plasmids expressing Cas9 and dual sgRNAs along with a homology template to knock-in a *3xP3-DsRed* eye-specific red fluorescence marker between two *AcAmt* DSB sites (Liu et al., 2020). The two sgRNAs targeted sequences at the start of both *Exon 1* and *Exon 4* to remove the majority of the three exons in between the DSBs of the *AcAmt* coding region (**Table 1**). The 2kb homology arms were designed to extend outward from the two DSB sites to insert the

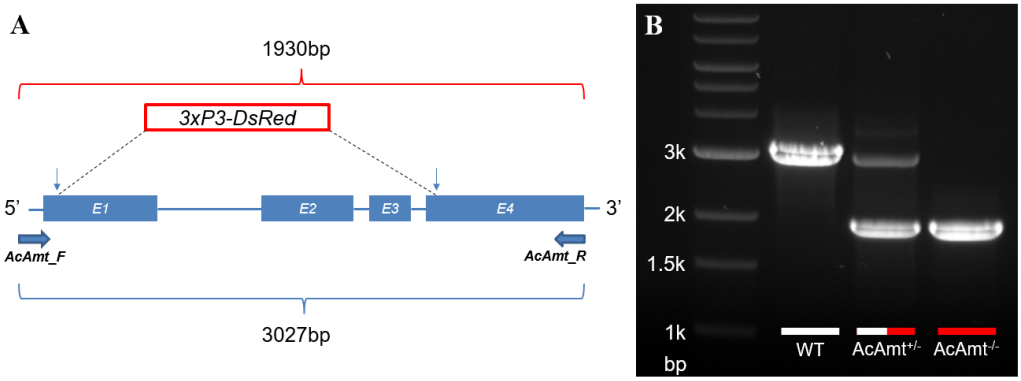

Figure 1. (**A**) Schematics of the CRISPR/Cas9 strategy that induced two double-stranded breaks (indicated by vertical arrows) on *Exon 1* (*E1*) and *Exon 4* (*E4*). A homology template was introduced to replace the sequences in between two double-stranded break sites with a red fluorescence marker *3xP3-DsRed*. A pair of primers (*AcAmt_F* and *AcAmt_R*) were used to determine the successful genetic manipulation. In theory, the wild-type produces a 3027-bp amplicon whereas the mutant renders a 1930-bp amplicon; (**B**) PCR determination of CRISPR/Cas9-mediated mutagenesis in the wild-type (WT), the heterozygotes (*AcAmt*$^{+/-}$), and the homozygotes (*AcAmt*$^{-/-}$).

3xP3-DsRed fluorescence marker (**Figure 1A**). The successful knock-out/knock-in was molecularly confirmed in progeny using both PCR (**Figure 1B**) and DNA sequencing. Homozygous and heterozygous individuals from subsequent backcross generations were selected based on the intensity of red fluorescence that directly correlates to the copy number of *3xP3-DsRed* alleles.

Olfactory Responses to Ammonia

AcAmt expression has been localized to ammonia-sensitive antennal coeloconic sensilla and grooved pegs (Ye et al., 2020), which corresponds to the ammonia-sensing deficit in ac1 sensilla in *Drosophila* (Menuz et al., 2014). Here, SSR studies were carried out to examine whether responses to ammonia in these sensilla are affected by the *AcAmt*$^{-/-}$ mutation (**Figure 2A&2B**). Surprisingly, and in contrast to the significant electrophysiological deficits observed in *DmAmt*$^{-/-}$ mutants (Menuz et al., 2014), indistinguishable dose-dependent responses to ammonia were observed in coeloconic sensilla (**Figure 2C**) and grooved pegs (**Figure 2D**) in both wild-type and *AcAmt*$^{-/-}$ females. Sensillar responses to repeated stimulations of ammonia were also assessed in order to saturate the sensillar lymph and potentially uncover a requirement for the putative clearance function of Amt (Menuz et al., 2014). Despite this additional challenge, no significant differences were observed in SSR responses across coeloconic sensilla (**Figure 2E**) and grooved pegs (**Figure 2F**) in wild-type and *AcAmt*$^{-/-}$ female antennae. To investigate whether the *AcAmt*$^{-/-}$ mutation alters sensillar responses to other odorants, we characterized the response profiles of coeloconic sensilla to an odorant panel of amines, acids, ketones, aldehydes, and alcohols (**Figure 3A**). Most amines and acids evoked strong, albeit not significantly different, responses in wild-type and *AcAmt*$^{-/-}$ females (**Figure 3B**), as opposed to the weak responses elicited by other general odorants (**Figure 3C**).

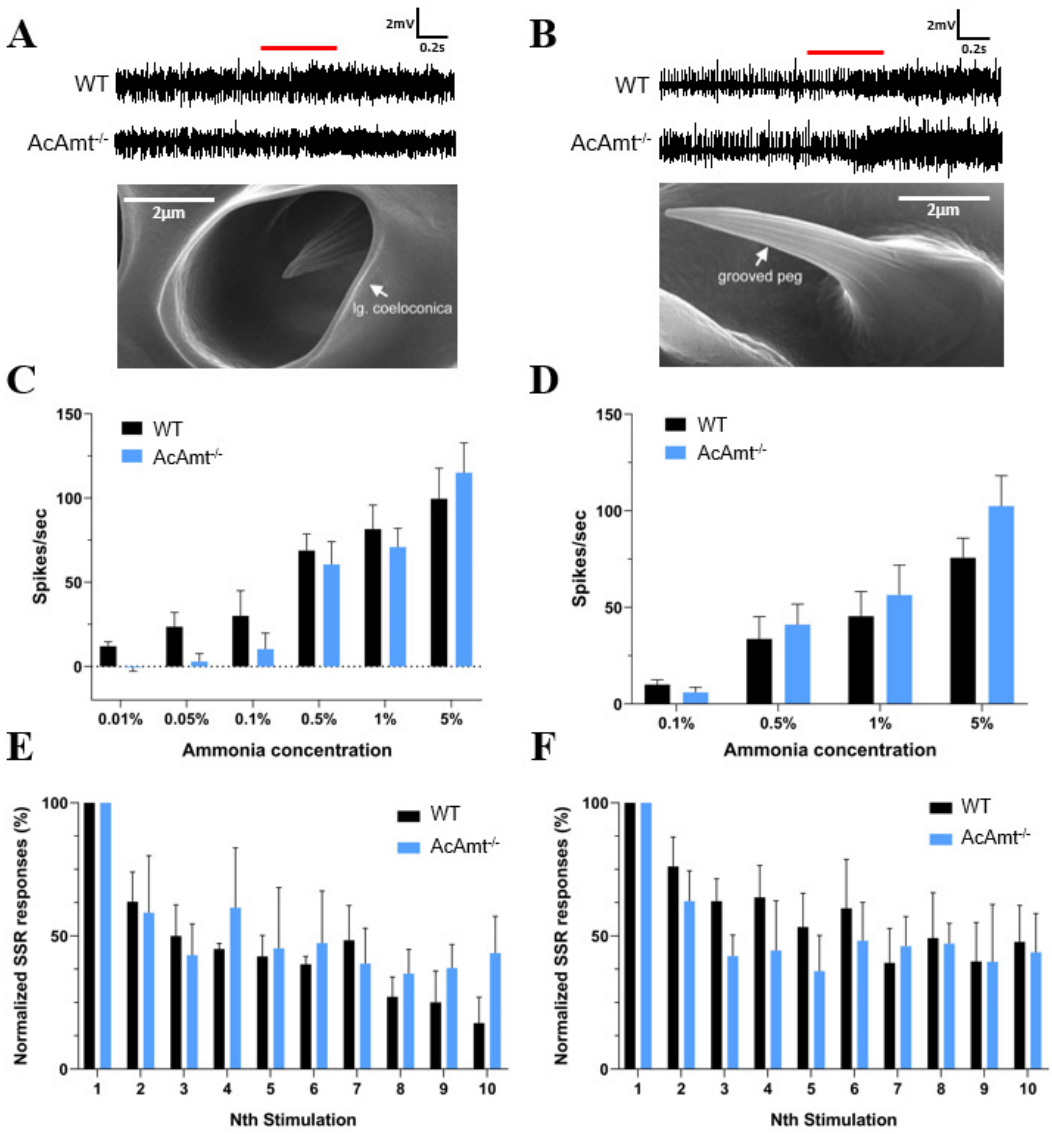

Figure 2. (**A**) Representative single-sensillum recordings from representative single-sensillum recording responses of coeloconic sensilla to 1% ammonia. Red bar indicates the duration of stimulations (0.5s). The scanning electron microscopy image showing the structure of a coeloconic sensillum is adopted from (Pitts and Zwiebel, 2006); (**B**) Representative single-sensillum recording responses of grooved pegs to 0.5% ammonia. Red bar indicates the duration of stimulations (0.5s). The scanning electron microscopy image showing the structure of a grooved peg is adopted from (Pitts and Zwiebel, 2006); (**C**) Single-sensillum responses of coeloconic sensilla to ammonia at different concentrations (N=5-7 for each concentration); (**D**) Single-sensillum responses of grooved pegs to ammonia at different concentrations (N=7-9 for each concentration);

(Continued from previous page)

(**E**) Multiple single-sensillum responses of coeloconic sensilla to 1% ammonia with 5-s intervals (N=3). The responses were normalized to the fraction of the first stimulation; (**F**) Multiple single-sensillum responses of grooved pegs to 0.5% ammonia with 5-s intervals (N=3-5). The responses were normalized to the fraction of the first stimulation. Multiple t-tests with Holm-Sidak method suggest no significant differences ($P > 0.05$) between the wild-type and *AcAmt*$^{-/-}$. Error bars = Standard error of the mean.

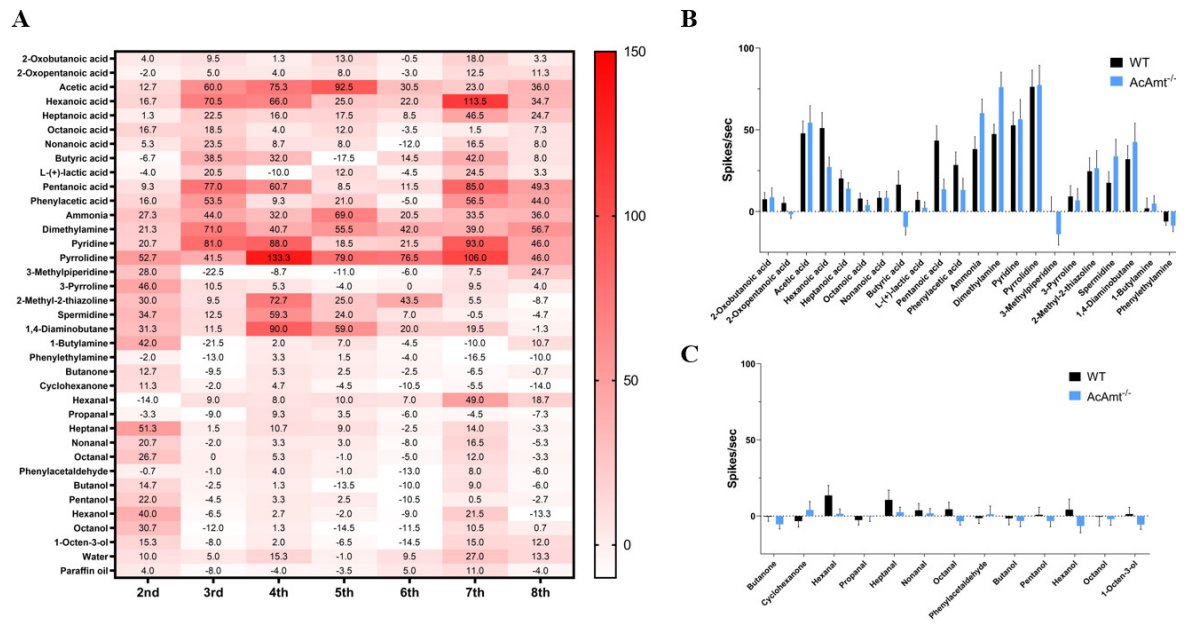

Figure 3. (**A**) Single-sensillum recording on wild-type female coeloconic sensilla. The heatmap showing mean responses to odorants (y-axis) in coeloconic sensilla on 2nd-8th flagellomeres (x-axis; N=3-4 for each flagellomere); (**B**) Comparison of single-sensillum responses to amines and acids on total coeloconic sensilla between wild-type and *AcAmt*$^{-/-}$ females (Multiple t-tests with Holm-Sidak method; N=2-4 for each from flagellomere 2nd-8th; N=23-25 in total); (**C**) Comparison of single-sensillum responses to ketones, aldehydes, and alcohols on total coeloconic sensilla between wild-type and *AcAmt*$^{-/-}$ females (Multiple t-tests using Holm-Sidak method; N=2-4 for each from flagellomere 2nd-8th; N=23-25 in total). Error bars = Standard error of the mean.

Transcuticular EAG studies were also used to examine peripheral dose-dependent responses to ammonia at the whole-appendage level. Inasmuch as wild-type

EAG responses to ammonia displayed both depolarization (downward) and hyperpolarization (upward) deflections relative to baseline (**Figure 4A**), these data were analyzed across both components. Once again, no significant differences were observed in dose-dependent antennal responses to ammonia (**Figure 4B&4C**) nor in response to the positive controls 1-octen-3-ol (**Figure 4D**) and butylamine (**Figure 4E**) which display robust dose-dependent depolarizations in both mutant and wild-type mosquitoes. Together, these data suggest ammonia responses across the antennae

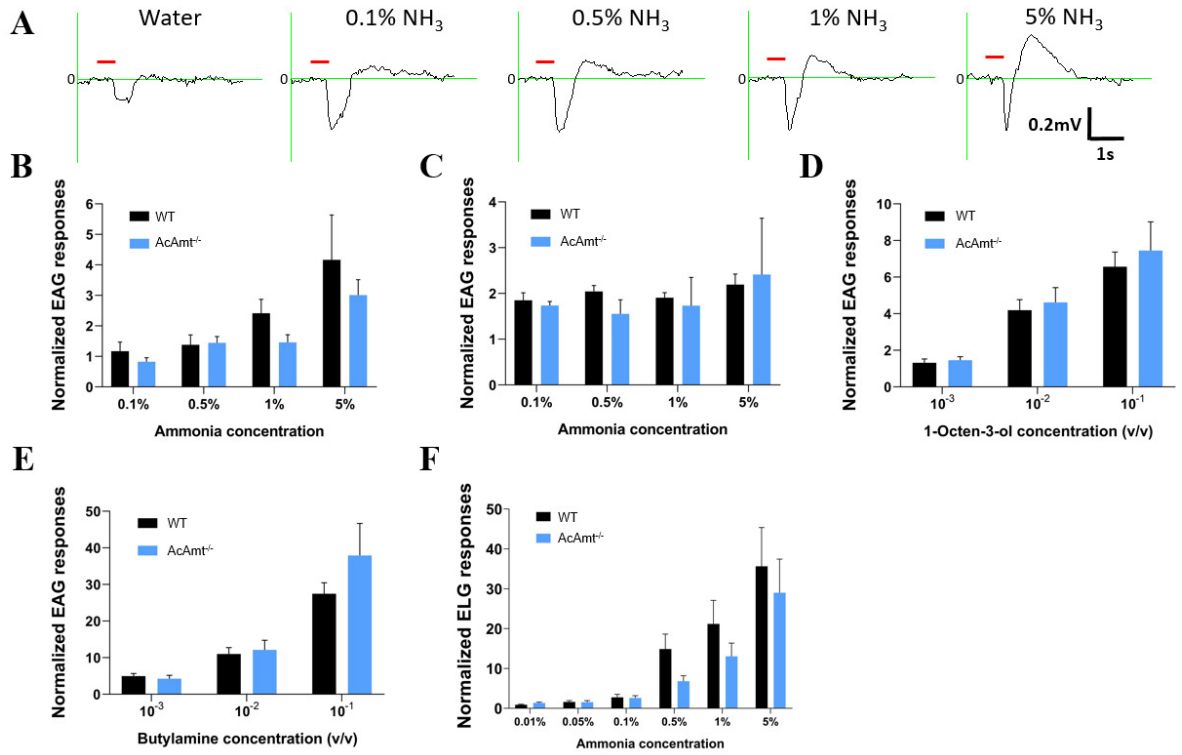

Figure 4. (**A**) Representative EAG responses of the wild-type to water and ammonia; Red bar indicates the duration of stimulations (0.5s). (**B**) Upward EAG responses to ammonia at different concentrations (N=6 for each concentration); (**C**) Downward EAG responses to ammonia at different concentrations (N=6 for each concentration); (**D**) EAG responses to 1-octen-3-ol at different concentrations (N=6 for each concentration); (**E**) EAG responses to butylamine at different concentrations (N=6 for each concentration); (**F**) ELG responses to ammonia at different concentrations (N=8-15 for each concentration). Multiple t-tests using Holm-Sidak method suggest no significant differences (P > 0.05) between the wild-type and *AcAmt*$^{-/-}$. Error bars = Standard error of the mean.

are not altered in *AcAmt*$^{-/-}$ females. We also examined the role of *AcAmt* in peripheral responses to ammonia on the mosquito labella where it is also highly expressed (Pitts et al. 2014a; Ye et al. 2020) using ELG recording preparations. As was the case for the antennae, these studies demonstrated that both wild-type and *AcAmt*$^{-/-}$ female labella display dose-dependent responses to ammonia with no significant differences (**Figure 4F**).

Reproductive Deficits in AcAmt Null Mutants

In contrast to the absence of mutant olfactory phenotypes in response to ammonia, *AcAmt*$^{-/-}$ mutants displayed a broad range of deficits associated with reproductive fitness and fecundity that resulted in a striking difficulty to propagate the *AcAmt*$^{-/-}$ mutant line. To assess this issue, we utilized a simple group mating bioassay (**Figure 5A**) to quantify female insemination rates (**Figure 5B**) which uncovered significant mating deficits in *AcAmt*$^{-/-}$ mutants compared with the wild-type and *AcAmt*$^{+/-}$ heterozygotes (**Figure 5C**). Importantly, this phenotype is not sex-specific as these mating deficits persist when pairing either female or male *AcAmt*$^{-/-}$ mosquitoes with wild-type counterparts (**Figure 5C**). In order to investigate whether these phenotypes derived from shared or sex-independent mechanisms, we first examined male-specific processes such as sperm mobility. Here, *AcAmt*$^{+/-}$ males, which produce both mutant and wild-type spermatozoa, were crossed with wild-type females thereby allowing the wild-type sperm to compete with mutant sperm throughout reproduction which is a multi-step process comprising insemination (i.e., the delivery of sperm to the female spermatheca) as well as subsequent sperm activation and oocyte fertilization.

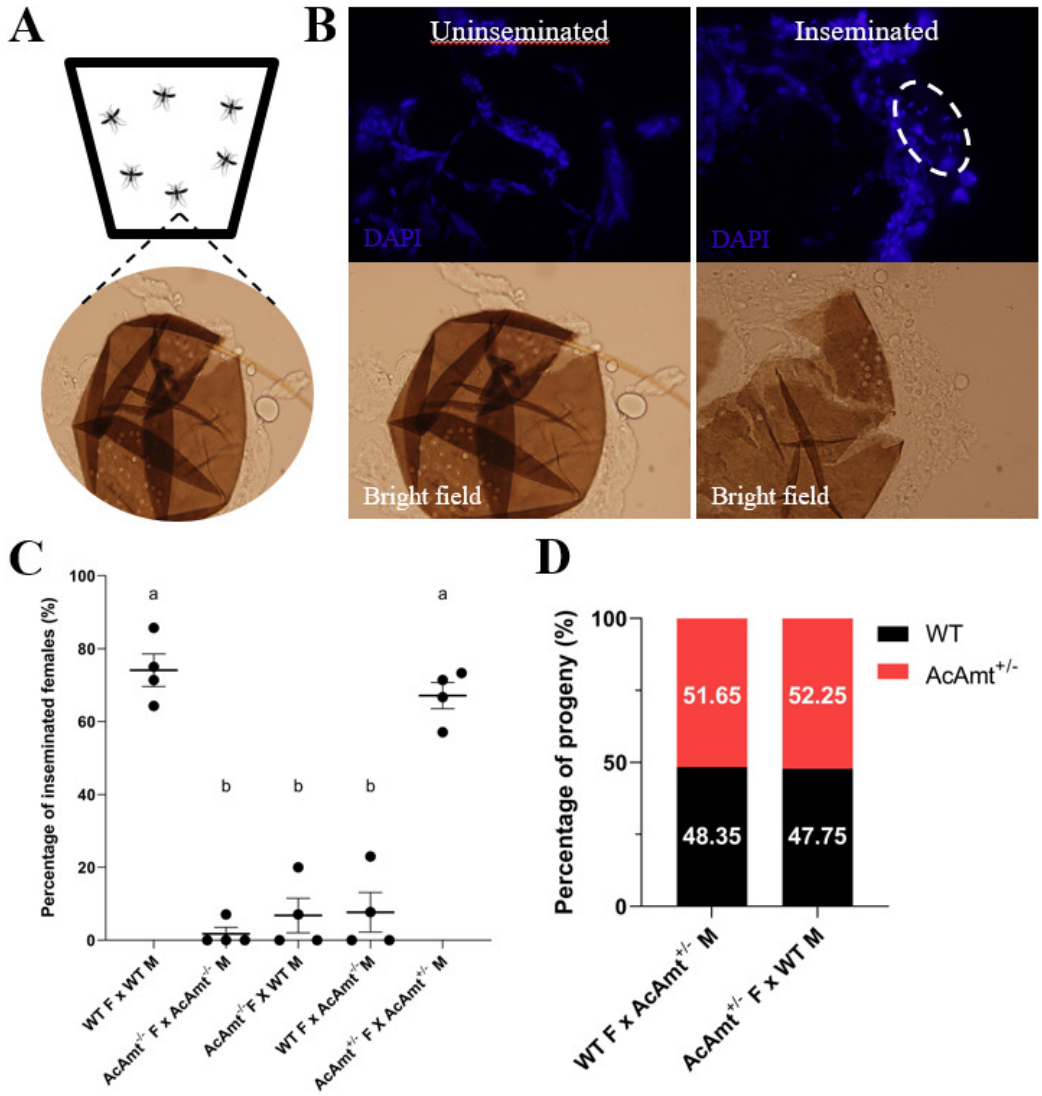

Figure 5. (**A**) Schematics of the mating bioassay. The females and males were allowed to mate in a bucket for 5 days before the female spermathecae were dissected; (**B**) Representation of inseminated and un-inseminated spermathecae stained with DAPI. The sperm heads are circled by dashed line; (**C**) Insemination rate of females in different mating pairs (F: females; M: males). Mean values with different grouping letters were significantly different (N=4; One-way ANOVA; $P < 0.05$); (**D**) Progeny ratio (wild-type versus *AcAmt*$^{+/-}$) from two mating pairs to test sperm competency. Chi-square test suggests the ratio is not significantly different from 50% versus 50% (N=3-4; $P > 0.05$). Error bars = Standard error of the mean.

In this context, we quantified the number of heterozygous versus wild-type larvae distinguished by means of DsRed-derived fluorescence. In these studies, the consistent ratios of larval progeny showed there is no significant difference between the wild-type and *AcAmt* mutant sperm (**Figure 5D**). This suggests that the *AcAmt*$^{-/-}$ mating deficits may be due to a reduction of the frequency of successful copulation, which raises the potential of broader deficits in overall metabolism that in turn impact general activity levels.

To assess activity profiles, individual male and female adult mosquitoes were digitally recorded in the scotophase between ZT12 and ZT17, which encompasses the peak period for Anopheline mating (Charlwood and Jones, 1980; Howell and Knols, 2009), and subsequently analyzed across several activity/mobility parameters, including distance travelled, the proportion of time spent near sugar water, the proportion of time spent moving, and the sum of clockwise and counterclockwise turns. Across the entire trial, both wild-type and *AcAmt*$^{-/-}$ mutant females displayed a burst of activity within the first hour of the scotophase, followed by a prolonged period of relative quiescence (**Figure 6A**). Although the mean distance travelled over the full duration of the trial was relatively lower in males than females, a similar trend of activity and quiescence was also observed in both wild-type and *AcAmt*$^{-/-}$ mutant males (**Figure 6B**). Furthermore, an analysis of all the activity/mobility parameters examined across the full duration of the bioassay failed to indicate any significant differences between wild-type or *AcAmt*$^{-/-}$ mutant genotypes for either female or male adult mosquitoes (**Figure 6C-6J**). That said, these cumulative data largely reflect the prolonged period of inactivity, resulting in mean

values that tend to converge the longer the mosquitoes remain inactive (**Figure 6A&6B**).

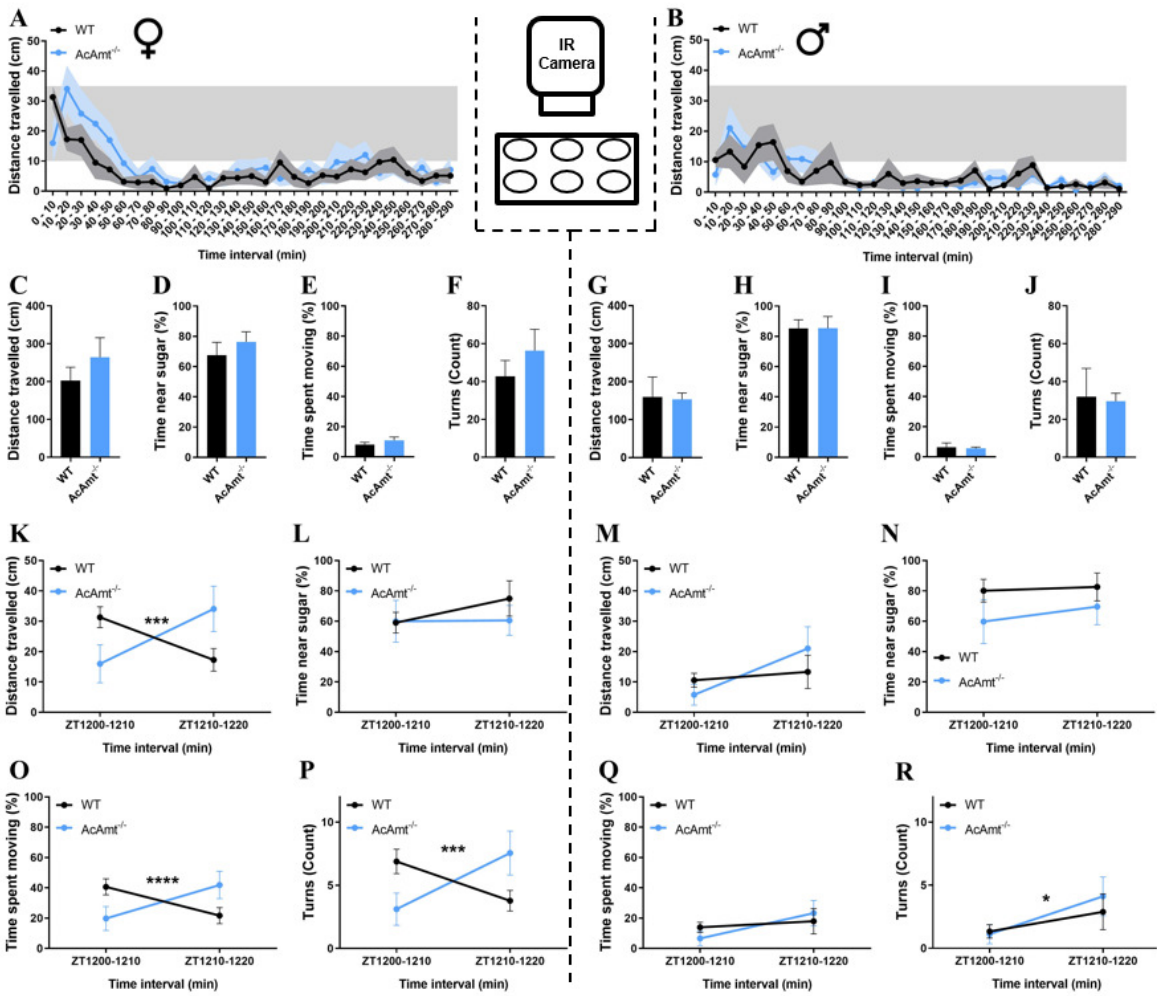

Figure 6. (**A-B**) Video recordings of individual mosquitoes showing distance travelled during the activity bioassay for wild-type and *AcAmt*$^{-/-}$ mutant females (**A**) and males (**B**) organized into 10-min bins. Sex-specific data are separated by dashed lines. (**C-J**) Mobility parameters, including mean distance travelled (cm), time spent near the sugar water (%), time spent moving (%), and turning frequency (count) for females (**C-F**) and males (**G-J**) over the full duration of the bioassay (N=9; t-test with Welch's correction); (**K-R**) Mobility parameters for females (**K-L**, **O-P**) and males (**M-N**, **Q-R**) over the first 20 min of the dark cycle organized into 10-min bins (N=9; Two-way repeated measures ANOVA; * < 0.05. *** = 0.0001. **** < 0.0001). Error bars = Standard error of the mean.

Inasmuch as the majority of mating in *An. coluzzii* occurs proximate to the dusk transition at start of the scotophase (Charlwood and Jones, 1980; Howell and Knols, 2009), we looked for more nuanced differences within this initial window. Here, wild-type females appeared to be more active within the first 10 min of the scotophase, while *AcAmt*$^{-/-}$ mutant females manifested a modest latency in movement, which subsequently was higher than the wild-type females (**Figure 6A**). To address this more formally, we statistically analyzed activity levels within two discrete 10-min intervals that together represent the initial 20 min of the dark component of the light:dark cycle (ZT1200-1220). In this interval, while female mosquitoes showed no significant difference in the time spent near the sugar water, a significant interaction effect was observed between genotype and time with respect to distance moved ($F(1, 16) = 26.28$, $P = 0.0001$), the proportion of time spent moving ($F(1, 16) = 27.99$, $P < 0.0001$), and turning frequency ($F(1, 16) = 24.59$, $P = 0.0001$) (**Figure 6K-6L&6O-6P**). In males, apart from a modest but nevertheless significant ZT-dependent effect on turning frequency, in which both wild-type and *AcAmt*$^{-/-}$ mutants turned more frequently in the ZT1210-ZT1220 interval than in ZT1200-ZT1210, no differences were observed (**Figure 6M-6N&6Q-6R**). Taken together, these results suggest that there are significant differences in activity levels between wild-type and *AcAmt*$^{-/-}$ mutant females that correspond to the onset of the dark cycle and the peak period of mating (Charlwood and Jones, 1980; Howell and Knols, 2009). Specifically, *AcAmt*$^{-/-}$ mutant females experience a delay in activity compared with their wild-type counterparts, which are most active at the onset of the dark cycle; this may contribute to mating deficiencies during this critical time window by desynchronization of peak activity between the sexes.

Eclosion Phenotypes

In addition to mating phenotypes, we also observed an interesting developmental deficit characterized by a significantly higher level of pharate mortality during eclosion of pupae to adults in *AcAmt*$^{-/-}$ mutants compared with wild-type individuals raised under identical conditions and larval density levels (**Figure 7A&7B**). This phenotype does not appear to have a gender bias as approximately equal ratios of male and female *AcAmt*$^{-/-}$ mosquitoes are represented in the reduced numbers of adults that nevertheless survive. Furthermore, *AcAmt*$^{-/-}$ mosquitoes displayed the same pupation rate (**Figure 7C**) and general development timing as their wild-type and *AcAmt*$^{+/-}$ counterparts, supporting the view that *AcAmt* mutations do not significantly influence larval or pupal stage development. Instead, these data suggest that post-eclosion reduction in viable *AcAmt*$^{-/-}$ adults results exclusively from the failure of pharate adult *AcAmt*$^{-/-}$ mutants to successfully eclose and fully emerge from their pupal cases. Taken together with the

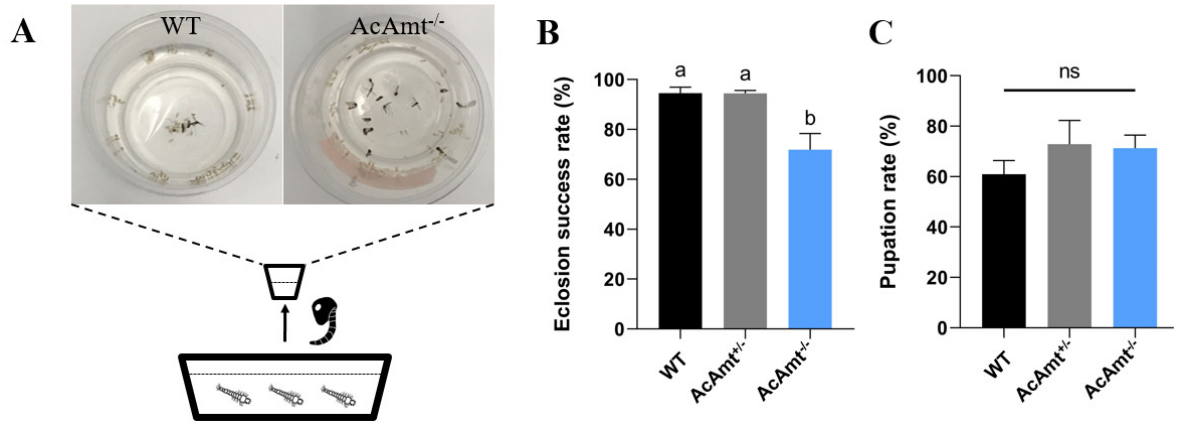

Figure 7. (**A**) Schematics of larval rearing in pan. Pupae were consequently placed in cups to examine eclosion rate. A representative image showing a higher mortality in *AcAmt*$^{-/-}$ during eclosion; (**B**) Eclosion success rate. Mean values with different grouping letters were significantly different (N=5; One-way ANOVA; $P < 0.05$); (**C**) Pupation rate. One-way ANOVA suggests no significant differences among the three groups (N=5; $P > 0.05$). Error bars = Standard error of the mean.

broad mating deficits of *AcAmt*$^{-/-}$ mutants, these phenotypes raise the possibility that these mutants have an inability to effectively excrete or otherwise manage metabolic ammonia during these two intensively active processes resulting in toxic levels of ammonia that ultimately impact these critical behaviors.

Elevated Ammonia Levels in AcAmt Null Mutants

RNAi-mediated silencing of *AeAmt1* has been shown to induce elevation of ammonia levels in the larval hemolymph of *Ae. aegypti* (Chasiotis et al., 2016). In order to assess this possibility in our *AcAmt*$^{-/-}$ mutants, we used a simple colorimetric reagent to enzymatically measure whole-body ammonia levels in mating-stage adults and late-stage pupae (**Figure 8A**). These quantitative data indicate that while there was no alteration in ammonia levels for adult males regardless of genotype, mating-stage

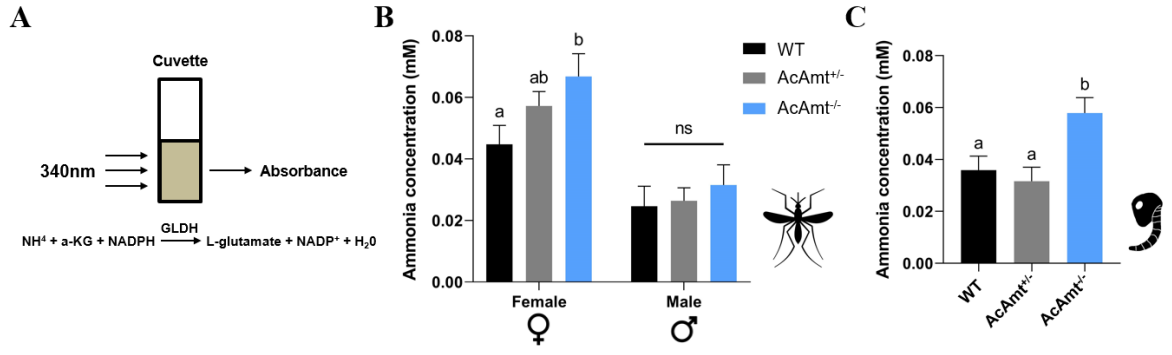

Figure 8. (**A**) Ammonia reacts with α-ketoglutarate (α-KG) and reduced nicotinamide adenine dinucleotide phosphate (NADPH) to form L-glutamate and NADP in a reaction catalyzed by glutamate dehydrogenase (GLDH) {L-glutamate: NAD(P) + oxidoreductase (deaminating), EC 1.4.1.3}, which is followed by a reduction of absorbance at 340nm; (**B**) Ammonia concentration in mosquito adults. Mean values with different grouping letters were significantly different (N=10-18; One-way ANOVA; $P < 0.05$); (**C**) Ammonia concentration in mosquito pupae. Mean values with different grouping letters were significantly different (N=12; One-way ANOVA; $P < 0.05$). Error bars = Standard error of the mean.

AcAmt$^{-/-}$ females exhibited significantly higher levels of ammonia than wild-type females or *AcAmt*$^{+/-}$ heterozygotes that displayed intermediate levels of ammonia (**Figure 8B**). Similarly, significant increases in ammonia levels were detected in unsexed late-stage *AcAmt*$^{-/-}$ pupae relative to wild-type or *AcAmt*$^{+/-}$ heterozygote counterparts (**Figure 8C**).

Sugar Feeding and Carbohydrate Levels in AcAmt Mutants

The mating/eclosion phenotypes may also be the result of a potential defect in energy content and/or sugar feeding that play an essential role in mosquito mating and other behaviors (Gary et al., 2009). To examine this, we used a modified capillary feeder (CAFE) bioassay (**Figure 9A**) to measure adult sugar feeding during the same ZT12-ZT18 interval when Anopheline mating is most likely to occur (Howell and Knols, 2009). In these studies, only *AcAmt*$^{-/-}$ males exhibited a significantly lower sugar consumption than the wild-type and *AcAmt*$^{+/-}$ males (**Figure 9B**). Water-only CAFE

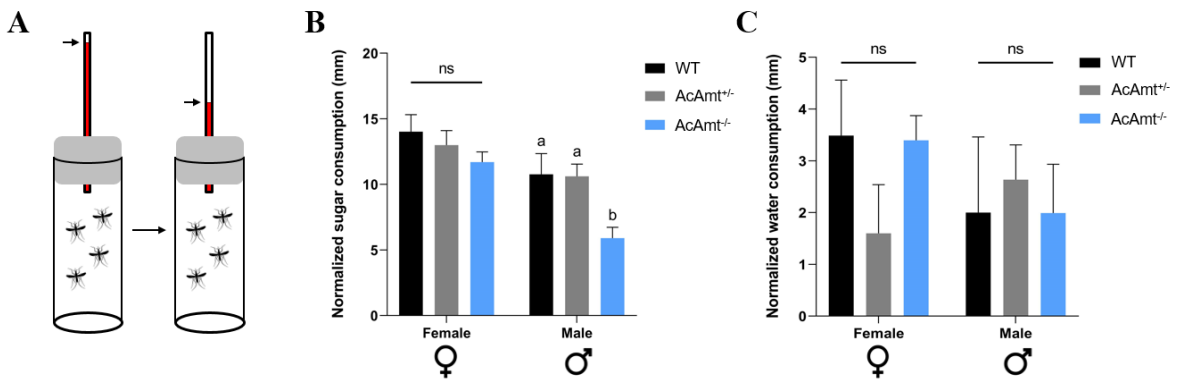

Figure 9. (**A**) Schematics of modified CAFE bioassay where the consumption was quantified by sugar level reduction marked on the capillary; (**B**) Sugar feeding ability in mosquito adults. Mean values with different grouping letters were significantly different (N=6-8; One-way ANOVA; $P < 0.05$); (**C**) Water consumption controls in mosquito adults. One-way ANOVA suggests no significant differences among the three groups (N=6-8). Error bars = Standard error of the mean.

controls were also conducted, which demonstrated that the male-specific defect is restricted to sugar feeding (**Figure 9C**).

To further examine the potential impact of sugar feeding deficits on adult mating and pupal eclosion, respectively, we collected adults at ZT11 just before the onset of mating and late-stage pupae 12h before eclosion and used the phenol-sulfuric acid method (Ahmed, 2013; Ellison et al., 2015) to assess whole-body carbohydrate levels across wild-type and *AcAmt* mutant genotypes. Once again, while there were no

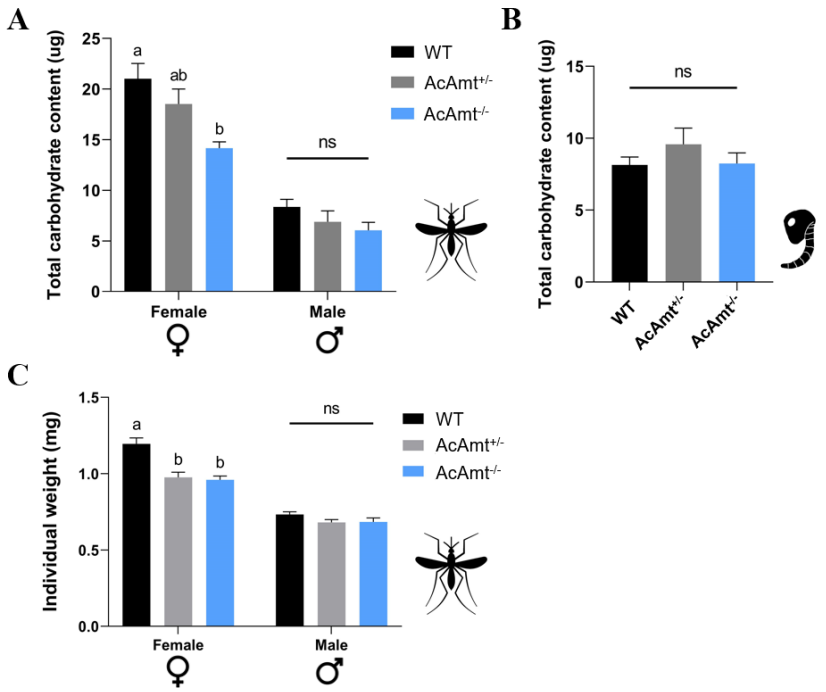

Figure 10. (**A**) Total carbohydrate content in mosquito adults. Mean values with different grouping letters were significantly different (N=8; One-way ANOVA; $P < 0.05$); (**B**) Total carbohydrate content in mosquito pupae. Mean values with different grouping letters were significantly different (N=6; One-way ANOVA; $P < 0.05$); (**C**) Individual mosquito adult weights. Mean values with different grouping letters were significantly different (N=10-15; One-way ANOVA; $P < 0.05$). Error bars = Standard error of the mean.

significant differences across adult male genotypes, *AcAmt*$^{-/-}$ females exhibited significantly lower total carbohydrate content than wild-type or the intermediate levels seen in *AcAmt*$^{+/-}$ heterozygotes (**Figure 10A&10B**). In order to control for larger individuals artifactually accounting for these higher carbohydrate contents, mosquitoes were sampled and weighed prior to homogenization. Correspondingly, this analysis revealed that both *AcAmt*$^{-/-}$ and *AcAmt*$^{+/-}$ females weighed significantly less than wild-type females (**Figure 10C**), which suggests their lower carbohydrate contents may, in part, reflect this physical characteristic.

Discussion

In *Drosophila*, *DmAmt* null mutants demonstrated a dramatic reduction of ac1 sensilla responses to ammonia where *DmAmt* is expressed in auxiliary cells and hypothesized to be involved in ammonium clearance (Menuz et al., 2014), while no such phenotype was observed in the labella where *DmAmt* is exclusively neuronal (Delventhal et al., 2017). We now report a comprehensive investigation in the malaria vector mosquito *An. coluzzii* of *AcAmt* null mutant olfactory responses to ammonia. This analysis encompasses both antennal grooved pegs and coeloconic sensilla, where *AcAmt* is primarily expressed in auxiliary cells, as well as the labella where *AcAmt* was observed in olfactory and non-olfactory neurons (Ye et al., 2020). In contrast to *Drosophila*, no significant reduction of peripheral neuron sensitivity to ammonia was found in either antennae or labella of *AcAmt*$^{-/-}$ mutants. It is noteworthy that, in addition to *AcAmt*, another ammonium transporter, *Rh50*, is highly expressed on the mosquito antennae (Pitts et al., 2014a), which in light of these data is to likely play a

complementary role in the ammonia-sensing and management pathways. This is consistent with a previous study in *Drosophila*, in which ammonia responses in ac3 and ac4 sensilla on female antennae where *DmRh50* is expressed were not impacted by the *DmAmt* mutation (Menuz et al., 2014).

While the receptors and other components underlying ammonia-sensing mechanisms in the mosquito olfactory system remain unknown, attraction to ammonia plays a significant role in host-seeking behaviors by *Anopheles* females (Braks et al., 2001; Smallegange et al., 2005). This makes it likely that sensitivity to ammonia is sufficiently essential in anautogenous mosquitoes to drive the evolution of parallel and complementary ammonia sensitivity processes. In light of the lack of *AcAmt*$^{-/-}$ deficits in *An. coluzzii* olfaction, comprehensive localization and characterization of the ammonium transporter *Rh50* will be critically informative. Indeed, it is reasonable to speculate that significant impairment of olfactory responses to ammonia might require mutations of both *AcAmt* and *Rh50*.

In addition to the peripheral olfactory responses to ammonia, ammonium transporters have recently been shown to be involved in other essential functions in the biology of insects including male fertility in *Ae. aegypti* (Durant and Donini, 2020) and larval muscle control in *Drosophila* (Lecompte et al., 2020). Here, CRISPR/Cas9-induced *AcAmt*$^{-/-}$ mutations similarly uncover several potentially non-olfactory phenotypes in *An. coluzzii* that are likely to significantly reduce the overall fitness of these mutants. Even so, while significant fecundity deficits are reported here in *AcAmt*$^{-/-}$ mutants and *AeAmt* RNAi treatments in *Ae. aegypti* (Durant and Donini, 2020), these phenotypes are likely to result from fundamentally different mechanisms working

synergistically. In *An. coluzzii*, the frequency of successful copulation (sperm delivery) is significantly reduced in both *AcAmt*$^{-/-}$ females and males, while the decrease of fecundity in *Ae. aegypti* appears to be due to a significant reduction in viable spermatozoa (Durant and Donini, 2020). Importantly, this latter phenotype is specifically not observed in *An. coluzzii* mating studies. Instead, data reported here suggest that the absence of *AcAmt* results in subtle but nevertheless significantly altered activity profiles during the circadian interval most associated with mating (Charlwood and Jones, 1980; Howell and Knols, 2009). Even more compelling is the *AcAmt*-dependent elevation of endogenous ammonia levels that may rise above physiologically toxic thresholds in mating-stage adults and late-stage pupae as the likely mechanism responsible for these mating as well as the eclosion deficits we report. This rationale aligns with increased ammonia levels and hemolymph acidification found in *Ae. aegypti* larvae treated with *AeAmt*/*AeRh50*-targeted RNAi (Chasiotis et al., 2016; Durant et al., 2017; Durant and Donini, 2018) and suggests that *AcAmt* is similarly involved in ammonia management/excretion systems in *Anopheles* mosquitoes. This is consistent with our recent hypothesis implicating *AcAmt* in neural toxicity and ammonia homeostasis (Ye et al., 2020).

During mating, both male and female mosquitoes monitor each other's wing beat frequency to actively modulate these activities toward convergence (Cator et al., 2009; Gibson et al., 2010; Gibson and Russell, 2006; Robert, 2009). This auditory interaction between females and males has been suggested to serve an important role in conspecific mating recognition and, in that context, directly contributes to mosquito reproductive fitness (Cator et al., 2009; Robert, 2009). This has indeed been shown to

contribute to the reproductive isolation between “M” and “S” forms of *An. gambiae* now recognized as distinct species (Coetzee et al., 2013), which utilize wing beat frequency to recognize potential mates within their own molecular form/species (Pennetier et al., 2010). Notably, this mating interaction requires not only auditory interactions, but also the coordination of wing movement to match the frequencies of corresponding partners (Robert, 2009). While uncharacterized in mosquitoes, *Drosophila* leg and wing muscles are innervated with glutamatergic neurons, and, not surprisingly, the malfunction of these neurons impairs fly movement (Gowda et al., 2018; Sadaf et al., 2015). Inasmuch as *Anopheles* mosquitoes rely on muscle coordination to achieve a matching of wing-beat frequencies between females and males for mating recognition (Pennetier et al., 2010), the absence of *AcAmt* function may impact neuronal function to impair muscle control and the auditory/wing beat frequency convergence required during mating.

With regard to the eclosion deficits displayed by *AcAmt* mutants, it is reasonable to conclude that successful emergence from the pupal case requires similarly substantial muscular coordination and effort such that failure to physiologically manage ammonia/acid levels could well be lethal.

In light of these data as well as recent studies in *Ae aegypti* demonstrating that volatile amines activate IR-mediated signaling in ORNs as well as CO_2-sensitive maxillary palp neurons (Younger et al., 2020), it appears likely that multiple complementary systems exist in mosquitoes to ensure ammonia and volatile amine detection, which is critical for host seeking and reproduction. Similarly, it seems likely that Amts, Rh50s, as well as other cryptic ammonium transporters are involved in distinct functional pathways where they play essential roles in supporting locomotion

and behavior. Taken together with our recent *AcAmt* localization study (Ye et al., 2020), the CRISPR/Cas9-mediated genome-editing studies reported here suggest that *AcAmt* is functional across a variety of systems that involve olfaction, reproduction, and ammonia metabolism. Whereas further integrative studies on different ammonium transporter genes will doubtlessly reveal more detail regarding these functions, the broad footprint of *AcAmt* activity, especially insofar as its impact on mosquito fecundity, supports its role as an important target for the development of novel vector-control strategies.

Acknowledgements

We thank Zhen Li for mosquito rearing and all members of the Zwiebel lab for critical suggestions, as well as Drs. Julian Hillyer, Maulik Patel, Wenbiao Chen, and Patrick Abbot (Vanderbilt University) for valuable advice throughout the course of this work. We also thank Dr. Samuel Ochieng for technical support in conducting ELGs, Dr. Willi Honegger for comments on the manuscript and Dr. AM McAinsh for scientific copy-editing. This work was conducted with the support of Vanderbilt University and funded by the National Institutes of Health (NIAID, R21-113960) to RJP and LJZ.

Author contributions

Conceived experiments: ZY, FL, STF, RJP and LJZ; Performed research: ZY, FL, and STF; Analyzed data: ZY, FL, STF, and AB; Wrote the paper: ZY, FL, STF, AB, RJP, and LJZ. Approved the final manuscript: ZY, FL, STF, AB, RJP, and LJZ.

References

Ahmed, A.M., 2013. Mosquito autogeny in *Aedes caspius* (Diptera: Culicidae): Alterations of larval nourishments reservation upon bacterial infection. Insect Sci. https://doi.org/10.1111/j.1744-7917.2012.01544.x

Andrade, S.L.A., Einsle, O., 2007. The Amt/Mep/Rh family of ammonium transport proteins (Review). Mol. Membr. Biol. 24, 357–365. https://doi.org/10.1080/09687680701388423

Benton, R., Vannice, K.S., Gomez-Diaz, C., Vosshall, L.B., 2009. Variant ionotropic glutamate receptors as chemosensory receptors in *Drosophila*. Cell 136, 149–162. https://doi.org/10.1016/j.cell.2008.12.001

Braks, M.A.H., Meijerink, J., Takken, W., 2001. The response of the malaria mosquito, *Anopheles gambiae*, to two components of human sweat, ammonia and L-lactic acid, in an olfactometer. Physiol. Entomol. 26, 142–148. https://doi.org/10.1046/j.1365-3032.2001.00227.x

Carey, A.F., Carlson, J.R., 2011. Insect olfaction from model systems to disease control. Proc. Natl. Acad. Sci. U. S. A. 108, 12987–12995. https://doi.org/10.1073/pnas.1103472108

Cator, L.J., Arthur, B.J., Harrington, L.C., Hoy, R.R., 2009. Harmonic convergence in the love songs of the dengue vector mosquito. Science (80-.). 323, 1077–1079. https://doi.org/10.1126/science.1166541

Charlwood, J.D., Jones, M.D.R., 1980. Mating in the mosquito, *Anopheles gambiae s.l.* II. Swarming behaviour. Physiol. Entomol. 5, 315–320.

https://doi.org/10.1111/j.1365-3032.1980.tb00241.x

Chasiotis, H., Ionescu, A., Misyura, L., Bui, P., Fazio, K., Wang, J., Patrick, M., Weihrauch, D., Donini, A., 2016. An animal homolog of plant Mep/Amt transporters promotes ammonia excretion by the anal papillae of the disease vector mosquito *Aedes aegypti*. J. Exp. Biol. 219, 1346–1355. https://doi.org/10.1242/jeb.134494

Coetzee, M., Hunt, R.H., Wilkerson, R., Torre, A. Della, Coulibaly, M.B., Besansky, N.J., 2013. *Anopheles coluzzii* and *Anopheles amharicus*, new members of the anopheles gambiae complex. Zootaxa 3619, 246–274. https://doi.org/10.11646/zootaxa.3619.3.2

Delventhal, R., Menuz, K., Joseph, R., Park, J., Sun, J.S., Carlson, J.R., 2017. The taste response to ammonia in *Drosophila*. Sci. Rep. 7. https://doi.org/10.1038/srep43754

Den Otter, C.J., Behan, M., Maes, F.W., 1980. Single cell responses in female *Pieris brassicae* (Lepidoptera: Pieridae) to plant volatiles and conspecific egg odours. J. Insect Physiol. 26, 465–472. https://doi.org/10.1016/0022-1910(80)90117-1

Dennis, E.J., Goldman, O. V., Vosshall, L.B., 2019. *Aedes aegypti* Mosquitoes Use Their Legs to Sense DEET on Contact. Curr. Biol. 29, 1551-1556.e5. https://doi.org/10.1016/j.cub.2019.04.004

Durant, A.C., Chasiotis, H., Misyura, L., Donini, A., 2017. *Aedes aegypti* Rhesus glycoproteins contribute to ammonia excretion by larval anal papillae. J. Exp. Biol. 220, 588–596. https://doi.org/10.1242/jeb.151084

Durant, A.C., Donini, A., 2020. Ammonium transporter expression in sperm of the

disease vector *Aedes aegypti* mosquito influences male fertility. Proc. Natl. Acad. Sci. U. S. A. 117, 29712–29719. https://doi.org/10.1073/pnas.2011648117

Durant, A.C., Donini, A., 2018. Ammonia excretion in an osmoregulatory syncytium is facilitated by AeAmt2, a novel ammonia transporter in *Aedes aegypti* larvae. Front. Physiol. 9. https://doi.org/10.3389/fphys.2018.00339

Ellison, H.E., Estévez-Lao, T.Y., Murphree, C.S., Hillyer, J.F., 2015. Deprivation of both sucrose and water reduces the mosquito heart contraction rate while increasing the expression of nitric oxide synthase. J. Insect Physiol. 74, 1–9. https://doi.org/10.1016/j.jinsphys.2015.01.011

Fox, A.N., Pitts, R.J., Robertson, H.M., Carlson, J.R., Zwiebel, L.J., 2001. Candidate odorant receptors from the malaria vector mosquito *Anopheles gambiae* and evidence of down-regulation in response to blood feeding. Proc. Natl. Acad. Sci. U. S. A. 98, 14693–14697. https://doi.org/10.1073/pnas.261432998

Gary, R.E., Cannon, J.W., Foster, W.A., 2009. Effect of sugar on male *Anopheles gambiae* mating performance, as modified by temperature, space, and body size. Parasites and Vectors 2. https://doi.org/10.1186/1756-3305-2-19

Ghaninia, M., Ignell, R., Hansson, B.S., 2007. Functional classification and central nervous projections of olfactory receptor neurons housed in antennal trichoid sensilla of female yellow fever mosquitoes, *Aedes aegypti*. Eur. J. Neurosci. 26, 1611–1623. https://doi.org/10.1111/j.1460-9568.2007.05786.x

Gibson, G., Russell, I., 2006. Flying in tune: Sexual recognition in mosquitoes. Curr. Biol. https://doi.org/10.1016/j.cub.2006.05.053

Gibson, G., Warren, B., Russell, I.J., 2010. Humming in tune: Sex and species recognition by mosquitoes on the wing. JARO - J. Assoc. Res. Otolaryngol. 11, 527–540. https://doi.org/10.1007/s10162-010-0243-2

Gowda, S.B.M., Paranjpe, P.D., Reddy, O.V., Thiagarajan, D., Palliyil, S., Reichert, H., Vijayraghavan, K., 2018. GABAergic inhibition of leg motoneurons is required for normal walking behavior in freely moving *Drosophila*. Proc. Natl. Acad. Sci. U. S. A. 115, E2115–E2124. https://doi.org/10.1073/pnas.1713869115

Hammond, A., Galizi, R., Kyrou, K., Simoni, A., Siniscalchi, C., Katsanos, D., Gribble, M., Baker, D., Marois, E., Russell, S., Burt, A., Windbichler, N., Crisanti, A., Nolan, T., 2016. A CRISPR-Cas9 gene drive system targeting female reproduction in the malaria mosquito vector *Anopheles gambiae*. Nat. Biotechnol. 34, 78–83. https://doi.org/10.1038/nbt.3439

Howell, P.I., Knols, B.G.J., 2009. Male mating biology. Malar. J. 8. https://doi.org/10.1186/1475-2875-8-S2-S8

Kwon, H.W., Lu, T., Rützler, M., Zwiebel, L.J., 2006. Olfactory response in a gustatory organ of the malaria vector mosquito *Anopheles gambiae*. Proc. Natl. Acad. Sci. U. S. A. 103, 13526–13531. https://doi.org/10.1073/pnas.0601107103

Lecompte, M., Cattaert, D., Vincent, A., Birman, S., Chérif-Zahar, B., 2020. *Drosophila* ammonium transporter Rh50 is required for integrity of larval muscles and neuromuscular system. J. Comp. Neurol. 528, 81–94. https://doi.org/10.1002/cne.24742

Liu, F., Chen, L., Appel, A.G., Liu, N., 2013. Olfactory responses of the antennal trichoid

sensilla to chemical repellents in the mosquito, *Culex quinquefasciatus*. J. Insect Physiol. 59, 1169–1177. https://doi.org/10.1016/j.jinsphys.2013.08.016

Liu, F., Ye, Z., Baker, A., Sun, H., Zwiebel, L.J., 2020. Gene editing reveals obligate and modulatory components of the CO_2 receptor complex in the malaria vector mosquito, *Anopheles coluzzii*. Insect Biochem. Mol. Biol. 127. https://doi.org/10.1016/j.ibmb.2020.103470

Menuz, K., Larter, N.K., Park, J., Carlson, J.R., 2014. An RNA-seq screen of the *Drosophila* antenna identifies a transporter necessary for ammonia detection. PLoS Genet. 10. https://doi.org/10.1371/journal.pgen.1004810

Min, S., Ai, M., Shin, S.A., Suh, G.S.B., 2013. Dedicated olfactory neurons mediating attraction behavior to ammonia and amines in *Drosophila*. Proc. Natl. Acad. Sci. U. S. A. 110, 1321–1329. https://doi.org/10.1073/pnas.1215680110

Montell, C., Zwiebel, L.J., 2016. Mosquito sensory systems. Adv. In Insect Phys. 51, 293–328. https://doi.org/10.1016/bs.aiip.2016.04.007

Pennetier, C., Warren, B., Dabiré, K.R., Russell, I.J., Gibson, G., 2010. “Singing on the wing” as a mechanism for species recognition in the malarial mosquito *Anopheles gambiae*. Curr. Biol. 20, 131–136. https://doi.org/10.1016/j.cub.2009.11.040

Pitts, R.J., Derryberry, S.L., Pulous, F.E., Zwiebel, L.J., 2014a. Antennal-expressed ammonium transporters in the malaria vector mosquito *Anopheles gambiae*. PLoS One 9. https://doi.org/10.1371/journal.pone.0111858

Pitts, R.J., Derryberry, S.L., Zhang, Z., Zwiebel, L.J., 2017. Variant ionotropic receptors in the malaria vector mosquito *Anopheles gambiae* tuned to amines and carboxylic

acids. Sci. Rep. 7. https://doi.org/10.1038/srep40297

Pitts, R.J., Fox, A.N., Zwiebeil, L.J., 2004. A highly conserved candidate chemoreceptor expressed in both olfactory and gustatory tissues in the malaria vector *Anopheles gambiae*. Proc. Natl. Acad. Sci. U. S. A. 101, 5058–5063. https://doi.org/10.1073/pnas.0308146101

Pitts, R.J., Liu, C., Zhou, X., Malpartida, J.C., Zwiebel, L.J., 2014b. Odorant receptor-mediated sperm activation in disease vector mosquitoes. Proc. Natl. Acad. Sci. U. S. A. 111, 2566–2571. https://doi.org/10.1073/pnas.1322923111

Pitts, R.J., Zwiebel, L.J., 2006. Antennal sensilla of two female anopheline sibling species with differing host ranges. Malar. J. 5. https://doi.org/10.1186/1475-2875-5-26

Pondeville, E., Puchot, N., Meredith, J.M., Lynd, A., Vernick, K.D., Lycett, G.J., Eggleston, P., Bourgouin, C., 2014. Efficient φc31 integrase-mediated site-specific germline transformation of *Anopheles gambiae*. Nat. Protoc. 9, 1698–1712. https://doi.org/10.1038/nprot.2014.117

Qiu, Y.T., Smallegange, R.C., Hoppe, S., van Loon, J.J.A., Bakker, E.-J., Takken, W., 2004. Behavioural and electrophysiological responses of the malaria mosquito *Anopheles gambiae* Giles *sensu stricto* (Diptera: Culicidae) to human skin emanations. Med. Vet. Entomol. 18, 429–438. https://doi.org/10.1111/j.0269-283X.2004.00534.x

Robert, D., 2009. Insect bioacoustics: Mosquitoes make an effort to listen to each other. Curr. Biol. https://doi.org/10.1016/j.cub.2009.04.021

Sadaf, S., Reddy, O.V., Sane, S.P., Hasan, G., 2015. Neural control of wing coordination in flies. Curr. Biol. 25, 80–86. https://doi.org/10.1016/j.cub.2014.10.069

Scaraffia, P.Y., Isoe, J., Murillo, A., Wells, M.A., 2005. Ammonia metabolism in *Aedes aegypti*. Insect Biochem. Mol. Biol. 35, 491–503. https://doi.org/10.1016/j.ibmb.2005.01.012

Smallegange, R.C., Qiu, Y.T., van Loon, J.A., Takken, W., 2005. Synergism between ammonia, lactic acid and carboxylic acids as kairomones in the host-seeking behaviour of the malaria mosquito *Anopheles gambiae sensu stricto* (Diptera: Culicidae). Chem. Senses 30, 145–152. https://doi.org/10.1093/chemse/bji010

Smallegange, R.C., Verhulst, N.O., Takken, W., 2011. Sweaty skin: An invitation to bite? Trends Parasitol. https://doi.org/10.1016/j.pt.2010.12.009

Soupene, E., Lee, H., Kustu, S., 2002. Ammonium/methylammonium transport (Amt) proteins facilitate diffusion of NH_3 bidirectionally. Proc. Natl. Acad. Sci. U. S. A. 99, 3926–3931. https://doi.org/10.1073/pnas.062043799

Suh, E., Choe, D.H., Saveer, A.M., Zwiebel, L.J., 2016. Suboptimal larval habitats modulate oviposition of the malaria vector mosquito *Anopheles coluzzii*. PLoS One 11. https://doi.org/10.1371/journal.pone.0149800

Sun, H., Liu, F., Ye, Z., Baker, A., Zwiebel, L.J., 2020. Mutagenesis of the orco odorant receptor co-receptor impairs olfactory function in the malaria vector *Anopheles coluzzii*. Insect Biochem. Mol. Biol. 127. https://doi.org/10.1016/j.ibmb.2020.103497

Thomas, G.H., Mullins, J.G.L., Merrick, M., 2000. Membrane topology of the Mep/Amt

family of ammonium transporters. Mol. Microbiol. 37, 331–344. https://doi.org/10.1046/j.1365-2958.2000.01994.x

Tremblay, P.L., Hallenbeck, P.C., 2009. Of blood, brains and bacteria, the Amt/Rh transporter family: Emerging role of Amt as a unique microbial sensor. Mol. Microbiol. 71, 12–22. https://doi.org/10.1111/j.1365-2958.2008.06514.x

World Health Organization, 2019. World Malaria Report, World Health.

Ye, Z., Liu, F., Sun, H., Barker, M., Pitts, R.J., Zwiebel, L.J., 2020. Heterogeneous expression of the ammonium transporter AgAmt in chemosensory appendages of the malaria vector, *Anopheles gambiae*. Insect Biochem. Mol. Biol. 120. https://doi.org/10.1016/j.ibmb.2020.103360

Younger, M.A., Herre, M., Ehrlich, A.R., Gong, Z., Gilbert, Z.N., Rahiel, S., Matthews, B.J., Vosshall, L.B., 2020. Non-canonical odor coding ensures unbreakable mosquito attraction to humans. bioRxiv. https://doi.org/10.1101/2020.11.07.368720

Zwiebel, L.J., Takken, W., 2004. Olfactory regulation of mosquito-host interactions. Insect Biochem. Mol. Biol. 34, 645–652. https://doi.org/10.1016/j.ibmb.2004.03.017

CHAPTER IV

SUMMARY AND FUTURE DIRECTIONS

This thesis project comprises comprehensive investigation of the cellular localization and function of the ammonium transporter *AcAmt* in the chemosensory system of the malaria mosquito *An. coluzzii* (formerly *An. gambiae sensu stricto* "M-form"; Coetzee et al. 2013). Functional studies have thus far been primarily focused on olfactory receptors including ORs, IRs, and GRs (Carey et al., 2010; Liu et al., 2010, 2020; Lu et al., 2007; Pitts et al., 2017; Sun et al., 2020; Wang et al., 2010), while non-receptor components have remained largely uncharacterized despite suggestions that they play essential roles in the olfactory sensing pathway (Leal, 2013). Here, we targeted the ammonium transporter Amt due to its potential role in olfactory sensitivity to ammonia, which is a potent human-derived attractant based on previous studies in *Anopheles* (Braks et al., 2001; Smallegange et al., 2005, 2002) and *Drosophila* (Menuz et al., 2014; Pitts et al., 2014a). Combining advanced genetic tools, cellular labelling techniques, an array of phenotypic assessments, and biochemical measurements, we successfully detailed the localization of *AcAmt* in mosquito chemosensory appendages and its function across the mosquito's olfactory, reproductive, and metabolic systems. This study sheds light on a novel ammonia sensing mechanism in mosquitoes compared to the fruit fly academic model and, in light of the novel degree of multifunctionality we revealed, illustrates a non-receptor alternative vector control strategy that targets these non-canonical olfactory components.

The first research component (Chapter 2) of this thesis focused on the localization of *AcAmt* using the binary expression Q system, which requires a genetic cross between an *AcAmt promoter-QF* driver line and a pre-defined *QUAS-GFP* effector line to allow GFP expression driven by *QF-QUAS* transcriptional activation in *AcAmt* expressing cells (Riabinina et al., 2016). In order to apply this genetic tool, we inserted the *AcAmt promoter-QF* element into a defined genomic location using the *phiC31* integration system (Meredith et al., 2011). The offspring of the driver line and the effector line is expected to display specific GFP fluorescence that indicates the expression of *AcAmt*. Immunohistochemical experiments incorporating antibodies against Orco and HRP (as ORN and general neuronal markers, respectively) as well as FISH riboprobes targeting *Ir76b* (as an ionotropic receptor neuron (IRN) marker) and *Gr15* (as a sugar-sensing gustatory receptor neuron (GRN) marker) were conducted to reveal *AcAmt* expression relative to several olfactory/gustatory elements in *An. coluzzii* adults and larvae. These studies revealed the following points: (1) In female antennae, *AcAmt* is expressed in both auxiliary cells surrounding *Ir76b*-expressing IRNs (marked by Ir76b riboprobes) as well as a subset of HRP antibody-labelled neurons likely located in coeloconic sensilla and grooved pegs; (2) In female maxillary palps, *AcAmt* is expressed in a subset of Orco antibody-labelled neurons in capitate pegs; (3) In female labella, *AcAmt* is expressed exclusively in HRP antibody-labelled neurons where *Ir76b*, Orco, and *Gr15* are labelled; (4) In female tarsi, *AcAmt* is expressed exclusively in HRP antibody-labelled neurons; (5) In larval antennae, *AcAmt* is expressed in both neuronal and auxiliary cells. Taken together, *AcAmt* is heterogeneously expressed in both neurons and auxiliary cells in antennae while being exclusively neuronal in other

chemosensory appendages in female *An. coluzzii*. The close association between AcAmt and Ir76b indicates they are likely involved in the same ammonia-sensing pathway, where Ir76b consists of a receptor complex with tuning Irs and AcAmt supports receptor activities by clearing ammonium and preventing desensitization.

Moreover, while the expression of *AcAmt* in the grooved pegs of *An. coluzzii* antennae was consistent with previous studies indicating that grooved pegs respond to ammonia (Meijerink et al., 2001; Qiu et al., 2006), the antennal coeloconic sensilla and maxillary palps capitate pegs that show *AcAmt* expression, as described above, have not been functionally characterized as sensitive to ammonia. We therefore conducted single sensillum recording (SSR) on these two classes of sensilla to investigate their potential as novel ammonia sensors.

From a technical perspective, in contrast to *Drosophila* where these approaches are well-established and wide-spread, thus far only a very limited number of studies have successfully employed genetic manipulations in *Anopheles* (Taning et al., 2017). To routinely accomplish this, I was able to utilize a *Anopheles* transgenic platform that combined phiC31 and Q system in order to generate driver lines with high efficiency (Pondeville et al., 2014). A similar workflow was used in Chapter 3 to generate CRISPR/Cas9-mediated *AcAmt* mutants and also been applied in the Zwiebel group to study additional genes in *An. coluzzii* (Liu et al., 2020; Sun et al., 2020). The accuracy of this genetic localization system is highly dependent on the understanding of the gene regulatory sequences, which is difficult to fully predict. To address this concern, instead of using difficult-to-predict promoters to regulate the QF transcriptional factor, recent studies have begun to employ CRISPR/Cas9 system modified to directly knock-in a

T2A-QF element into the target gene exon. The T2A peptide mediates ribosomal skipping during translation to facilitate the independent expression of *QF* under regulation of the native promoter and generate unambiguous labelling signals (Matthews et al., 2019; Younger et al., 2020). Considering the high CRICPR/Cas9 efficiency detailed in Chapter 3, this novel system should be able to be introduced to *Anopheles* in future studies to greatly improve fidelity and reduce the antibody/FISH-based validation processes in Q system-mediated genetic localization studies.

In the next experimental component (Chapter 3), the function of *AcAmt* in ammonia sensitivity was investigated using CRISPR/Cas9-mediated mutagenesis. The knock-out strategy relies on homology-directed repair to insert a *3xP3-DeRed* fluorescence marker at the exon of the target gene, allowing for easy selection of mutants. In order to ensure a more robust/complete gene knock-out phenotype, we employed two sgRNAs to target the beginning of *AcAmt exon1* and *exon4* in order to replace the sequences in between with *3xP3-DsRed*, which is the majority of the coding sequence. Whole antennal/labellar responses of *AcAmt*$^{-/-}$ females to ammonia were investigated using electroantennogram/electrolabellogram (EAG/ELG) and single sensillum recording (SSR) studies focused on antennal coeloconic sensilla and grooved pegs where extensive *AcAmt* expression was observed in Chapter 2. In contrast to the dramatic reduction of ammonia responses in *Drosophila Amt* mutants (Menuz et al., 2014), EAG, ELG, and SSR data in *An. coluzzii* collectively suggest there are no significant differences between *AcAmt* null mutants and wild type mosquitoes across these broad electrophysiological responses to ammonia. Instead, we observed a range of phenotypic deficits related to reproduction and fitness in *AcAmt* mutants. Behavioral

bioassays showed significantly lower efficiency in adult mating and significantly higher mortality rates during eclosion in the *AcAmt*$^{-/-}$ mutants. Abnormal adult locomotor activities were observed within the timeframe during which mating mostly occurs. To deepen our understanding of these mating and eclosion phenotypes, biochemical experiments were conducted to test the sugar content and ammonia levels in the adults and pupae, and a behavioral bioassay was performed to test sugar feeding ability in the adult mosquitoes. In these experiments, *AcAmt*$^{-/-}$ males showed significantly lower sugar consumption, while *AcAmt*$^{-/-}$ females and pupae displayed significantly higher ammonia levels than their wild-type counterparts. Additionally, video recordings were conducted to monitor mosquito locomotor activity during scotophase, revealing that *AcAmt*$^{-/-}$ females experience a delay in activity that may contribute to mating deficiency.

Overall, these data support the existence of an unique ammonia-sensing mechanism in *An. coluzzii* that may have evolved as a consequence of the importance of this semiochemical in blood feeding mosquitoes. It is likely that the importance of ammonia in host-seeking/preference behaviors that are necessary to satisfy the mosquito's blood feeding reproductive requirements provide sufficient selective pressure to give rise to other complementary mechanisms involving other ammonium transporters. Indeed, previous studies have revealed the expression of another, namely the *Rh50* gene in *Anopheles* and *Drosophila* antennae (Menuz et al., 2014; Pitts et al., 2014). While the localization and function of Rh50 remains cryptic, it is reasonable to postulate that antennal Rh50 might be involved in diverse ammonia sensing pathways and, in that context, play a similar role as Amt.

Future studies focusing on comparison of Rh50 and Amt could significantly contribute to the understanding of ammonia-detecting mechanisms in mosquitoes. According to the heterogenous expression pattern of *AcAmt* in cells that are functionally divergent, our data suggest that neuronally-expressed *AcAmt* is likely involved in sensory/non-sensory mechanisms distinct from those occurring in auxiliary cells. Furthermore, in Chapter 3, we have hypothesized that neuronal Amt might be involved in ammonia homeostasis of glutamatergic neurons likely to be associated with neuro-muscular pathways in the mosquito, which was suggested to be the function of Rh50 in *Drosophila* larvae (Lecompte et al., 2020). In this regard, *Amt* mutations could presumably impair mosquito muscle control and result in abnormal wing-beat frequencies that would be expected to impair the sexual recognition required for conspecific mating restrictions (Pennetier et al., 2010). In any case, the function of the neuronal Amt remains an interesting topic that should be further investigated using high-sensitivity mosquito monitoring systems. Beyond this academic interest, the data reported here makes it reasonable to speculate that, taken together, mosquito Amts represent a viable molecular target for the design of novel vector control strategies.

References

Braks, M.A.H., Meijerink, J., Takken, W., 2001. The response of the malaria mosquito, *Anopheles gambiae*, to two components of human sweat, ammonia and L-lactic acid, in an olfactometer. Physiol. Entomol. 26, 142–148. https://doi.org/10.1046/j.1365-3032.2001.00227.x

Carey, A.F., Wang, G., Su, C.Y., Zwiebel, L.J., Carlson, J.R., 2010. Odorant reception in the malaria mosquito *Anopheles gambiae*. Nature 464, 66–71. https://doi.org/10.1038/nature08834

Leal, W.S., 2013. Odorant reception in insects: Roles of receptors, binding proteins, and degrading enzymes. Annu. Rev. Entomol. 58, 373–391. https://doi.org/10.1146/annurev-ento-120811-153635

Lecompte, M., Cattaert, D., Vincent, A., Birman, S., Chérif-Zahar, B., 2020. *Drosophila* ammonium transporter Rh50 is required for integrity of larval muscles and neuromuscular system. J. Comp. Neurol. 528, 81–94. https://doi.org/10.1002/cne.24742

Liu, C., Pitts, R.J., Bohbot, J.D., Jones, P.L., Wang, G., Zwiebel, L.J., 2010. Distinct olfactory signaling mechanisms in the malaria vector mosquito *Anopheles gambiae*. PLoS Biol. 8, 27–28. https://doi.org/10.1371/journal.pbio.1000467

Liu, F., Ye, Z., Baker, A., Sun, H., Zwiebel, L.J., 2020. Gene editing reveals obligate and modulatory components of the CO_2 receptor complex in the malaria vector mosquito, *Anopheles coluzzii*. Insect Biochem. Mol. Biol. 127. https://doi.org/10.1016/j.ibmb.2020.103470

Lu, T., Qiu, Y.T., Wang, G., Kwon, J.Y., Rutzler, M., Kwon, H.W., Pitts, R.J., van Loon,

J.J.A., Takken, W., Carlson, J.R., Zwiebel, L.J., 2007. Odor coding in the maxillary palp of the malaria vector mosquito *Anopheles gambiae*. Curr. Biol. 17, 1533–1544. https://doi.org/10.1016/j.cub.2007.07.062

Matthews, B.J., Younger, M.A., Vosshall, L.B., 2019. The ion channel ppk301 controls freshwater egg-laying in the mosquito *Aedes aegypti*. Elife 8. https://doi.org/10.7554/eLife.43963

Meijerink, J., Braks, M.A.H., Van Loon, J.J.A., 2001. Olfactory receptors on the antennae of the malaria mosquito *Anopheles gambiae* are sensitive to ammonia and other sweat-borne components. J. Insect Physiol. 47, 455–464. https://doi.org/10.1016/S0022-1910(00)00136-0

Menuz, K., Larter, N.K., Park, J., Carlson, J.R., 2014. An RNA-seq screen of the *Drosophila* antenna identifies a transporter necessary for ammonia detection. PLoS Genet. 10. https://doi.org/10.1371/journal.pgen.1004810

Meredith, J.M., Basu, S., Nimmo, D.D., Larget-Thiery, I., Warr, E.L., Underhill, A., McArthur, C.C., Carter, V., Hurd, H., Bourgouin, C., Eggleston, P., 2011. Site-specific integration and expression of an anti-malarial gene in transgenic *Anopheles gambiae* significantly reduces *Plasmodium* infections. PLoS One 6. https://doi.org/10.1371/journal.pone.0014587

Pennetier, C., Warren, B., Dabiré, K.R., Russell, I.J., Gibson, G., 2010. “Singing on the wing” as a mechanism for species recognition in the malarial mosquito *Anopheles gambiae*. Curr. Biol. 20, 131–136. https://doi.org/10.1016/j.cub.2009.11.040

Pitts, R.J., Derryberry, S.L., Pulous, F.E., Zwiebel, L.J., 2014. Antennal-expressed ammonium transporters in the malaria vector mosquito *Anopheles gambiae*. PLoS

One 9. https://doi.org/10.1371/journal.pone.0111858

Pitts, R.J., Derryberry, S.L., Zhang, Z., Zwiebel, L.J., 2017. Variant ionotropic receptors in the malaria vector mosquito *Anopheles gambiae* tuned to amines and carboxylic acids. Sci. Rep. 7. https://doi.org/10.1038/srep40297

Pondeville, E., Puchot, N., Meredith, J.M., Lynd, A., Vernick, K.D., Lycett, G.J., Eggleston, P., Bourgouin, C., 2014. Efficient φc31 integrase-mediated site-specific germline transformation of *Anopheles gambiae*. Nat. Protoc. 9, 1698–1712. https://doi.org/10.1038/nprot.2014.117

Qiu, Y.T., van Loon, J.J.A., Takken, W., Meijerink, J., Smid, H.M., 2006. Olfactory coding in antennal neurons of the malaria mosquito, *Anopheles gambiae*. Chem. Senses 31, 845–863. https://doi.org/10.1093/chemse/bjl027

Riabinina, O., Task, D., Marr, E., Lin, C.C., Alford, R., O'Brochta, D.A., Potter, C.J., 2016. Organization of olfactory centres in the malaria mosquito *Anopheles gambiae*. Nat. Commun. 7. https://doi.org/10.1038/ncomms13010

Smallegange, R.C., Geier, M., Takken, W., 2002. Behavioural responses of *Anopheles gambiae* to ammonia, lactic acid and a fatty acid in a y-tube olfactometer. Proc. Exp. Appl. Entomol. 13, 147–152.

Smallegange, R.C., Qiu, Y.T., van Loon, J.A., Takken, W., 2005. Synergism between ammonia, lactic acid and carboxylic acids as kairomones in the host-seeking behaviour of the malaria mosquito *Anopheles gambiae sensu stricto* (Diptera: Culicidae). Chem. Senses 30, 145–152. https://doi.org/10.1093/chemse/bji010

Sun, H., Liu, F., Ye, Z., Baker, A., Zwiebel, L.J., 2020. Mutagenesis of the orco odorant receptor co-receptor impairs olfactory function in the malaria vector *Anopheles*

coluzzii. Insect Biochem. Mol. Biol. 127. https://doi.org/10.1016/j.ibmb.2020.103497

Taning, C.N.T., Van Eynde, B., Yu, N., Ma, S., Smagghe, G., 2017. CRISPR/Cas9 in insects: Applications, best practices and biosafety concerns. J. Insect Physiol. 98, 245–257. https://doi.org/10.1016/j.jinsphys.2017.01.007

Wang, G., Carey, A.F., Carlson, J.R., Zwiebel, L.J., 2010. Molecular basis of odor coding in the malaria vector mosquito *Anopheles gambiae*. Proc. Natl. Acad. Sci. U. S. A. 107, 4418–4423. https://doi.org/10.1073/pnas.0913392107

Younger, M.A., Herre, M., Ehrlich, A.R., Gong, Z., Gilbert, Z.N., Rahiel, S., Matthews, B.J., Vosshall, L.B., 2020. Non-canonical odor coding ensures unbreakable mosquito attraction to humans. bioRxiv. https://doi.org/10.1101/2020.11.07.368720